

HIGH FIELD MAGNETIC STUDIES  
ON DISPERSED NICKEL CATALYSTS

---

A Thesis  
Presented to  
the Faculty of the Department of Chemical Engineering  
University of Houston

---

In Partial Fulfillment  
of the Requirements for the Degree  
Master of Science in Chemical Engineering

---

by  
Lonnie Reed Vincent

December, 1973

691982

## ACKNOWLEDGEMENT

The completion of this study is indebted to the following:

My parents and wife: for their encouragement.

Messrs. Lee Bennett and Roy Priest: for their many helpful suggestions and excellent work in building the equipment.

Doctors W. I. Honeywell and J. E. Vevai: for many helpful discussions on the experimental equipment and technique and for operation of the superconducting solenoid.

Mr. R. N. McGill: for useful discussion of the experimentation and for assistance in performing the high field measurements.

Dr. J. T. Richardson: for discussions of the theoretical and experimental aspects of this study.

Mr. C.-Y. P. Huang: for making the surface area measurements and assisting with the high field measurements.

Mr. T. H. Chen and D. Bruns: for their comments on the proposed methods for determining crystallite distributions.

Mr. Herb Kent and the staff of the Chemical Engineering Department: for valuable assistance in administrative and logistical matters.

The Welch Foundation: to whom we are most indebted for financial support of this project.

To all are extended sincere appreciation and best wishes.

HIGH FIELD MAGNETIC STUDIES  
ON DISPERSED NICKEL CATALYSTS

---

An Abstract of a Thesis  
Presented to  
the Faculty of the Department of Chemical Engineering  
University of Houston

---

In Partial Fulfillment  
of the Requirements for the Degree  
Master of Science in Chemical Engineering

---

by  
Lonnie Reed Vincent  
December, 1973

## ABSTRACT

The magnetization of thirteen dispersed nickel catalyst samples was measured for magnetic field strengths in the 0 to 90,000 oersted range. Measurements were made in this range to better estimate the saturation magnetization of the dispersed systems and to obtain the low and high magnetic field strength average crystallite sizes as a means of measuring the dispersion of the nickel.

Methods for determining the average crystallite sizes and crystallite size distributions are discussed. Two measures of dispersion are presented and two methods proposed and tested for approximating crystallite size distributions from the magnetic data. One of the methods was used to approximate the crystallite size distributions of several of the dispersed nickel catalysts.

## TABLE OF CONTENTS

CHAPTER	PAGE
I. INTRODUCTION .....	1
II. THEORY OF FERROMAGNETIC CRYSTALLITES .....	5
III. EXPERIMENTAL EQUIPMENT AND PROCEDURE .....	25
IV. EXPERIMENTAL DATA AND RESULTS .....	37
V. CONCLUSIONS AND RECOMMENDATIONS .....	64
BIBLIOGRAPHY	
APPENDIX	
A. LANGEVIN AND BRILLOUIN FUNCTIONS .....	69
B. EXPERIMENTAL DATA .....	73
C. COMPUTER PROGRAM .....	86
D. SAMPLE CALCULATIONS .....	98
NOMENCLATURE .....	101

## LIST OF FIGURES

FIGURE	PAGE
2.1	RELATIVE MAGNETIZATION FOR MONODISPERSE SYSTEM AND SYSTEM WITH NARROW DISTRIBUTION OF CRYSTALLITE SIZES ..... 8
2.2	EXAMPLE OF RESULTS OF FOURIER INTEGRAL METHOD ( ● ) FOR DETERMINING CRYSTALLITE DISTRIBUTION FROM RELATIVE MAGNETIZATION CURVE CALCULATED FROM GIVEN DISTRIBUTION ..... 23
2.3	EXAMPLE OF RESULTS OF FOURIER INTEGRAL METHOD ( ● ) FOR DETERMINING CRYSTALLITE DISTRIBUTION FROM RELATIVE MAGNETIZATION CURVE CALCULATED FROM GIVEN DISTRIBUTION ..... 24
3.1	GENERAL ARRANGEMENT OF SUPERCONDUCTING MAGNET, MEASURING COILS, SAMPLE CELL AND SAMPLE USED FOR HIGH MAGNETIC FIELD STRENGTH MEASUREMENTS ..... 28
3.2	RLC CIRCUIT OF Q-METER USED TO MEASURE NICKEL CONCENTRATION ..... 31
3.3	SCHEMATIC DIAGRAM OF SAMPLE PREPARATION AND SURFACE AREA APPARATUS ..... 32
4.1	TYPICAL EXPERIMENTAL SIGNAL FROM HIGH FIELD SYSTEM. TWO SIGNALS ( OFFSET ) DEMONSTRATE REPRODUCIBILITY. SAMPLE 12 AT 15.5 KILO-OERSTEDS .. 39
4.2	EXPERIMENTAL DATA FROM HIGH FIELD MEASUREMENTS FOR SAMPLE 1 (BULK NICKEL) AND SAMPLE 3 AT 295 DEGREES KELVIN ..... 40
4.3	EXPERIMENTAL DATA FOR OBTAINING SIGNAL AT SATURATION FOR SAMPLE 1 (BULK NICKEL) AT 295 DEGREES KELVIN ... 42
4.4	EXPERIMENTAL DATA FOR OBTAINING SIGNAL AT SATURATION FOR SAMPLE 3 AT 295 DEGREES KELVIN ..... 43

FIGURE	PAGE
4.5	EXPERIMENTAL DATA FOR OBTAINING SIGNAL AT SATURATION FOR SAMPLE 3 at 295 DEGREES KELVIN ..... 44
4.6	EXPERIMENTALLY DETERMINED RELATIVE MAGNETIZATION VERSUS H / T FOR SAMPLES 1 AND 4 (BULK NICKEL) AT 295 DEGREES KELVIN ..... 47
4.7	EXPERIMENTALLY DETERMINED RELATIVE MAGNETIZATION VERSUS H / T FOR SAMPLES 2 AND 3 AT 295 DEGREES KELVIN ..... 48
4.8	EXPERIMENTALLY DETERMINED RELATIVE MAGNETIZATION VERSUS H / T FOR SAMPLES 5, 6 AND 7 AT 295 DEGREES KELVIN. SERIES REDUCED AT 350 DEGREES CENTIGRADE .. 49
4.9	EXPERIMENTALLY DETERMINED RELATIVE MAGNETIZATION VERSUS H / T FOR SAMPLES 8 AND 9 AT 295 DEGREES KELVIN. SERIES REDUCED AT 450 DEGREES CENTIGRADE .. 50
4.10	EXPERIMENTALLY DETERMINED RELATIVE MAGNETIZATION VERSUS H / T FOR SAMPLES 10 AND 11 AT 295 DEGREES KELVIN. SERIES REDUCED AT 600 DEGREES CENTIGRADE .. 51
4.11	EXPERIMENTALLY DETERMINED RELATIVE MAGNETIZATION VERSUS H / T FOR SAMPLE 12 AND 13 AT 295 DEGREES KELVIN. SERIES SINTERED IN HELIUM ..... 52
4.12	FOURIER SERIES APPROXIMATION TO CRYSTALLITE SIZE DISTRIBUTION FOR SAMPLE 2 ..... 55
4.13	FOURIER SERIES APPROXIMATION TO CRYSTALLITE SIZE DISTRIBUTION FOR SAMPLE 3 ..... 56
4.14	FOURIER SERIES APPROXIMATION TO CRYSTALLITE SIZE DISTRIBUTION FOR SAMPLE 5 ..... 57
4.15	FOURIER SERIES APPROXIMATION TO CRYSTALLITE SIZE DISTRIBUTION FOR SAMPLE 6 ..... 58
4.16	FOURIER SERIES APPROXIMATION TO CRYSTALLITE SIZE DISTRIBUTION FOR SAMPLE 7 ..... 59
4.17	FOURIER SERIES APPROXIMATION TO CRYSTALLITE SIZE DISTRIBUTION FOR SAMPLE 8 ..... 60

FIGURE	PAGE
4.18 FOURIER SERIES APPROXIMATION TO CRYSTALLITE SIZE DISTRIBUTION FOR SAMPLE 9 .....	61
4.19 FOURIER SERIES APPROXIMATION TO CRYSTALLITE SIZE DISTRIBUTION FOR SAMPLE 10 .....	62
4.20 FOURIER SERIES APPROXIMATION TO CRYSTALLITE SIZE DISTRIBUTION FOR SAMPLE 11 .....	63
B.1 EXPERIMENTAL DATA FROM HIGH FIELD MEASUREMENTS FOR SAMPLE 2 AT 295 DEGREES KELVIN .....	74
B.2 EXPERIMENTAL DATA FROM HIGH FIELD MEASUREMENTS FOR SAMPLE 4 (BULK NICKEL) AT 295 DEGREES KELVIN ..	75
B.3 EXPERIMENTAL DATA FROM HIGH FIELD MEASUREMENTS FOR SAMPLE 5 AT 295 DEGREES KELVIN .....	76
B.4 EXPERIMENTAL DATA FROM HIGH FIELD MEASUREMENTS FOR SAMPLE 6 AT 295 DEGREES KELVIN .....	77
B.5 EXPERIMENTAL DATA FROM HIGH FIELD MEASUREMENTS FOR SAMPLE 7 AT 295 DEGREES KELVIN .....	78
B.6 EXPERIMENTAL DATA FROM HIGH FIELD MEASUREMENTS FOR SAMPLE 8 AT 295 DEGREES KELVIN .....	79
B.7 EXPERIMENTAL DATA FROM HIGH FIELD MEASUREMENTS FOR SAMPLE 9 AT 295 DEGREES KELVIN .....	80
B.8 EXPERIMENTAL DATA FROM HIGH FIELD MEASUREMENTS FOR SAMPLE 10 AT 295 DEGREES KELVIN .....	81
B.9 EXPERIMENTAL DATA FROM HIGH FIELD MEASUREMENTS FOR SAMPLE 11 AT 295 DEGREES KELVIN .....	82
B.10 EXPERIMENTAL DATA FROM HIGH FIELD MEASUREMENTS FOR SAMPLE 12 AT 295 DEGREES KELVIN .....	83
B.11 EXPERIMENTAL DATA FROM HIGH FIELD MEASUREMENTS FOR SAMPLE 13 AT 295 DEGREES KELVIN .....	84
B.12 COMPARISON OF HIGH FIELD SYSTEM DATA WITH FARADAY SYSTEM DATA. FARADAY DATA AFTER ROSSER ( 33 ) .....	85

LIST OF TABLES

TABLE		PAGE
4.1	SAMPLE PREPARATION DATA .....	38
4.2	EXPERIMENTALLY DETERMINED CATALYST CHARACTERISTICS .....	53
4.3	EXPERIMENTALLY DETERMINED AVERAGE CRYSTALLITE SIZES AND MEASURES OF DISPERSION AS CALCULATED BY DIFFERENT APPROXIMATIONS .....	54

## CHAPTER I

### INTRODUCTION

The successful interpretation and utilization of catalytic kinetic data for both fundamental and industrial applications depends upon proper characterization of the catalyst. Early attempts to relate catalytic activity to bulk quantities such as the mass of catalyst yielded information of little or no value. The realization that catalytic processes are site or surface phenomena has brought catalytic kinetics more into perspective and has yielded a better understanding of heterogeneous catalysis. It has also been observed that the activity of certain reactions depends not only upon the surface area but also upon the crystallite size of the supported metal. Boudart and coworkers ( 1 ) have classified those reactions which depend upon crystallite size as demanding reactions and those reactions which are insensitive to changes of crystallite size as facile reactions. Demanding reactions are further classified as (a) having a positive intrinsic factor when the specific activity decreases with crystallite size, (b) having a negative intrinsic factor when the specific activity increases with crystallite size and (c) those reactions for which the specific activity is a maximum at an intermediate size.

The surface area of a supported catalyst is usually measured by gas chemisorption. A measure of the average crystallite size

can then be obtained from the chemisorption surface area or by means of electron micrographs, x-ray line broadening or magnetic measurements. Luss ( 2 ) has shown that the specific activity will depend upon the crystallite size distribution and hence the average crystallite size will not yield meaningful correlation of specific activity since different distributions can have the same average crystallite size. It is therefore desirable to know not only the average crystallite size but also some measure of the dispersion about the average size. This work will be concerned with obtaining this data via magnetic measurements.

Magnetic measurements have been used for various purposes in the study of heterogeneous catalysis such as measuring the extent of reduction, adsorbate bonding, and average crystallite sizes. The latter measurements have been useful in comparing different catalysts, in crystallite growth studies, and in studies of demanding and facile reactions. Magnetic measurements are relatively simple and versatile and have been used by several investigators as a routine characterization of supported catalyst. Although generally limited to ferromagnetic materials, magnetic methods have proved to be a very useful tool in catalytic research.

Catalyst characterization by magnetic methods has generally been limited to relatively low magnetic field strengths (less than 20 kilo-oersteds) which means that the sample does not approach magnetic saturation unless low temperatures are used. These

measurements have been utilized for the calibration of equipment and for the measurement of the saturation magnetization and average crystallite size by methods to be discussed in a subsequent chapter. It is known that measurements at small and large relative saturations yield different crystallite size averages. The validity of the saturation magnetization determined from low field data is also questionable. However, the use of low temperatures to approach saturation is to be avoided if possible because the maximum crystallite size which exhibits superparamagnetism is greatly reduced as temperature is reduced.

The objectives of this study are as follows:

- (1) Compare the low and high field estimates of the saturation magnetization from data at approximately 300 degrees Kelvin.
- (2) Determine the low and high magnetic field strength estimates of the average crystallite size as a measure of the dispersion of several catalysts.
- (3) Propose and test methods for determining the crystallite size distribution from the magnetization curves of supported catalysts.
- (4) Determine the crystallite size distribution from the magnetization curve for several catalysts samples using the proposed methods.

This thesis will provide evidence that the use of the

high magnetic field measurements provides a better estimate of the saturation magnetization than low magnetic field measurements and that differences in catalysts with approximately the same low field estimate of the average crystallite size may be noted by measuring the dispersion of the crystallite sizes. Two different methods for estimating crystallite size distributions will be investigated. One of these methods may make possible the determination of crystallite size distributions utilizing relative magnetization data extending into the high magnetic field strength region.

## CHAPTER II

### THEORY OF FERROMAGNETIC CRYSTALLITES

#### SUPERPARAMAGNETISM

One of the first successful descriptions of the magnetic behavior of small particles based on a classical continuous energy distribution was given by Langevin ( 3 ). Consideration of the more recent theories of quantized energy levels leads to a description of small magnetic particles by the Brillouin function,  $B_r$  ( 4 ). Except at very low temperatures and for systems of very few atoms or ions, the Langevin function,  $L$ , will adequately describe the behavior of the systems presently under study ( 5 ). The basis for these two functions and their relation are discussed further in Appendix A.

Several different names have been used to describe the behavior of ferromagnetic crystallites, however, the terminology superparamagnetism appears to be more generally accepted and hence will be used herein. The measurements of Heukelom et al. ( 6 ) on nickel/silica catalysts at 80 and 300 degrees Kelvin appear to be one of the first published results of clearly superparamagnetic behavior. Since then, numerous examples of superparamagnetic behavior have been presented. Notable among these were the data of Bean and Jacobs ( 7 ), Becker ( 8 ) and Luborsky and Lawrence ( 9 ). Only those aspects of superparamagnetism pertinent to this study will be presented. More

thorough discussions have been presented elsewhere ( 4, 5, 10, 11 ).

Consider a system of single domain, uniform volume crystallites of a ferromagnetic material. The relative magnetic saturation of this system in thermal equilibrium with an applied field is given by the Langevin function

$$M / M_{\infty} = L( \mu H / kT ) \quad 2.1$$

$$M / M_{\infty} = \text{COTH}( \mu H / kT ) - ( kT / \mu H ) \quad 2.2$$

or alternately

$$M / M_{\infty} = \text{COTH}( M_{sp} V H / kT ) - ( kT / M_{sp} V H ) \quad 2.3$$

where

$$\mu = M_{sp} V \quad 2.4$$

for a ferromagnetic material.

Neel ( 12 ) and Brown ( 13 ) have considered the question of the approach to thermal equilibrium and have shown that when an applied magnetic field is removed from magnetized particles, the remanance decays according to

$$M_r / M_{\infty} = \text{EXP}( -t / \tau ) \quad 2.5$$

The relaxation time,  $\tau$ , is related to the volume by

$$1 / \tau = C_0 \text{EXP}( - C_1 V / kT ) \quad 2.6$$

where  $C_0$  is of the order of  $10^9$  per second and  $C_1$  is the anisotropy energy per unit volume. The question of thermal equilibrium has also been discussed by Jacobs and Bean ( 10 ) and by Selwood ( 5 ) who have shown, for ferromagnetic crystallites of the size usually encountered on supported catalysts, at 300 degrees Kelvin, that thermal equilibrium with the applied magnetic field is achieved in a time period of at most several seconds.

Monodisperse systems, however, are an ideality which are seldom encountered. For systems of practical importance, there are usually distributions of crystallite volumes and hence distributions of crystallite moments. The magnetization is then given by

$$M / M_{\infty} = \int_0^{\infty} L( \mu H / kT ) f_1 ( \mu ) d\mu \quad 2.7$$

or for a ferromagnetic material

$$M / M_{\infty} = \int_0^{\infty} L( M_{sp} V H / kT ) f_2 ( V ) dV \quad 2.8$$

A comparison of the relative magnetizations for a monodisperse and a system with a narrow distribution of crystallite sizes is given in Figure 2.1.

The theory of superparamagnetism thus gives at least two conditions for classifying the behavior of crystallites as

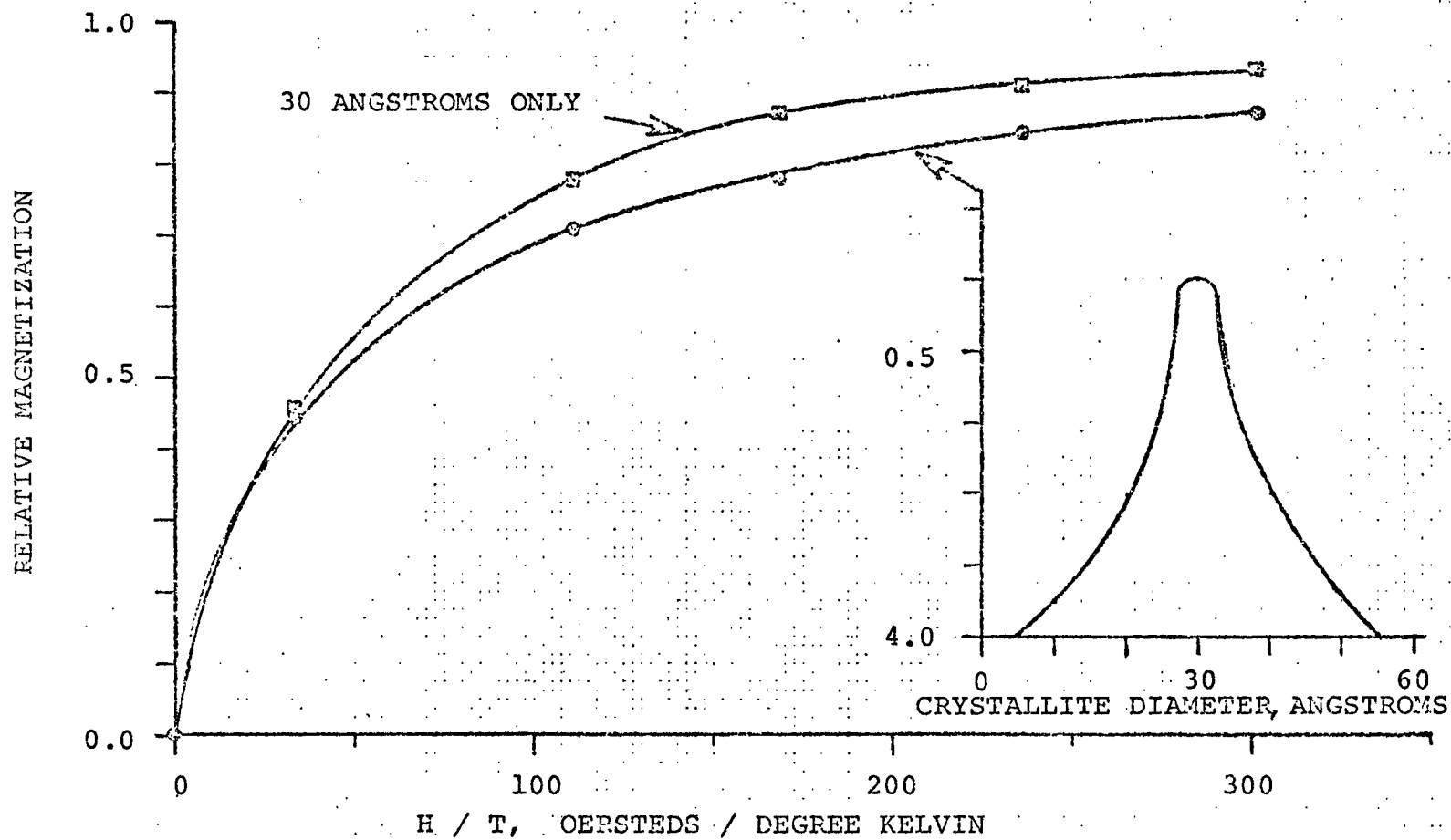


FIGURE 2.1. RELATIVE MAGNETIZATION FOR MONODISPersed SYSTEM AND SYSTEM WITH NARROW DISTRIBUTION OF CRYSTALLITE SIZES.

superparamagnetic. First, the magnetization curve does not exhibit hysteresis. The second condition is that the magnetizations measured at different temperatures over a range of field strengths superimpose when plotted versus  $( H / T )$  or  $( T / H )$ . This second condition implies, at least for ferromagnetic crystallites with a distribution of volumes, that the dependence of the spontaneous magnetization,  $M_{sp}$ , on temperature and volume is known.

One approach to determining the spontaneous magnetization of ferromagnetic crystallites, at least in a qualitative manner, is to measure the magnetization as a function of field strength over a range of temperatures for several 'monodisperse' systems with different crystallite sizes. Values of the spontaneous magnetization may then be determined which best fit the experimental data. Measurements of this type have been attempted with the results providing insight into the behavior of ferromagnetic crystallites.

Measurement of the low magnetic field strength magnetization at different temperatures for systems with known crystallite sizes cause variations in the spontaneous magnetization to be detected by changes in the initial slope of the magnetization curve. This can be shown by noting that the initial slope of the magnetization curve for a monodisperse system is obtained from equation (2.1) where, for small values of the argument of the Langevin function, the relative magnetization may be approximated by

$$M / M_{\infty} = M_{sp} V H / 3kT \quad 2.9$$

where  $V$  is the known crystallite volume. Measurements of this type have been made by Knappwost ( 14 ) on cobalt crystallites approximately 15 Angstroms in diameter at temperatures up to 580 degrees Kelvin, and by Vogt ( 15 ) on nickel crystallites approximately 35 Angstroms in diameter at temperatures up to 500 degrees Kelvin. Their results indicate that the temperature dependence of the spontaneous magnetization for ferromagnetic crystallites is very similar to that of the bulk material, that is

$$M_{sp} / M_{\infty} = \text{TANH} ( [ M_{sp} / M_{\infty} ] / [ T / T_c ] ) \quad 2.10$$

Measurements of the saturation magnetization on systems with different crystallite sizes yields some information on the volume dependence of the spontaneous magnetization. It is known for bulk ferromagnetics, as shown by equation ( 2.10 ), that the spontaneous magnetization at absolute zero of temperature is the same as the saturation magnetization. Two methods can be used to obtain the saturation magnetization. The first method is based on the approach to saturation given by the Langevin equation. The magnetization is plotted verses (  $1 / H$  ), and if sufficiently high field strengths are used, an extrapolation may be made with some confidence to the saturation magnetization at infinite field strength, that is at (  $1 / H$  ) = 0. A second method is based on

the observation of Heukelom et al. ( 6 ) that magnetization curves at room temperature over a range of field strengths approaching saturation could be represented by the empirical relation

$$M / M_{\infty}(0) = ( C_2 H )^{0.9} / [ 1 + ( C_2 H )^{0.9} ] \quad 2.11$$

where  $M_{\infty}(0)$  is the saturation magnetization at zero degrees Kelvin. The saturation magnetization may therefore be obtained by extrapolating to  $( 1 / H )^{0.9} = 0$  on a plot of  $( 1 / M )$  verses  $( 1 / H )^{0.9}$ . Measurements on samples of known composition and approximate crystallite size have been made that show that the saturation magnetization and hence the spontaneous magnetization of ferromagnetic crystallites is essentially that of the bulk material. One of the most comprehensive set of measurements of this type was those of Luborsky and Lawrence ( 9 ) who made measurements on iron crystallites between 15 and 40 Angstroms in diameter suspended in mercury over a temperature range of 4 to 300 degrees Kelvin and at field strengths up to 150,000 oersteds. Their measurements, however, were made using non-equilibrium pulsed magnetic fields. Bean, Livingston and Rodbell ( 16 ) used different methods than those described above and conclude that cobalt crystallites of approximately 42 to 154 Angstroms in diameter in copper exhibit essentially the same saturation magnetization as the bulk material.

## METHODS FOR DETERMINING CRYSTALLITE SIZES

Several methods are available for obtaining crystallite sizes of supported metals. These methods include x-ray line broadening, gas adsorption, low angle x-ray diffraction, electron microscopy, and magnetic measurements. Whereas x-ray line broadening and gas adsorption give only average crystallite sizes, it is possible to determine the size distribution as well as averages from the other methods. X-ray line broadening is generally limited to samples with metal crystallites larger than 40 Angstroms in diameter. Developments in electron microscopy have made the observation of crystallites of approximately 20 Angstroms in diameter possible. Dorling and Moss ( 17 ) for instance, have used x-ray line broadening and electron microscopy to determine average crystallite sizes on platinum/silica catalysts. Gas adsorption has also been used in research and industrial applications, however, the average crystallite size determined in this manner depends upon assumption of the crystallite shape and the fraction of the crystallite exposed to the adsorbate. There is also the unresolved question as to the effect of the support on the adsorption. Crystallite distributions may be measured with low angle x-ray diffraction or electron microscopy but the methods of preparation of the samples for use by these techniques leaves doubt as to how representative the sample is of the original catalyst. Further examples of the use and limitations of these techniques are discussed by Spenadel and Boudart ( 18 ), Adams et al. ( 19 ) and by Reinen and Selwood ( 20 ).

The primary consideration of this study will be the use of magnetic measurements to determine the crystallite size distribution of a supported metal. Low magnetic field strength measurements using the Faraday method have been developed to the point of routine measurements as has been reported by Richardson and Beauxis ( 21 ). Low field strength measurements have also been made using direct current permeameters similar to that described by Barnett ( 22 ) and by Selwood ( 5 ), and with alternating current permeameters similar to that described by Broersma ( 23 ). Magnetic measurements make possible the measurement of the average crystallite size or the crystallite distribution and have the advantage of preserving the sample in the form of the original catalyst. Magnetic measurements are therefore suitable for in situ characterization of the catalyst.

Cahn ( 24 ) and Dietz ( 25 ) as discussed by Selwood ( 5 ) have shown how approximations of the average crystallite size may be obtained from the initial and final slope of the relative magnetization curve. At low field strengths or small values of  $( H / T )$ , the relative magnetization for a monodisperse system of ferromagnetic crystallites can be approximated by equation ( 2.9 )

$$M / M_{\infty} = M_{sp} V H / 3kT \quad 2.12$$

from which the volume,  $V$ , can be determined if  $M_{sp}$  is known. For a system with a distribution of volumes, the relative magnetization is then

$$M / M_{\infty} = ( M_{sp} H / 3 kT ) ( \sum_i n_i V_i^2 / \sum_i n_i V_i ) \quad 2.13$$

or

$$M / M_{\infty} = ( M_{sp} H / 3kT ) ( \overline{V^2} / \bar{V} ) \quad 2.14$$

from which the average volume is given by

$$( \overline{V^2} / \bar{V} ) = ( 3kT / M_{sp} H ) ( M / M_{\infty} ) \quad 2.15$$

At high field strengths or larger values of  $( H / T )$ , the system approaches saturation and the relative magnetization of a monodisperse system of ferromagnetic crystallites is approximated by

$$M / M_{\infty} = [ 1 - ( kT / M_{sp} V H ) ] \quad 2.16$$

For a system with a distribution of volumes, the relative magnetization then becomes

$$M / M_{\infty} = 1 - [ kT / M_{sp} H ( \sum_i n_i V_i / \sum_i n_i ) ] \quad 2.17$$

or

$$M / M_{\infty} = 1 - [ kT / M_{sp} H \bar{V} ] \quad 2.18$$

from which the average volume is

$$\bar{V} = [ kT / M_{sp} H ] [ 1 / ( 1 - [ M / M_{\infty} ] ) ] \quad 2.19$$

A measure of the dispersion can be made if the dispersion is defined as the positive square root of the sums of squares of the deviations divided by the number of crystallites, as for a normal distribution, that is

$$s = [ \sum_i ( \bar{v} - v_i )^2 / n ]^{1/2} \quad 2.20$$

which in terms of the values determined from equation ( 2.15 ) and ( 2.19 ) is approximately

$$s = [ ( \overline{v^2} / \bar{v} ) - \bar{v} ] [ \bar{v} ] \quad 2.21$$

for a large number of crystallites, n.

An alternate method for determining the average crystallite size and dispersion is based on the observation that the radial distribution function for many supported catalyst systems can be represented by a log-normal distribution function ( 26 ) such that

$$f_{\text{1nd}}( r ) = \frac{1}{2\pi r \text{LN}( s )} \text{EXP} \left( - \frac{1}{2} \left[ \frac{\text{LN}( r ) - \text{LN}( \bar{r} )}{\text{LN}( s )} \right]^2 \right) \quad 2.22$$

By noting that at low field strengths equation ( 2.13 ) can be written as

$$M / M_{\infty} = ( M_{\text{sp}}^H / 3kT ) ( 4\pi / 3 ) \int_0^{\infty} f_{\text{1nd}}( r ) r^3 dr \quad 2.23$$

or

$$M / M_{\infty} = ( 4\pi M_{sp} H / 9kT ) \bar{r}^3 \quad 2.24$$

from which

$$\bar{r}^3 = ( M / M_{\infty} ) ( 9kT / 4\pi M_{sp} H ) \quad 2.25$$

At high field strengths equation ( 2.17 ) can be written as

$$M / M_{\infty} = 1 - [ ( 3kT / 4\pi M_{sp} H ) \int_0^{\infty} f_{lnd}( r ) r^{-3} dr ] \quad 2.26$$

or

$$M / M_{\infty} = 1 - ( 3kT / 4\pi M_{sp} H ) \bar{r}^{-3} \quad 2.27$$

from which

$$\bar{r}^{-3} = [ 1 - ( M / M_{\infty} ) ] [ 4\pi M_{sp} H / 3 kT ] \quad 2.28$$

It is also noted that

$$\bar{r}^P = \int_0^{\infty} r^P f_{lnd}( r ) dr \quad 2.29$$

$$\bar{r}^P = \text{EXP}( p \text{LN}( \bar{r} ) + ( p^2 / 2 ) \text{LN}^2( s ) ) \quad 2.30$$

hence

$$\text{LN}( \bar{r}^3 ) = 3 \text{LN}( \bar{r} ) + ( 9 / 2 ) \text{LN}^2( s ) \quad 2.31$$

and

2.32

$$\text{LN}(\overline{r^{-3}}) = -3 \text{LN}(\overline{r}) + (9/2) \text{LN}^2(s)$$

Using experimental data to determine  $\overline{r^3}$  and  $\overline{r^{-3}}$  from equation ( 2.25 ) and ( 2.28 ), equations ( 2.31 ) and ( 2.32 ) can be solved simultaneously to yield  $\overline{r}$  and  $s$ .

Most methods previously proposed for determining crystallite size distributions depend upon achieving thermal equilibrium with the applied magnetic field. Weil ( 27, 28 ) however, suggested and used the decay of remance at different temperatures as described by equations ( 2.5 ) and ( 2.6 ) to determine crystallite size distributions. Weil's results were consistent with the averages determined by the previously mentioned magnetic methods. Luborsky and Lawrence ( 9 ) compared Weil's method with the average crystallite sizes obtained from the low field and the high field approximations and have found the results to be consistent. Luborsky ( 29 ) compared the crystallite sizes determined from electron micrographs, Weil's method, and magnetization curves with comparable results.

Only several other methods have been suggested for determining crystallite sizes and distributions. These include the assumption of a distribution function and calculating the resulting magnetization curve as done by Becker ( 8 ) and by Elmore ( 30 ), and the solution of a set of simultaneous equations via linear programming as done by Dreyer ( 31 ). Most of these

methods utilize relatively low magnetic field strength magnetization curves which are biased by the larger crystallites.

PROPOSED METHODS FOR DETERMINING CRYSTALLITE SIZE DISTRIBUTIONS

Two methods different from those discussed in the previous section will be presented in the present section as possible means of determining crystallite size distributions from magnetic data.

The first method consists of rewriting the integral in equation ( 2.8 ) as

$$M / M_{\infty} = \int_0^{\infty} L( M_{sp} V H / kT ) f( V ) dV \quad 2.33$$

for  $M_{sp}$  approximately independent of volume. Solution of this linear integral equation for the measured values of the relative magnetization as a function of magnetic field strength and temperature yields the volume distribution,  $f( V )$ .

Equation ( 2.33 ) can be approximated by

$$M / M_{\infty} = \sum_{i=1}^{\infty} L( M_{sp} V_i H / kT ) f( V_i ) \quad 2.34$$

A set of simultaneous linear equations can thus be written such that

$$\begin{aligned} ( M / M_{\infty} )_1 &= f_1 L_{11} + f_2 L_{21} + f_3 L_{31} + \dots \\ ( M / M_{\infty} )_2 &= f_1 L_{12} + f_2 L_{22} + f_3 L_{32} + \dots \\ ( M / M_{\infty} )_3 &= f_1 L_{13} + f_2 L_{23} + f_3 L_{33} + \dots \\ &\vdots \end{aligned} \quad 2.35$$

where

$$f_i = f( V_i ) \quad 2.36$$

$$L_{ij} = L( M_{sp} V_i [ H / T ]_j / k ) \quad 2.37$$

Equations ( 2.35 ) may be solved using standard matrix solution techniques to yield the  $f( V_i )$  for the experimentally measured values of  $( M / M_\infty )$  as a function of  $( H / T )$ .

A second method starts with the definition of the variables

$$\beta = ( H / T ) \quad 2.38$$

$$\beta' = \beta \pi / \beta_{max} \quad 2.39$$

$$V' = V \pi / V_{max} \quad 2.40$$

so that equation ( 2.33 ) may be rewritten as

$$M / M_\infty = \int_0^{V_{max}} L( M_{sp} V \beta / k ) f( V ) dV \quad 2.41$$

or as

$$M / M_\infty = \int_0^\pi L( M_{sp} V' V_{max} \beta' \beta_{max} / \pi^2 k ) f_2( V' ) dV' \quad 2.42$$

The next step is to rewrite the kernel of the integral in equation ( 2.42 ) as the double Fourier series

$$L = \sum_{i=1}^{\infty} \sum_{j=1}^{\infty} W( i, j ) \text{SIN}( i \beta' ) \text{SIN}( j V' ) \quad 2.43$$

where

$$W( i, j ) = \frac{1}{\pi^2} \int_{-\pi}^{\pi} \int_{-\pi}^{\pi} L \text{ SIN}( i\beta' ) \text{ SIN}( jv' ) dv' d\beta' \quad 2.44$$

which can be determined since the function L is known. Using equation ( 2.43 ) in equation ( 2.42 ) yields

$$M / M_{\infty} = \int_0^{\pi} f_2( v' ) \sum_{i=1}^{\infty} \sum_{j=1}^{\infty} W( i, j ) \text{ SIN}( i\beta' ) \text{ SIN}( jv' ) dv' \quad 2.45$$

or

$$M / M_{\infty} = \sum_{i=1}^{\infty} \sum_{j=1}^{\infty} W( i, j ) W_2( j ) \text{ SIN}( i\beta' ) \quad 2.46$$

where the

$$W_2( j ) = \int_0^{\pi} f_2( v' ) \text{ SIN}( jv' ) dv' \quad 2.47$$

By noting that

$$W_3( i ) = \sum_{j=1}^{\infty} W( i, j ) W_2( j ) \quad 2.48$$

is equivalent to a matrix product, then equation ( 2.46 ) may be rewritten as the Fourier series

$$M / M_{\infty} = \sum_{i=1}^{\infty} W_3( i ) \text{ SIN}( i\beta' ) \quad 2.49$$

where the  $W_3( i )$  are determined from

$$W_3( i ) = \frac{1}{\pi} \int_{-\pi}^{\pi} [ M / M_{\infty} ] \text{SIN}( i\beta' ) d\beta' \quad 2.50$$

Since the  $W( i, j )$  are found from the Langevin function and equation ( 2.44 ), and the  $W_3( i )$  from experimental data by means of equation ( 2.50 ), then the  $W_2( j )$  may be calculated from equation ( 2.48 ) by a suitable matrix method. The crystallite size distribution is then given by

$$f_2( V' ) = \frac{1}{\pi} \sum_{j=1}^{\infty} W_2( j ) \text{SIN}( jV' ) \quad 2.51$$

The distribution  $f( V )$  can be easily obtained by an appropriate change of scale.

Both of these methods were tested on a digital computer (IBM 360, using FORTRAN IV G ) using relative magnetization data calculated from given crystallite size distributions. From the results, the ability of each method to determine the given distribution was assessed.

The first method, which will be referred to as the direct matrix method, was found to be generally unacceptable for determining crystallite distributions from experimental data. For arrays large enough to obtain an adequate description of the distribution, the problem of digital round-off accumulation usually encountered in matrix type solutions became significant and for arrays small enough to overcome this problem, the solution approximation of the original distribution was not satisfactory.

It was also noted that the required accuracy of the magnetization data was greater than could be expected from the experimental data.

The second method, which will be referred to as the Fourier integral method, yielded more acceptable results on the test cases. The main limitation of this method was the accurate calculation of the Fourier coefficients of the Langevin function given by equation ( 2.44 ). Once this difficulty was minimized, the results were representative of the test distributions. Figures 2.2 and 2.3 are examples of results computed from relative magnetization data which was calculated from the given distributions. Five coefficients were used in each of these cases. The results of the use of such a relatively small number of coefficients was the difficulty of representing distributions with maxima near the end of the interval under consideration as demonstrated by Figure 2.3. This however can be overcome by the use of more coefficients or by changing the interval under consideration.

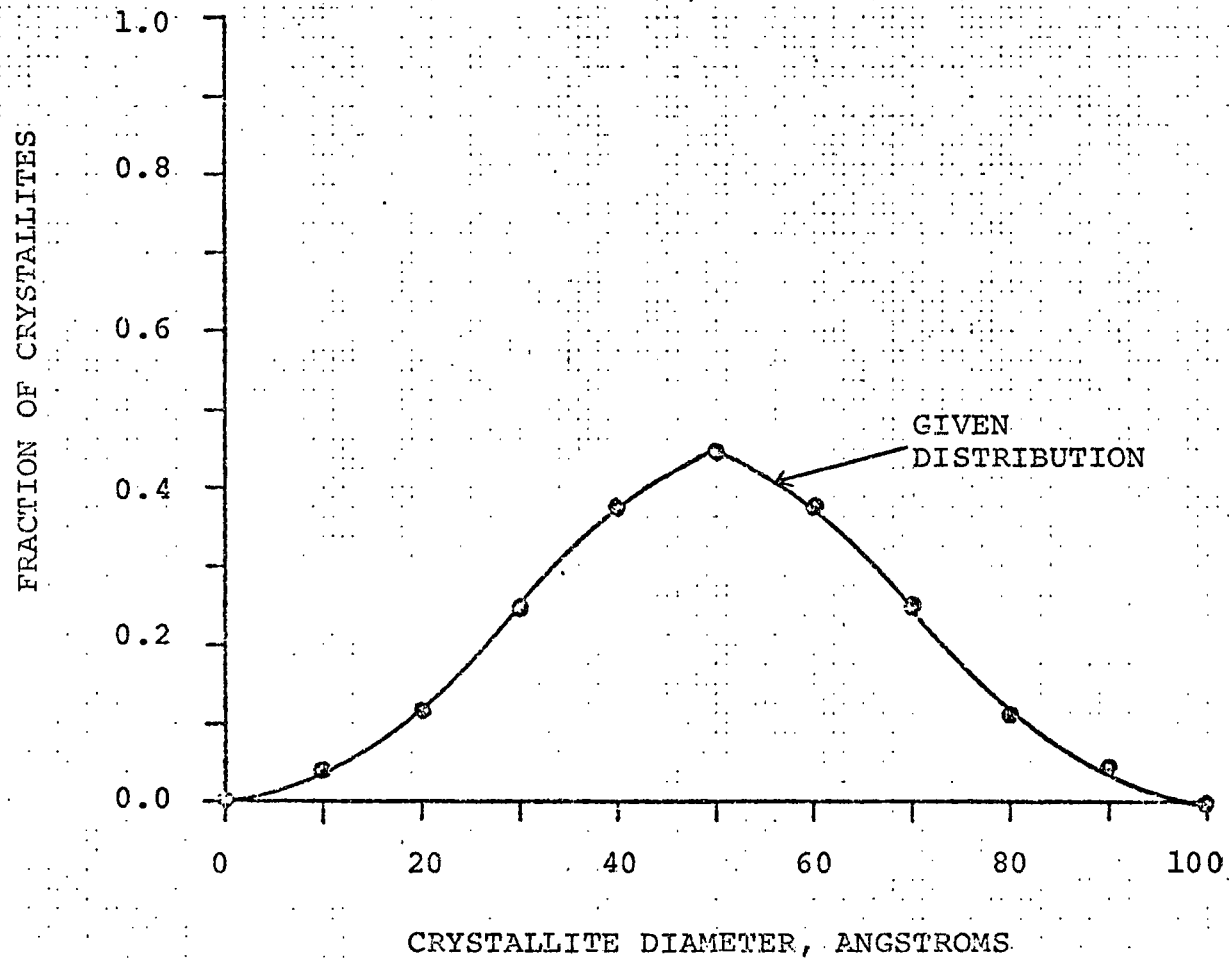


FIGURE 2.2 EXAMPLE OF RESULTS OF FOURIER INTEGRAL METHOD ( ● ) FOR DETERMINING CRYSTALLITE DISTRIBUTION FROM RELATIVE MAGNETIZATION CURVE CALCULATED FROM GIVEN DISTRIBUTION.

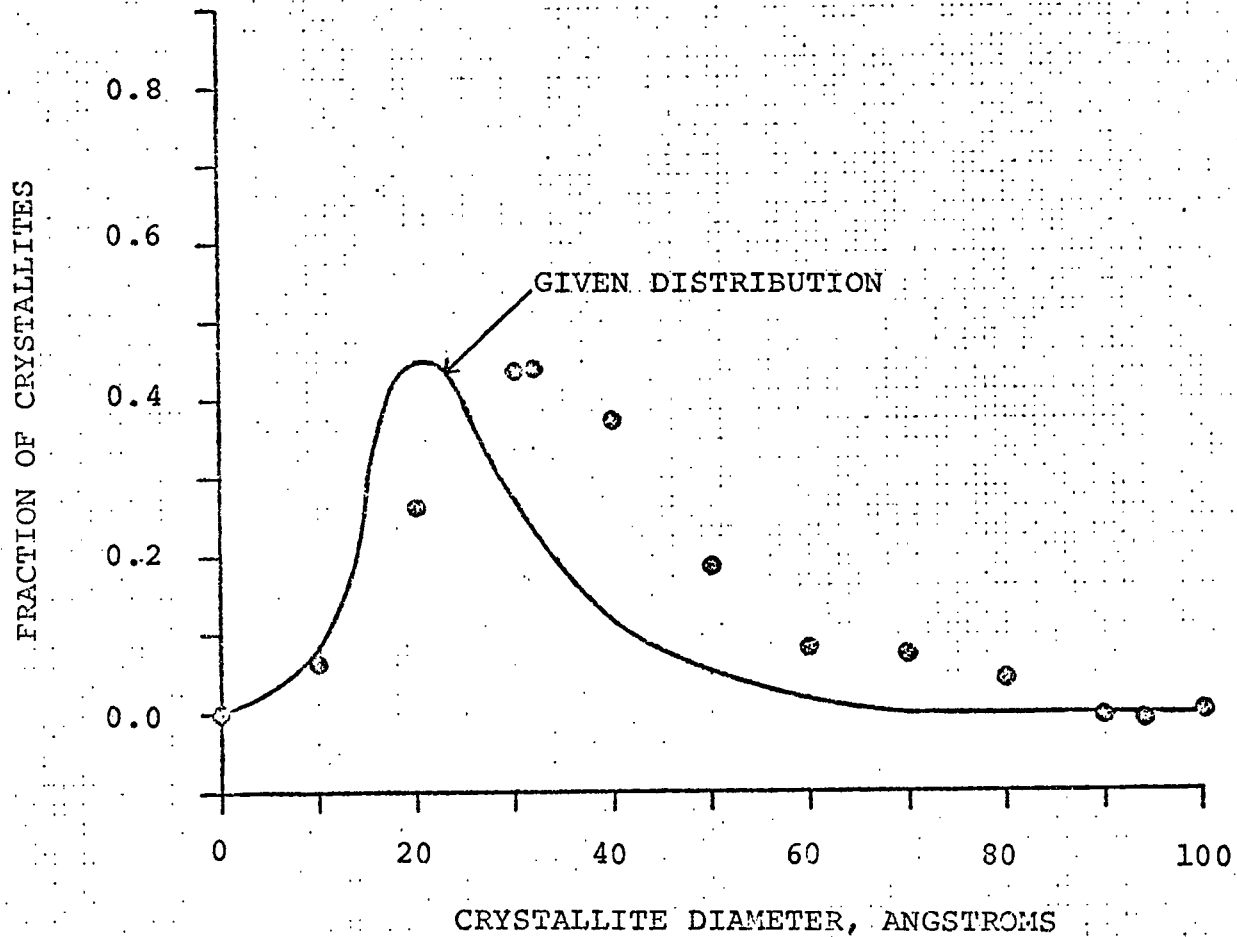


FIGURE 2.3 EXAMPLE OF RESULTS OF FOURIER INTEGRAL METHOD ( • ) FOR DETERMINING CRYSTALLITE DISTRIBUTION FROM RELATIVE MAGNETIZATION CURVE CALCULATED FROM GIVEN DISTRIBUTION.

## CHAPTER III

### EXPERIMENTAL EQUIPMENT AND PROCEDURE

#### HIGH FIELD STRENGTH SYSTEM

A permeameter similar to the direct current permeameters described by Barnett ( 22 ) was chosen as the flux measuring device due to its simplicity, ease of construction, and sensitivity. It is known from elementary electromagnetic theory, that if a solenoid is placed in a region of uniform magnetic field, that a given quantity of magnetic flux traverses the area of the solenoid. If the quantity of flux is suddenly changed, say by the introduction of a material into the solenoid with a susceptibility different than the material originally in the solenoid, then an emf is produced in the windings of the solenoid which is proportional to the difference in susceptibility of the two materials. Similarly, if the second material is suddenly removed and the original material replaced, then an emf of opposite polarity is produced. If two similar oppositely wound solenoids are connected in series and a material originally in one solenoid is moved into the second one, an emf twice the magnitude of one solenoid is produced.

The magnetic field used in this study for the measurements in the 0 - 100,000 oersted range was produced by a superconducting magnet which has been described elsewhere ( 32 ). The superconducting magnet was powered by a factory calibrated direct current

power supply which had an output ripple of less than 50 millivolts ( Magnion Incorporated, CF-100 ). The magnet provided a working volume ( uniformity of field better than 5 percent ) which was 5.08 centimeters in diameter with a minimum length of five centimeters and a maximum length of 7.6 centimeters. A gaussmeter ( F. W. Bell Incorporated Model 620 ) was used to verify the field strength and uniformity. The measured uniformity of the field over the length of the measuring coils was within 3 percent of the set field strength.

The measuring coils used in this study consisted of two opposingly wound solenoids connected in series. Each solenoid was two ( 2 ) centimeters long and consisted of three ( 3 ) layers of #36 Heavy Formvar insulated wire ( Alpha Wire Corporation ) with a total of 380 turns per solenoid. The two solenoids and 30 centimeters of leads were made of one continuous piece of wire ( total resistance at 25 degrees Centigrade was 58.1 ohms ) and were wound two ( 2 ) centimeters apart on a brass tube machined from brass rod ( A.S.T.M. B36 ) such that the internal diameter of the solenoids was 1.650 centimeters. The internal diameter of the brass tube was 1.300 centimeters. Plexiglass alignment plates were attached to the ends of the brass tube and a support consisting of one 0.635 centimeter aluminum rod ( A.S.T.M. B211 ) was attached to one plexiglass plate so that the measuring coils could be suspended in the center of the superconducting solenoid's work space. The coil arrangement has

been used before to make magnetic measurements as a means of eliminating magnetic field variations ( 5 ). Also, if the same material which is in the second solenoid before the sample is moved is also in the first solenoid after the sample is moved, then the flux change will be due to the sample only and not the change relative to a second material as in single solenoid systems ( 22 ). The measuring coil and sample arrangement are shown in Figure 3.1.

The movement of the sample from one solenoid into the other produces a voltage across the measuring coils, which according to Faraday's law is

$$E = C_3 ( d\Phi / dt ) \quad 3.1$$

or

$$E ( dt ) = C_3 [ NAC_4 ( dB ) ] \quad 3.2$$

where  $C_4$  is a coil constant. Integrating over the time and the distance that the sample moves yields

$$\int_0^t E dt = C_5 \int_0^1 [ d( H + 4\pi M ) ] \quad 3.3$$

that is

$$M = C_6 \int_0^t E dt \quad 3.4$$

or

$$\sigma = C_7 \int_0^t E dt \quad 3.5$$

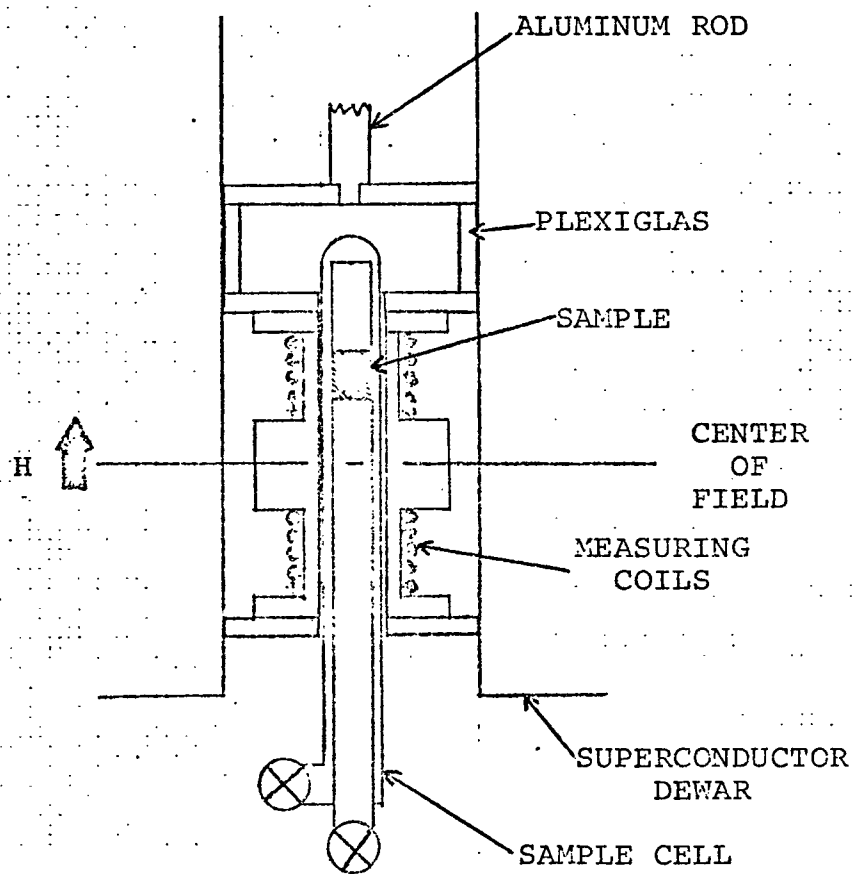


FIGURE 3.1 GENERAL ARRANGEMENT OF SUPERCONDUCTING MAGNET, MEASURING COILS, SAMPLE CELL AND SAMPLE USED FOR HIGH MAGNETIC FIELD MAGNETIZATION MEASUREMENTS.

The voltage as a function of time was measured using an oscilloscope ( Hewlett-Packard Model 1200A Dual Trace ) and recorded on film ( Polaroid Type 107 ) with an oscilloscope camera ( Hewlett-Packard Model 198A ). The recorded signal could then be integrated using any available methods. By use of a calibration standard, such as bulk nickel, the constants  $C_6$  and  $C_7$  could be determined from the experimental data.

The sample cell was a 13 millimeter outside diameter ( 10.6 millimeters inside diameter ) Vycor tube which was sealed at one end and inside of which was a concentric tube of 9 millimeter outside diameter ( 7 millimeters inside diameter ) Vycor tubing. Each tube was sealed at one end of the cell with high vacuum grade stopcocks (Kontes KG-151 ) connected by 14/35 standard taper joints.

The sample cell was held by a plexiglas clamp which was mechanically connected to a piston. The sample cell was moved by the pneumatically operated piston with oscilloscope timing accomplished by a pneumatic switch.

#### LOW FIELD STRENGTH SYSTEM

Low magnetic field strengths ( up to 8000 oersteds ) were obtained with a Faraday system which has been described previously ( 33 ). Data from the Faraday system was compared with the high field system for consistency and as a calibration verification.

### Q-METER SYSTEM

The quantity of reduced nickel in the samples was measured using a Q-meter method described by Richardson ( 34 ). The Q-meter is essentially an RLC circuit, as shown in Figure 3.2, where the Q of the system is

$$Q_{\max} = 1 / 2\pi\nu R C \quad 3.6$$

if  $\nu$  is the natural resonance frequency of the circuit. The introduction of a material into the inductor of the circuit changes the resonance properties. Richardson ( 34 ) has noted that the change in frequency or capacitance necessary to re-establish resonance is linearly dependent upon the mass of material that is introduced into the inductor. By calibrating the Q-meter with known quantities of nickel, the instrument was then used to determine the mass of reduced nickel in the samples. The Q-meter was a Boonton type 260A.

### SAMPLE PREPARATION-SURFACE AREA SYSTEM

Samples were prepared and surface areas were measured by hydrogen chemisorption using the system shown schematically in Figure 3.3. All fittings downstream of the metering valves were 1/4 inch brass Swagelok. The shutoff valves were brass vacuum grade bellows valves ( Nupro-4BK ). Metering valves were made of 316 stainless steel ( Nupro-4M ). All tubing was 1/4 inch outside diameter copper tubing. The sample cell connector was an adapter tee from 1/4 inch tubing ( Swagelok ) to 10 millimeter

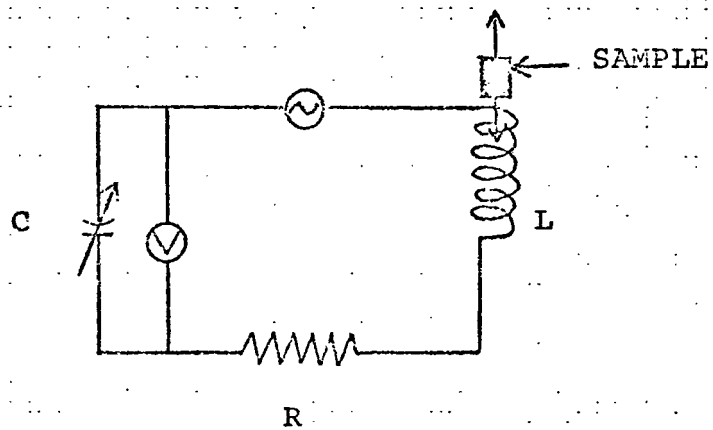


FIGURE 3.2 RLC CIRCUIT OF Q-METER USED TO MEASURE NICKEL CONCENTRATION.

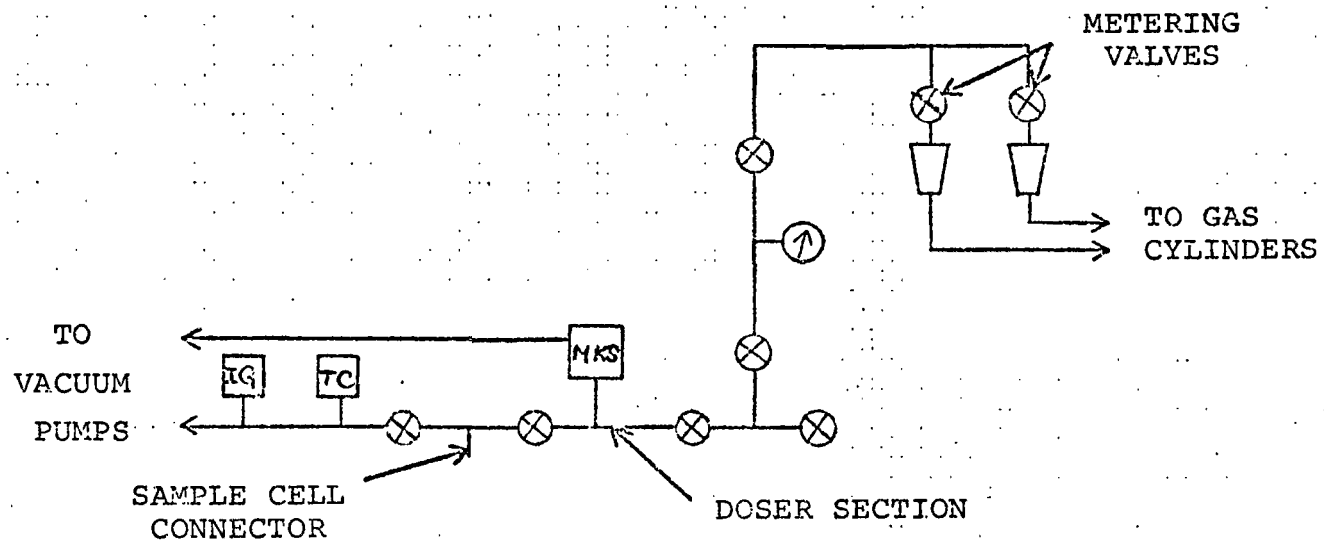


FIGURE 3.3 SCHEMATIC DIAGRAM OF SAMPLE PREPARATION AND SURFACE AREA APPARATUS.

tubing ( CAJON ) using a Viton O-ring for a seal on the sample cell. The rotameters were Brooks Instrument Company Type 2-1355-V ( Hydrogen: Serial Number 6312-58410 ; Helium: Serial Number 6312-58409 ). Vacuum was produced by a fore pump (Welch Duo-Seal Model 1402, Serial Number 42283 ) and a diffusion pump ( NRC Equipment Company Type 0148 using silicon pump oil ). The vacuum was monitored above  $10^{-3}$  torr with a thermocouple ( TC ) gage ( Veeco Model TG-7 ) and below  $10^{-3}$  torr with an ionization gage ( IG ) ( Veeco Model RG-81 ). The quantity of gas chemisorbed was determined by measuring the pressure in the calibrated doser volume before dosing the sample and the pressure in the doser-cell volume after dosing. For this purpose a differential pressure capacitive manometer ( MKS Baratron Type 144E-300, Serial Number J4664 ) was used with the vacuum as reference pressure. Calibration of the doser was performed by expansion of low pressure helium from the doser into a known cell volume. Measurement of cell and sample dead volume was similarly accomplished by helium expansion.

Cylinder helium ( IWECO of Union Carbide, 99.99% purity ) was passed through drying beds of silica gel ( Davidson Chemical Company ) and molecular sieves ( Davidson 13A ) before entering the rotameters. Cylinder hydrogen ( IWECO of Union Carbide, 99.9% purity ) was passed through a Deoxo unit ( Englehard Industries ) to remove trace quantities of oxygen and then through drying beds similar to those used for the helium.

The system was also equipped with temperature control apparatus for reduction and cleaning purposes. The controller was a Barber-Coleman 530 Series using a type K thermocouple. The control point was at the surface of the sample cell, however prior comparison of the thermocouple-controller arrangement against a calibrated thermocouple inside the cell under flow conditions allowed the temperature of the sample to be controlled to within five ( 5 ) degrees Centigrade.

#### EXPERIMENTAL PROCEDURE

The samples used in this study were commercial catalysts obtained in 1/8 inch by 1/8 inch pellet form. The catalysts were first crushed and screened to the 0.354-0.595 millimeter range. Samples of each catalyst could then be used for several different experiments. A nickel standard was prepared by mixing nickel powder ( Fischer N40 ) into a silica paste ( Cabot Corporation Cab-O-Sil HS-5 and water ), drying at 150 degrees Centigrade for 48 hours, crushing, screening and mixing. This resulted in a 33.78 weight percent nickel mixture.

Weight loss measurements were made by weighing the sample on a recording electrobalance ( Cahn #2000 RG Electrobalance ) while heating the sample in flowing helium at 175 degrees Centigrade. This allowed calculations to be based on the dry catalyst weight.

The samples for the high field magnetic measurements were generally loaded with sufficient catalyst to give between 1-1.5

centimeters of bed length in the inner tube of the cell. Glass or quartz wool was used as a packing material on both ends of the bed such that when the sample was in the region of one measuring coil the other coil contained a part of the sample cell filled with the packing. The sample cell was then positioned in the sample cell connector of the surface area system and evacuated to about  $50 \times 10^{-3}$  torr with the fore pump. The cell pressure was increased to atmospheric with helium and helium was then allowed to flow at 3 cubic centimeters per minute for 15 minutes. The sample was then heated to 150 degrees Centigrade until indications of physically adsorbed water were out of the cell. The temperature of the sample was then increased to the reduction temperature at approximately 5 degrees Centigrade per minute. At 50 degrees Centigrade less than the reduction temperature, a hydrogen flow of 3-5 cubic centimeters per minute was started and the helium flow stopped. The sample was left to reduce for the specific time, after which it was evacuated to at least  $40 \times 10^{-3}$  torr at the reduction temperature, filled to atmospheric pressure with helium and then cooled to ambient temperature.

The high magnetic field and the Q-meter measurements were made after the samples were prepared. The gaussmeter probe was inserted into the measuring coil tube, and the desired field set. After the superconductor's field stabilized, the gaussmeter reading was noted. Each sample in turn was clamped into position

and allowed to come to equilibrium with the field. After recording the signal and other data for each sample, the gaussmeter was reinserted and the field strength and uniformity remeasured. The magnetic field strength was increased and the above sequence repeated.

Surface areas could be measured on the same samples and in the same cells used for the high field measurements. However, surface areas were generally measured on different samples of the catalyst in surface area cells consisting of a single segment of 10 millimeter glass tubing with a high vacuum fitting and plug ( CAJON 6UT-6 ) on one end. This allowed a lower dead volume with increased accuracy. The same reduction procedure as used for the high magnetic field measurements was generally followed using approximately one gram of catalyst. However, after the reduction, evacuation at the reduction temperature was to about  $10^{-5}$  torr. The sample was then cooled to ambient temperature and doses of hydrogen were admitted to the cell until sufficient isotherm data was obtained. The cell was then reevacuated and the dead volume measured using helium expansion.

## CHAPTER IV

### EXPERIMENTAL DATA AND RESULTS

A total of thirteen samples were prepared for use in this study. Sample preparation data are given in Table 4.1. The weights given in Table 4.1 are those of the dried catalysts. Of the thirteen samples, nine were the same catalyst prepared at different reduction temperatures for varying lengths of time in order to study the effect of those variables on the crystallite size distribution.

Figure 4.1 is a photograph of a typical oscilloscope trace. The voltage scale of the oscilloscope ranged from 0.5 to 2.0 millivolts per division while the time scale was usually set at 20 milliseconds per division. Usually two traces were recorded for each sample at each field strength but for various samples at different field strengths, several traces were recorded and analyzed. These indicated the experimental deviation in determining the integrals of the signal was approximately  $\pm 3$  percent. The voltage integrals were plotted versus  $(H / T)$  as shown in Figure 4.2 for samples 1 and 3. The experimental data of this form for the other samples is given in Appendix B. Plots of  $(1 / H^2)$  for bulk nickel and  $(1 / H)$  and  $(1 / H^{0.9})$ , as suggested by equations ( 2.3 ) and ( 2.11 ), for the dispersed nickel were made to determine the appropriate ranges, if any, over which straight line extrapolations could be made. These

TABLE 4.1 SAMPLE PREPARATION DATA.

SAMPLE NUMBER	CATALYST (SUPPORT)	SAMPLE WEIGHT, GRAMS	NOMINAL PERCENT NICKEL	REDUCTION TEMPERATURE, DEGREES CENTIGRADE	REDUCTION TIME, HOURS	ADDITIONAL TREATMENT
1 <sup>(1)</sup>	NICKEL (SILICA)	0.2717	33.8	350	12	NONE
2	GIRDLER T-1233RS	0.5410	60.0	350	12	NONE
3	C (KIESELGUHR)	0.3082	40.0	350	12	NONE
4 <sup>(1)</sup>	NICKEL (SILICA)	0.3377	33.8	350	12	NONE
5	A (ALUMINA)	0.4939	75.0	350	12	NONE
6	A (ALUMINA)	0.3791	75.0	350	36	NONE
7	A (ALUMINA)	0.4144	75.0	350	72	NONE
8	A (ALUMINA)	0.4317	75.0	450	12	NONE
9	A (ALUMINA)	0.4292	75.0	450	48	NONE
10	A (ALUMINA)	0.3569	75.0	600	12	NONE
11	A (ALUMINA)	0.4273	75.0	600	24	NONE
12	A (ALUMINA)	0.4939	75.0	350	12	500°C, 12 HOURS IN HELIUM
13	A (ALUMINA)	0.3772	75.0	350	12	800°C, 12 HOURS IN HELIUM

1) USED AS CALIBRATION STANDARD, ASSUMED ALL NICKEL WAS REDUCED

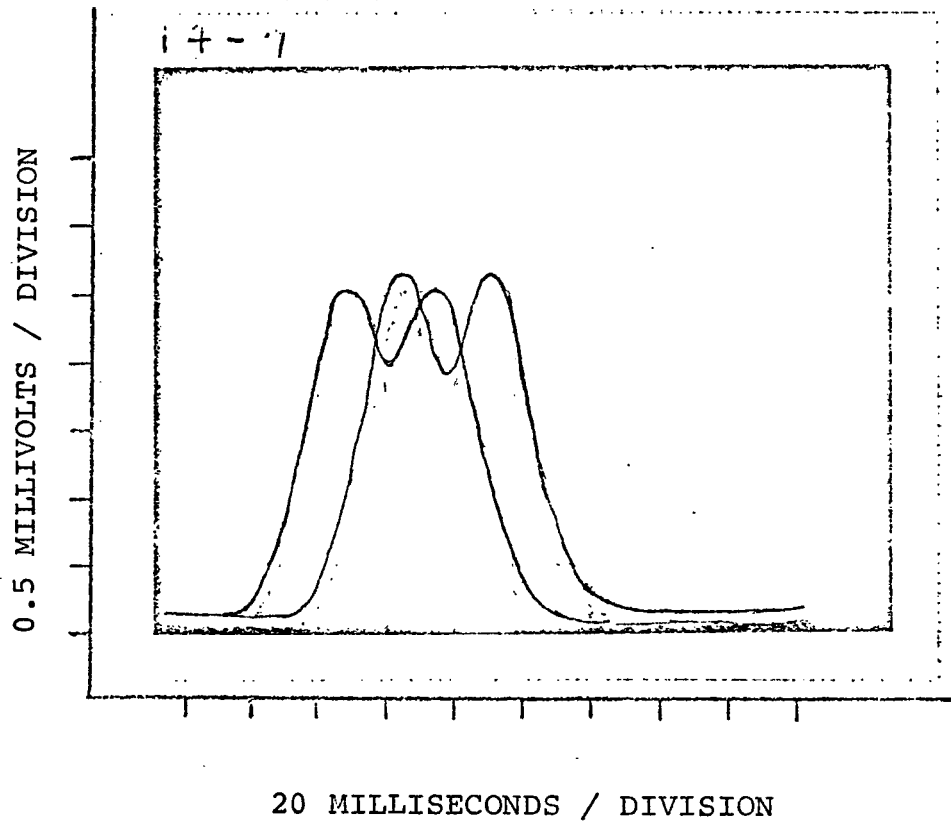


FIGURE 4.1 TYPICAL EXPERIMENTAL SIGNALS FROM HIGH FIELD SYSTEM. TWO SIGNALS (OFFSET) DEMONSTRATE REPRODUCIBILITY. SAMPLE 12 AT 15.5 KILO-OERSTEDS.

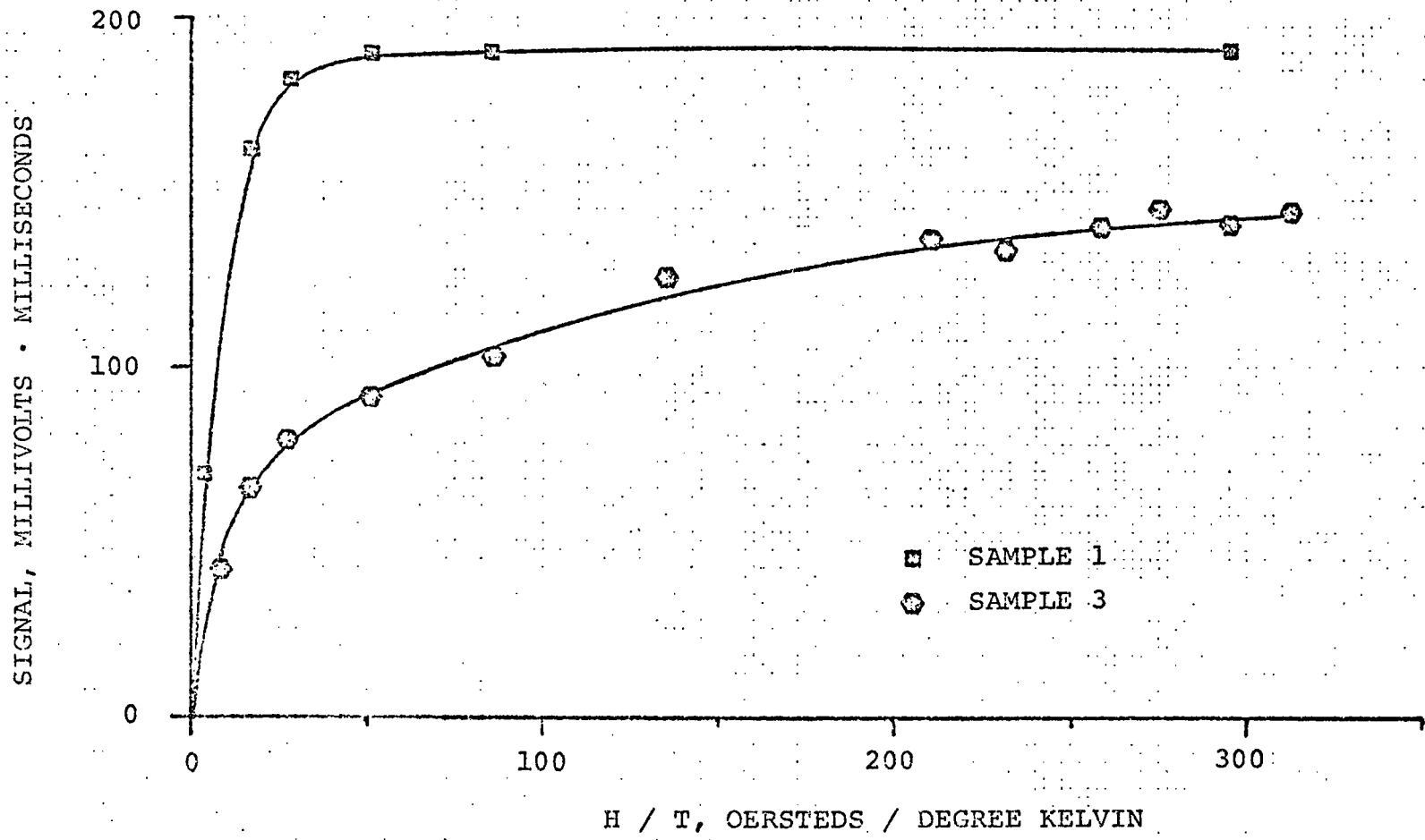


FIGURE 4.2 EXPERIMENTAL DATA FROM HIGH FIELD MEASUREMENTS FOR SAMPLE 1 (BULK NICKEL) AND SAMPLE 3 AT 295 DEGREES KELVIN

plots are shown for samples 1 and 3 in Figure 4.3 to 4.5. A linear least squares program was then used to find the zero intercepts which are the signals at magnetic saturation given in Table 4.2. These values were used to determine the relative magnetization as a function of  $(H / T)$  as shown in Figure 4.6 to 4.11. From these data, the low and high field strength approximations of the average crystallite size were calculated from equations ( 2.15 ) and ( 2.19 ) and the log-normal average size was calculated from equation ( 2.31 ) and ( 2.32 ). The measures of dispersion were calculated from equation ( 2.21 ) and from equations ( 2.31 ) and ( 2.32 ). These values are given in Table 4.3.

The weight percent reduced nickel was calculated from the Q-meter measurements and where used with the saturation signal and the calibration constant  $C_7$  ( $C_7 = 2.50 \times 10^{-2}$ ) to determine the specific magnetization at saturation,  $\sigma_{\infty}$ . These values are also given in Table 4.2.

The experimental relative magnetization data was used as input to a computer program ( see Appendix C ) which approximated the crystallite size distribution using the Fourier integral method. The results of the computations are given in Figures 4.12 and 4.20. Due to the results on the test cases, it was decided not to use the direct matrix method.

The relative magnetization data demonstrate that the samples exhibited superparamagnetic behavior over the magnetic field strengths investigated. It is also noted from Figures 4.4 and

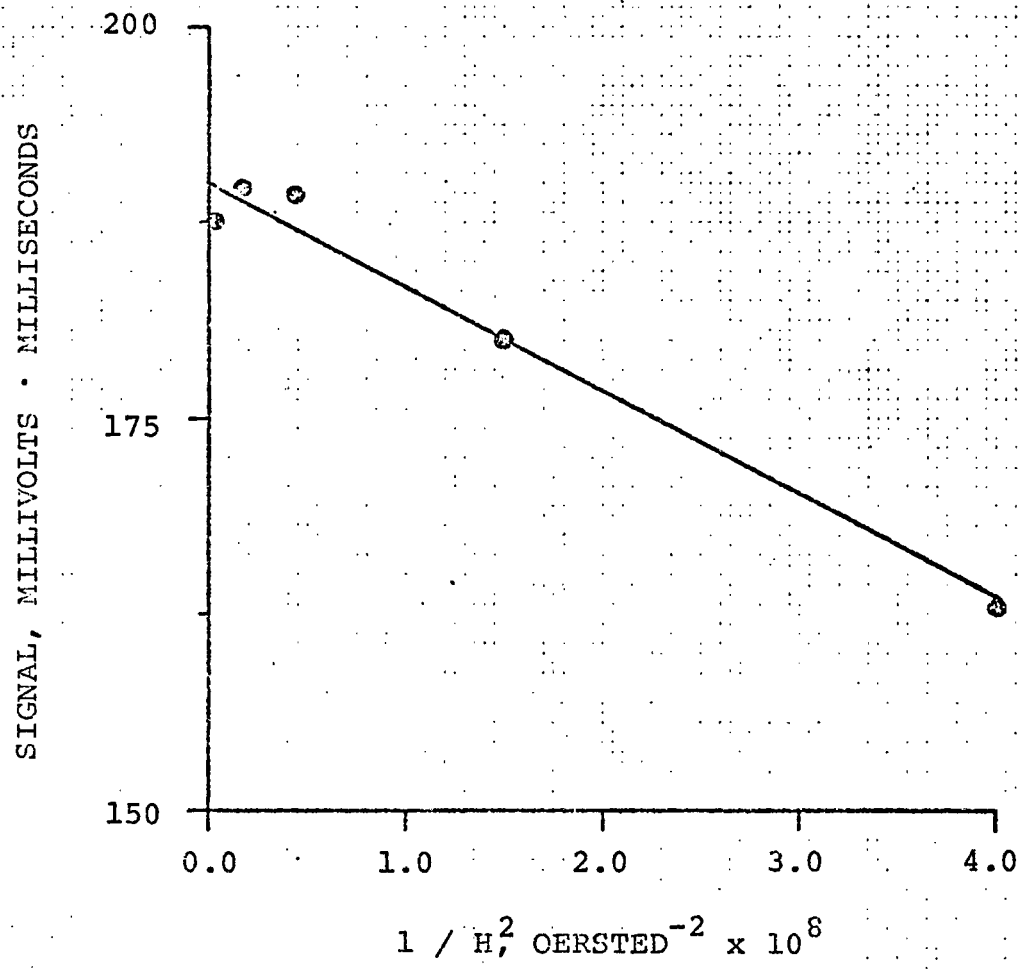


FIGURE 4.3 EXPERIMENTAL DATA FOR OBTAINING SIGNAL AT SATURATION FOR SAMPLE 1 (BULK NICKEL) AT 295 DEGREES KELVIN.

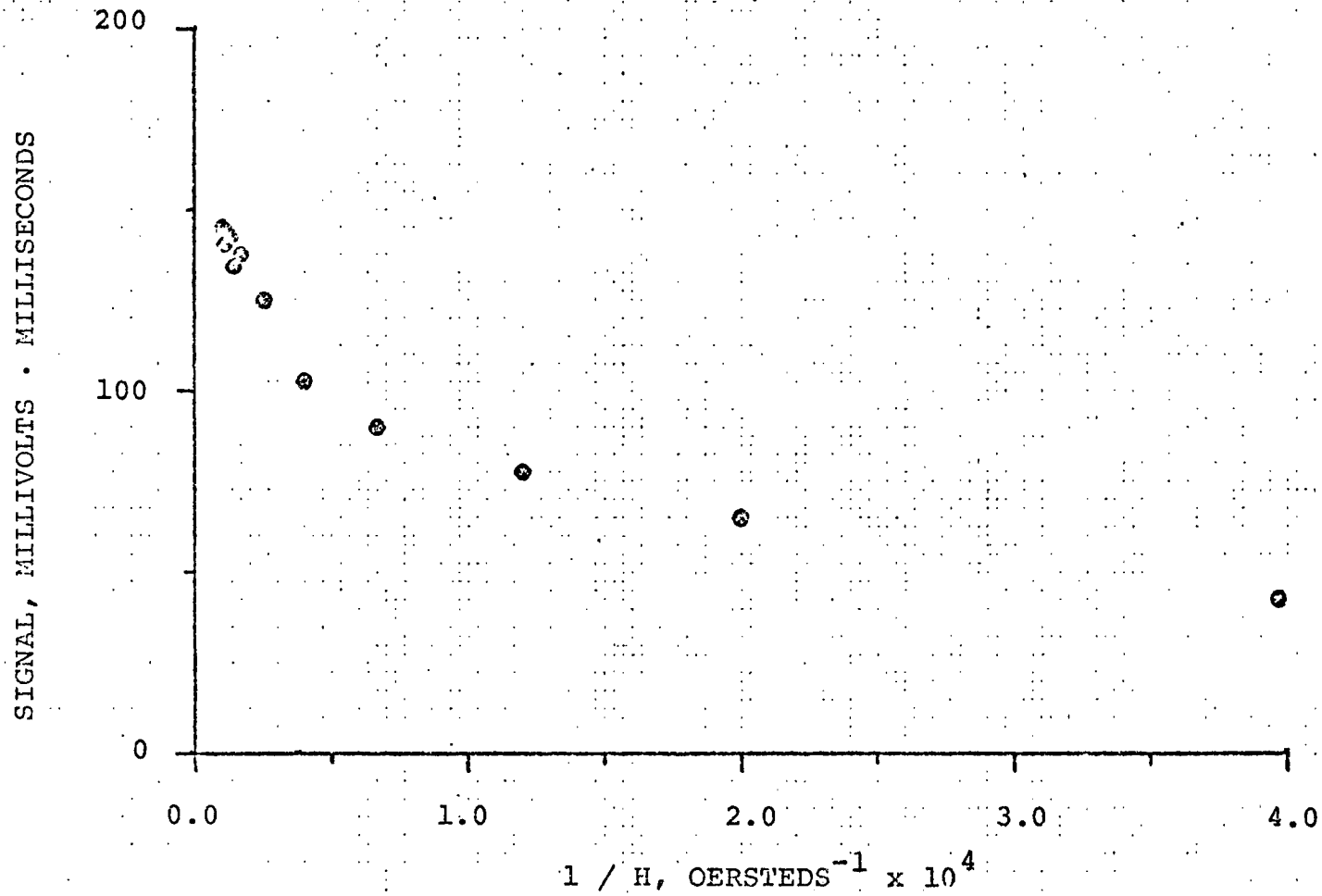


FIGURE 4.4 EXPERIMENTAL DATA FOR OBTAINING SIGNAL AT SATURATION FOR SAMPLE 3 AT 295 DEGREES KELVIN.

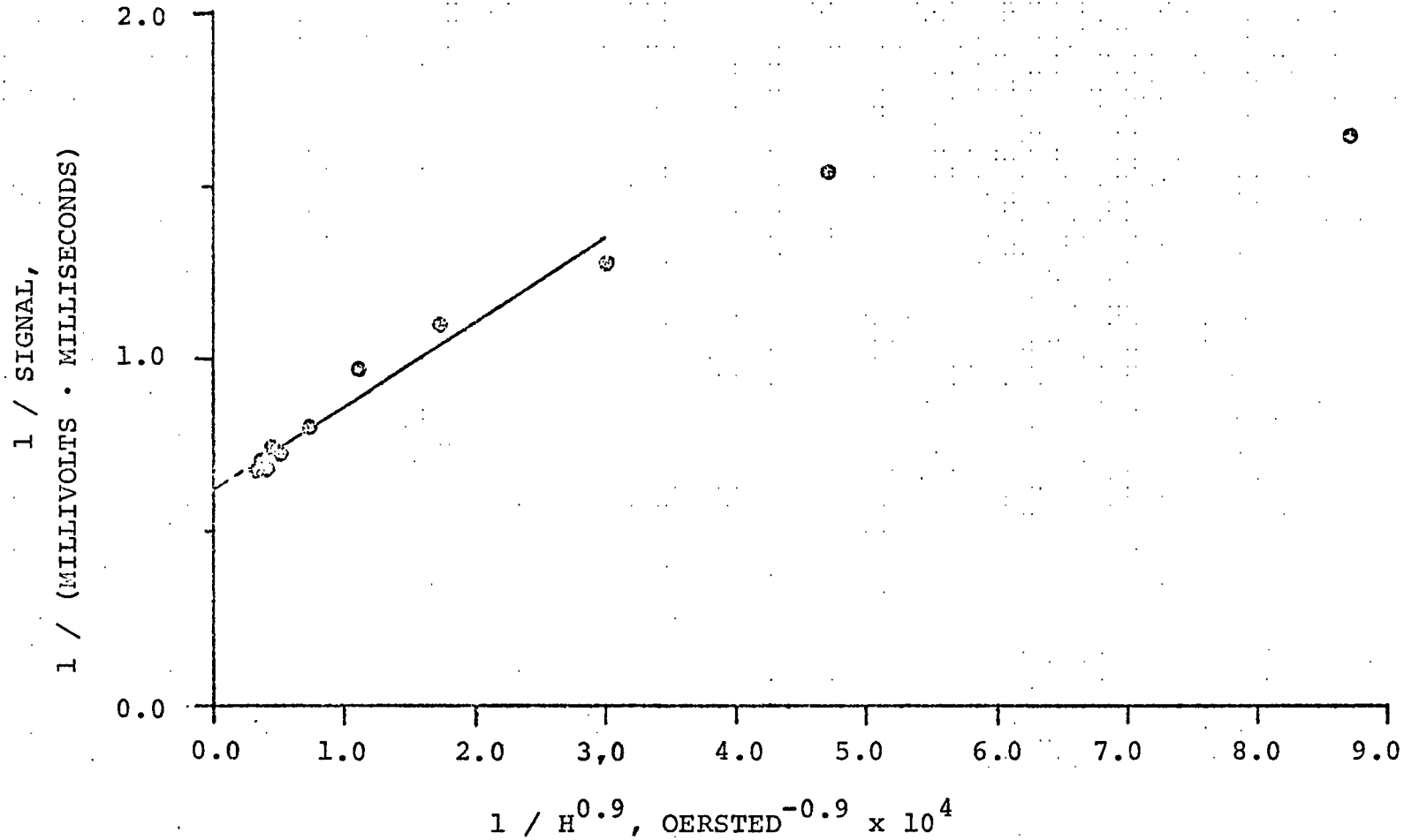


FIGURE 4.5 EXPERIMENTAL DATA FOR OBTAINING SIGNAL AT SATURATION FOR SAMPLE 3 AT 295 DEGREES KELVIN.

and 4.5, that unless magnetic field strengths in excess of 20 kilo-oersteds are used near 300 degrees Kelvin, that extrapolation to infinite field strength will yield saturation magnetization values considerably smaller than those obtained by obtaining data at larger field strengths. The saturation specific magnetizations given in Table 4.2 do not exhibit any significant variation and are an average of 3 percent lower than the bulk value, due possibly to low values of the extrapolated saturation signal.

The approximation of the crystallite distributions given in Figures 4.12 to 4.20 give at least a qualitative estimate of the shape of the crystallite distribution. These results should be interpreted with the understanding that Figures 4.12 to 4.20 are attempts to approximate the crystallite size distribution with a truncated Fourier series. Hence, Figure 4.14 for sample 5 would appear to be the results expected from representing a function similar to an impulse function by a Fourier series. Therefore it is suspected that sample 5 has a relatively narrow crystallite size distribution with a maxima at approximately 50 Angstroms. Figures 4.15 and 4.16 for samples 6 and 7 show that reducing the catalyst at the same temperature ( 350 degrees Centigrade ) for longer periods of time causes the increase in the relative number of both large and small crystallites with essentially no change in the crystallite diameter at which the maxima occurs. This is in agreement with the average crystallite

Sizes given in Table 4.3. No attempt to estimate the crystallite size distribution from the Fourier approximation was made at this stage of the development of the method. However, familiarity with Fourier series representations make the estimation of the distribution possible until further development of the method is tested for better results. The Fourier representation and the estimated distribution can then be used to calculate the magnetization curves and the average crystallite sizes for comparison with the experimental values as a means of assessing their ability to approximate the actual distribution.

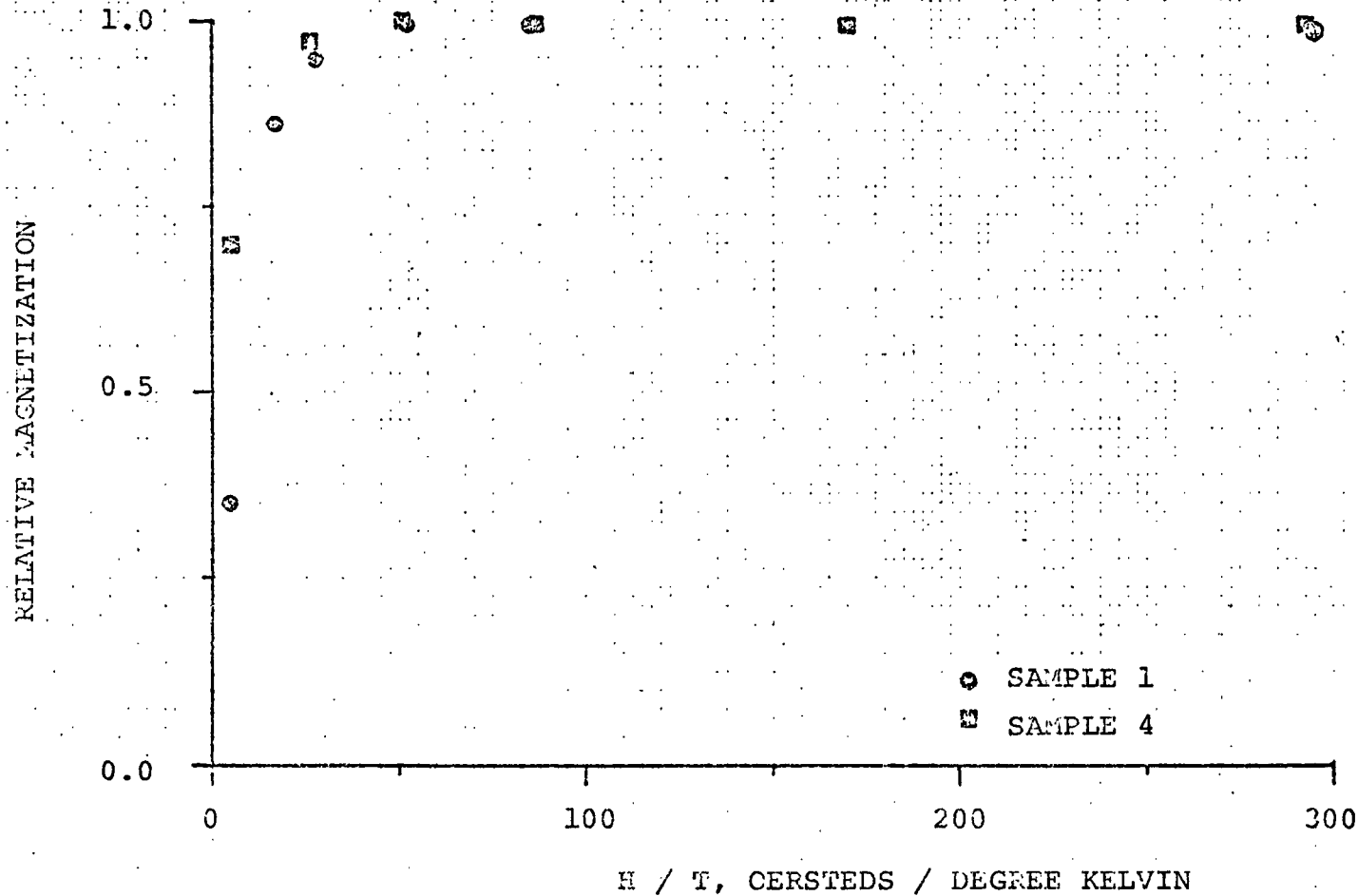


FIGURE 4.6. EXPERIMENTALLY DETERMINED RELATIVE MAGNETIZATION VERSUS H / T FOR SAMPLES 1 AND 4 (BULK NICKEL) AT 295 DEGREES KELVIN

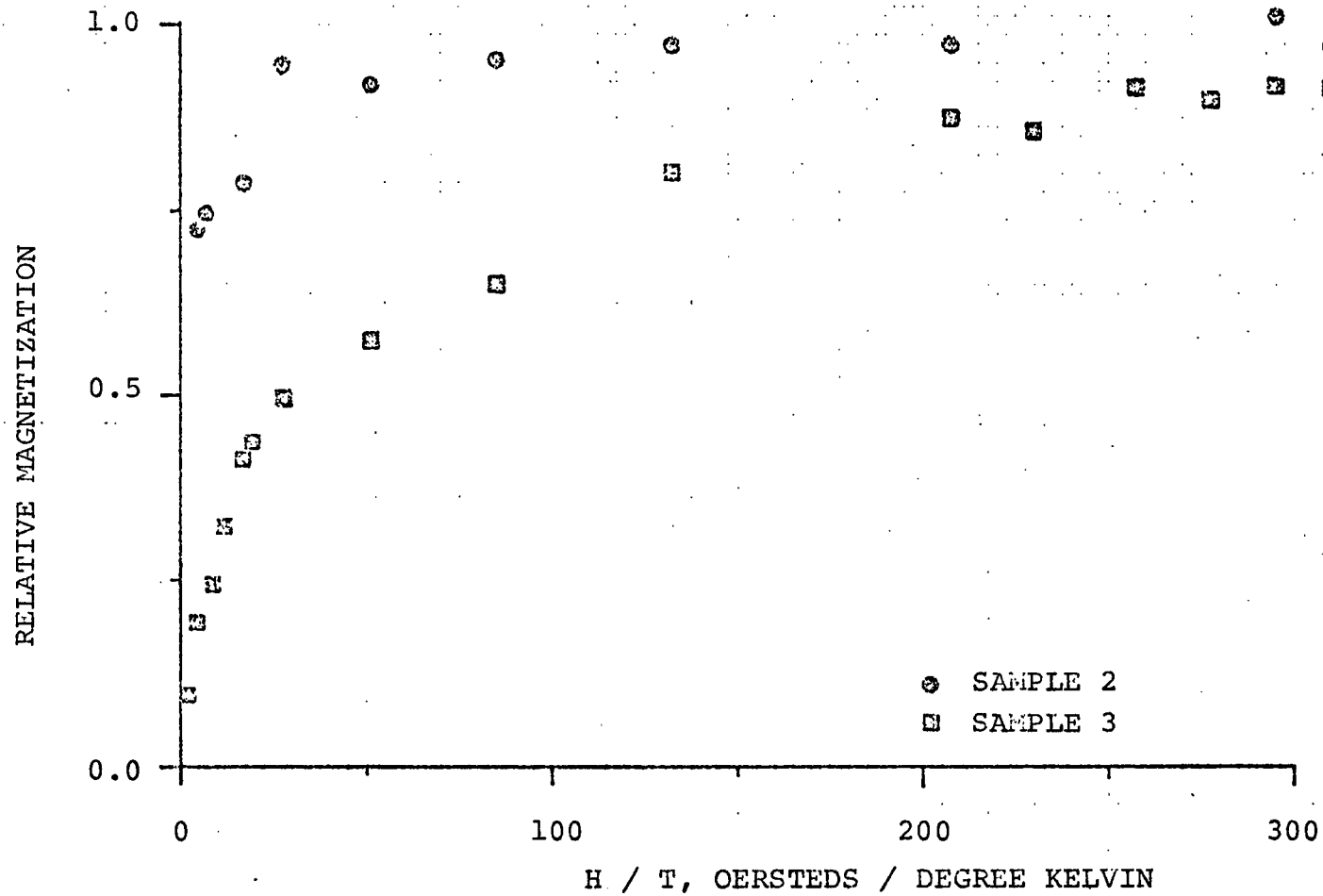


FIGURE 4.7 EXPERIMENTALLY DETERMINED RELATIVE MAGNETIZATION VERSUS H / T FOR SAMPLES 2 AND 3 AT 295 DEGREES KELVIN.

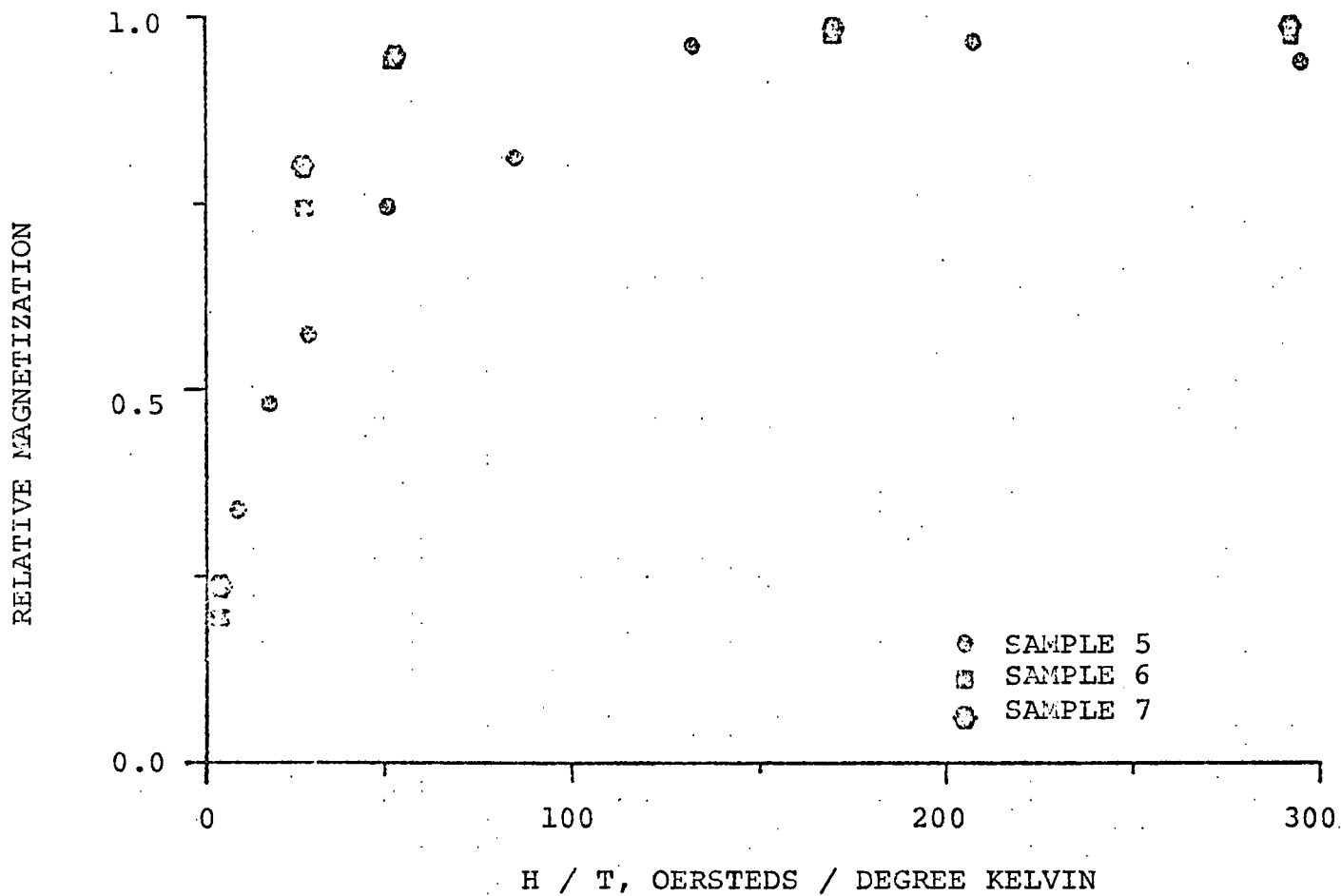


FIGURE 4.8 EXPERIMENTALLY DETERMINED RELATIVE MAGNETIZATION VERSUS H / T FOR SAMPLES 5, 6 AND 7 AT 295 DEGREES KELVIN. SERIES REDUCED AT 350 DEGREES CENTIGRADE.

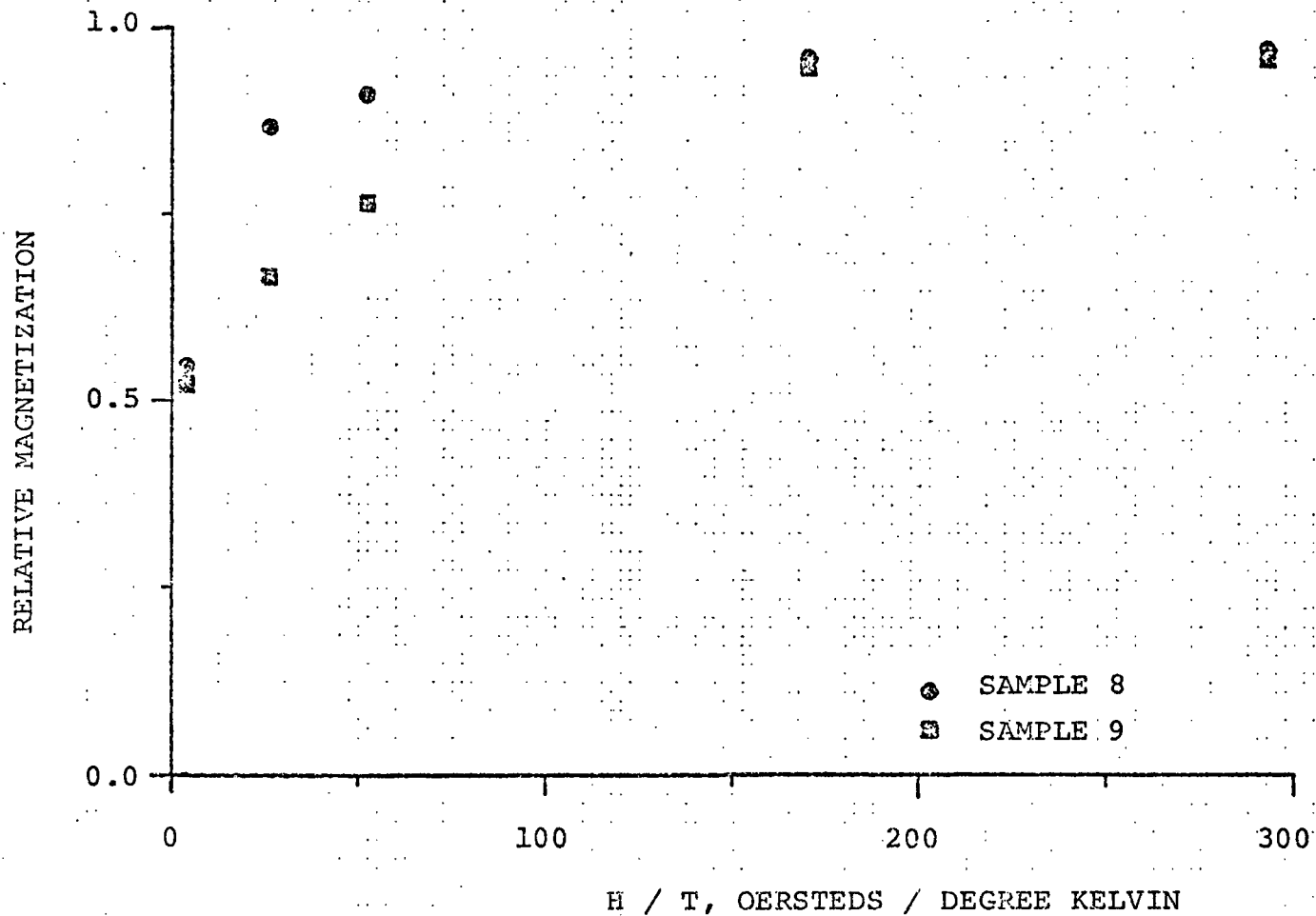


FIGURE 4.9 EXPERIMENTALLY DETERMINED RELATIVE MAGNETIZATION VERSUS H / T FOR SAMPLES 8 AND 9 AT 295 DEGREES KELVIN. SERIES REDUCED AT 450 DEGREES CENTIGRADE.

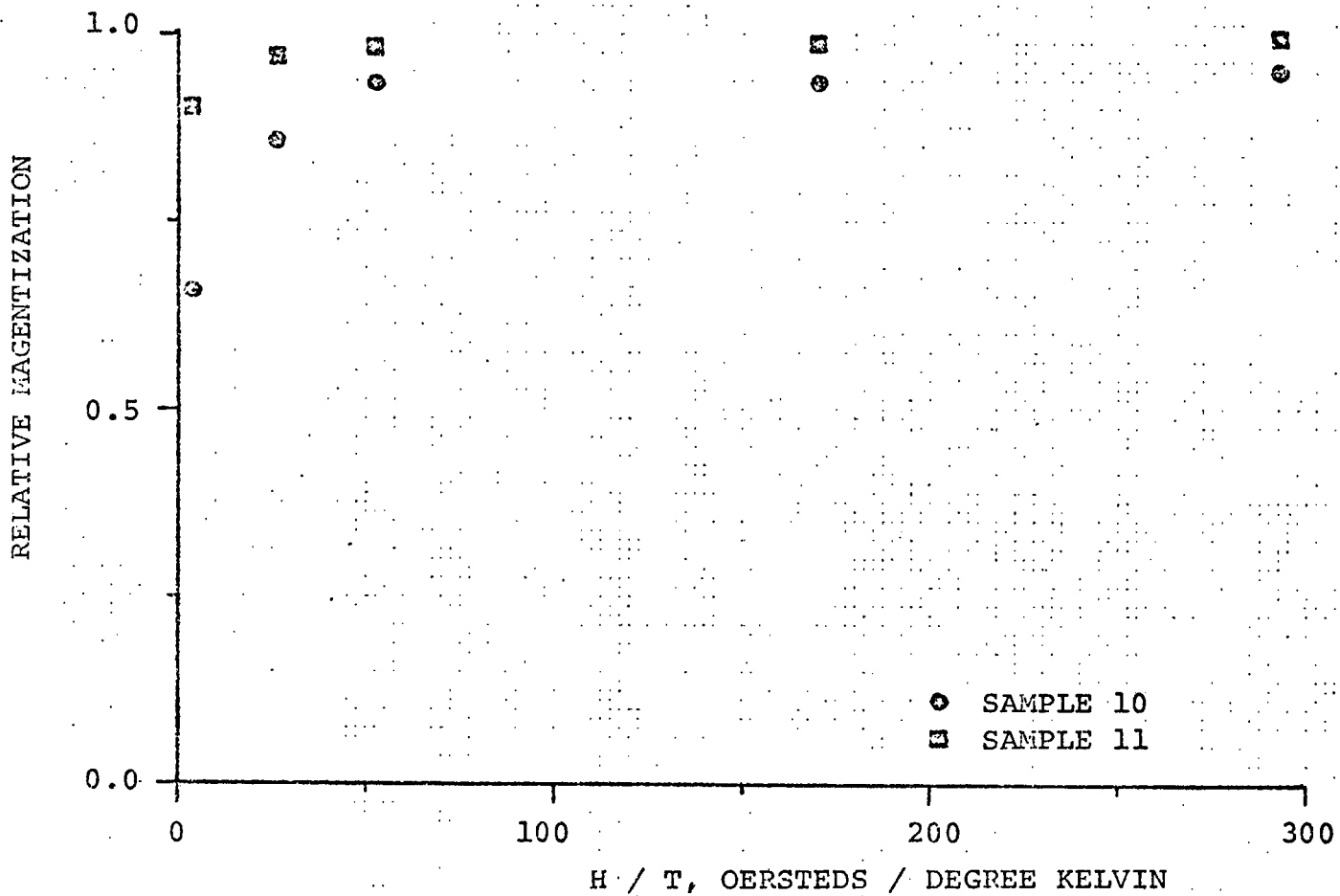


FIGURE 4.10 EXPERIMENTALLY DETERMINED RELATIVE MAGNETIZATION VERSUS H / T FOR SAMPLES 10 AND 11 AT 295 DEGREES KELVIN. SERIES REDUCED AT 600 DEGREES CENTIGRADE.

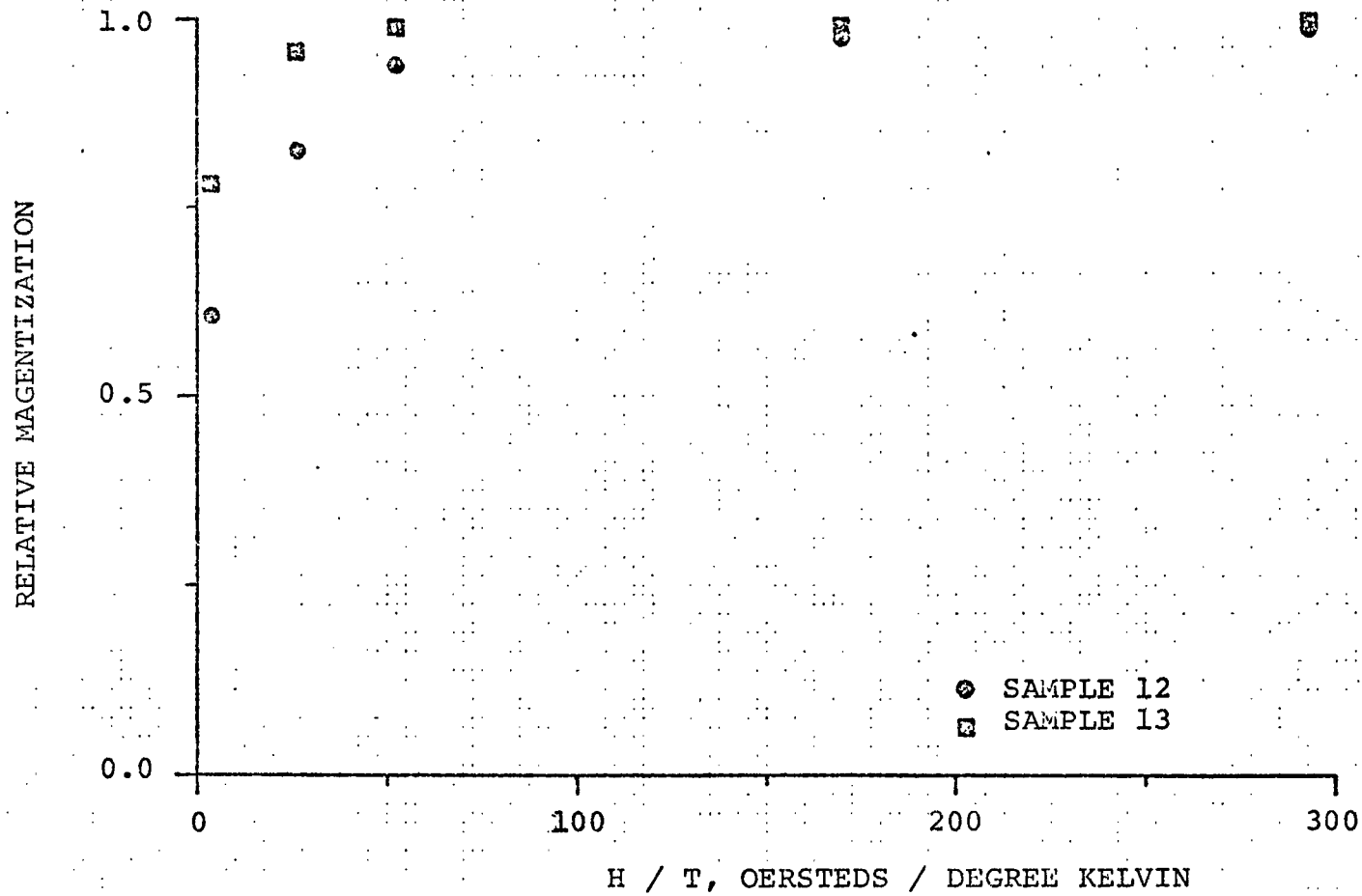


FIGURE 4.11 EXPERIMENTALLY DETERMINED RELATIVE MAGNETIZATION VERSUS H / T FOR SAMPLES 12 AND 13 AT 295 DEGREES KELVIN. SERIES SINTERED IN HELIUM.

TABLE 4.2 EXPERIMENTALLY DETERMINED CATALYST CHARACTERISTICS.

SAMPLE NUMBER	REDUCED NICKEL WEIGHT PERCENT	$(\int E dt)_{\infty}^{(2)}$ MILLIVOLTS . MILLISECONDS $\times 10^{-2}$	SATURATION SPECIFIC MAGNETIZATION, CGS/GRAM REDUCED NICKEL	SURFACE AREA, (5) METERS SQUARED/ GRAM REDUCED NICKEL
1 <sup>(4)</sup>	33.8	1.90	54.4	(3)
2	(3)	2.40	(3)	(3)
3	(3)	1.57	(3)	(3)
4 <sup>(4)</sup>	33.8	2.62	54.4	(3)
5	(3)	1.54	(3)	(3)
6	20.7	1.70	51.1	95.0
7	19.7	1.70	49.5	167
8	20.6	1.92	51.0	(3)
9	54.1	5.30	54.0	(3)
10	55.8	4.30	51.0	26.8
11	48.2	4.42	50.6	13.6
12	12.6	1.39	53.1	(3)
13	30.8	2.62	53.4	(3)

1) FROM Q-METER MEASUREMENTS

2) AVERAGE OF LEAST SQUARES INTERCEPT OF  $(1/H)$  and  $(1/H^{0.9})$ ,  
INTERCEPT OF  $(1/H^2)$  FOR BULK NICKEL

3) NOT AVAILABLE

4) USED AS CALIBRATION STANDARD

5) AT 295 DEGREES KELVIN

TABLE 4.3 EXPERIMENTALLY DETERMINED AVERAGE CRYSTALLITE SIZES AND MEASURES OF DISPERSION AS CALCULATED BY DIFFERENT APPROXIMATIONS.

SAMPLE NUMBER	AVERAGE CRYSTALLITE DIAMETER, ANGSTROMS			MEASURE OF DISPERSION	
	LOW FIELD	HIGH FIELD	LOG-NORMAL	NORMAL DISTRIBUTION	LOG-NORMAL DISTRIBUTION
1	43.6	37.8	40.6	14.8	1.25
2	65.0	30.3	44.4	32.4	1.66
3	42.5	29.1	34.8	19.7	1.44
4	67.8	122	91.4	--	--
5	46.6	40.4	43.4	15.8	1.24
6	44.4	36.2	40.0	17.2	1.30
7	47.2	40.0	43.4	17.0	1.27
8	62.5	38.7	49.2	30.3	1.13
9	62.0	37.2	48.0	30.4	1.51
10	66.9	34.5	48.0	33.4	1.60
11	73.6	77.4	75.4	--	--
12	64.6	57.0	60.8	20.8	1.23
13	70.4	77.4	73.8	--	--

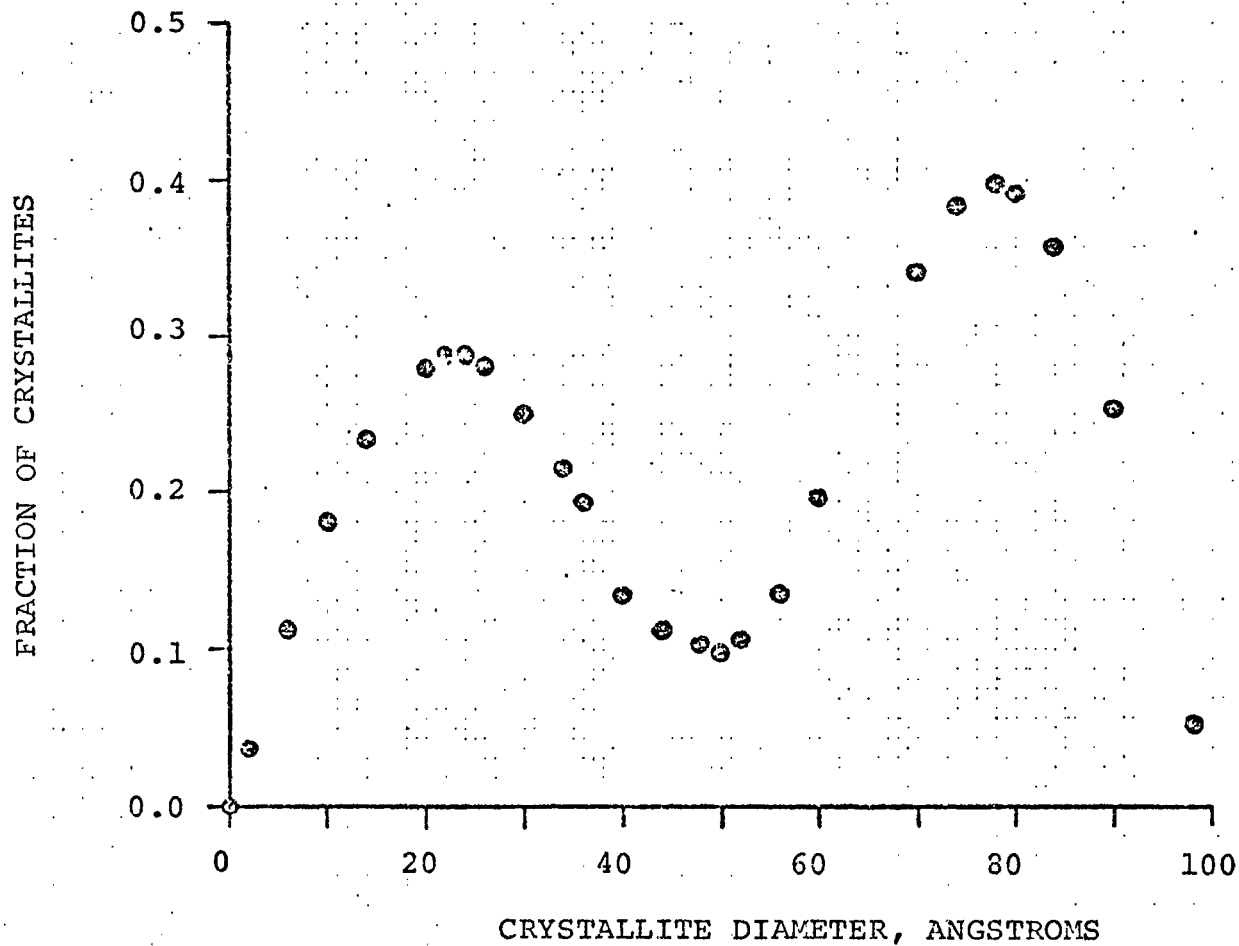


FIGURE 4.12 FOURIER SERIES APPROXIMATION TO CRYSTALLITE SIZE DISTRIBUTION FOR SAMPLE 2.

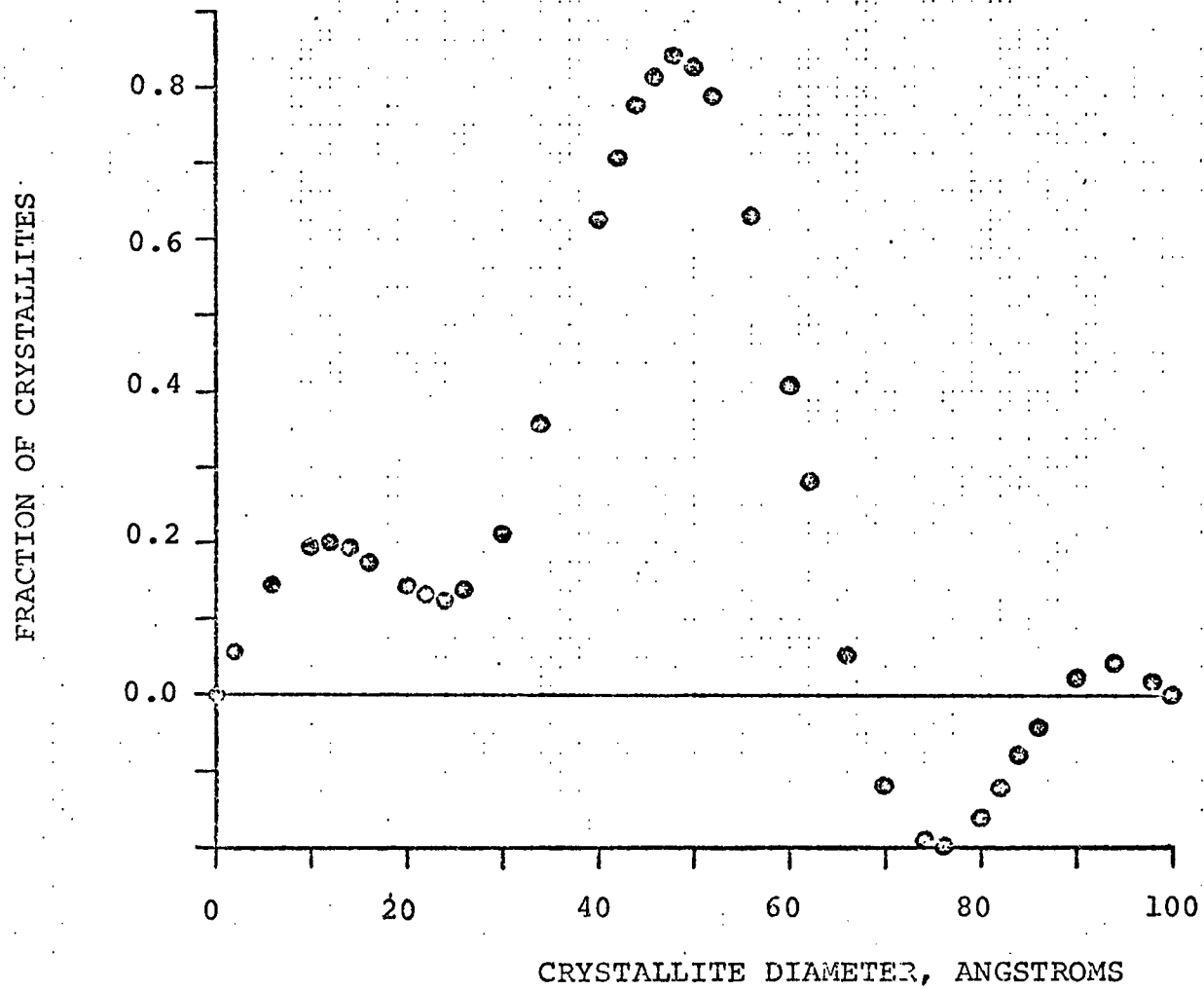


FIGURE 4.13 FOURIER SERIES APPROXIMATION TO CRYSTALLITE SIZE DISTRIBUTION FOR SAMPLE 3.

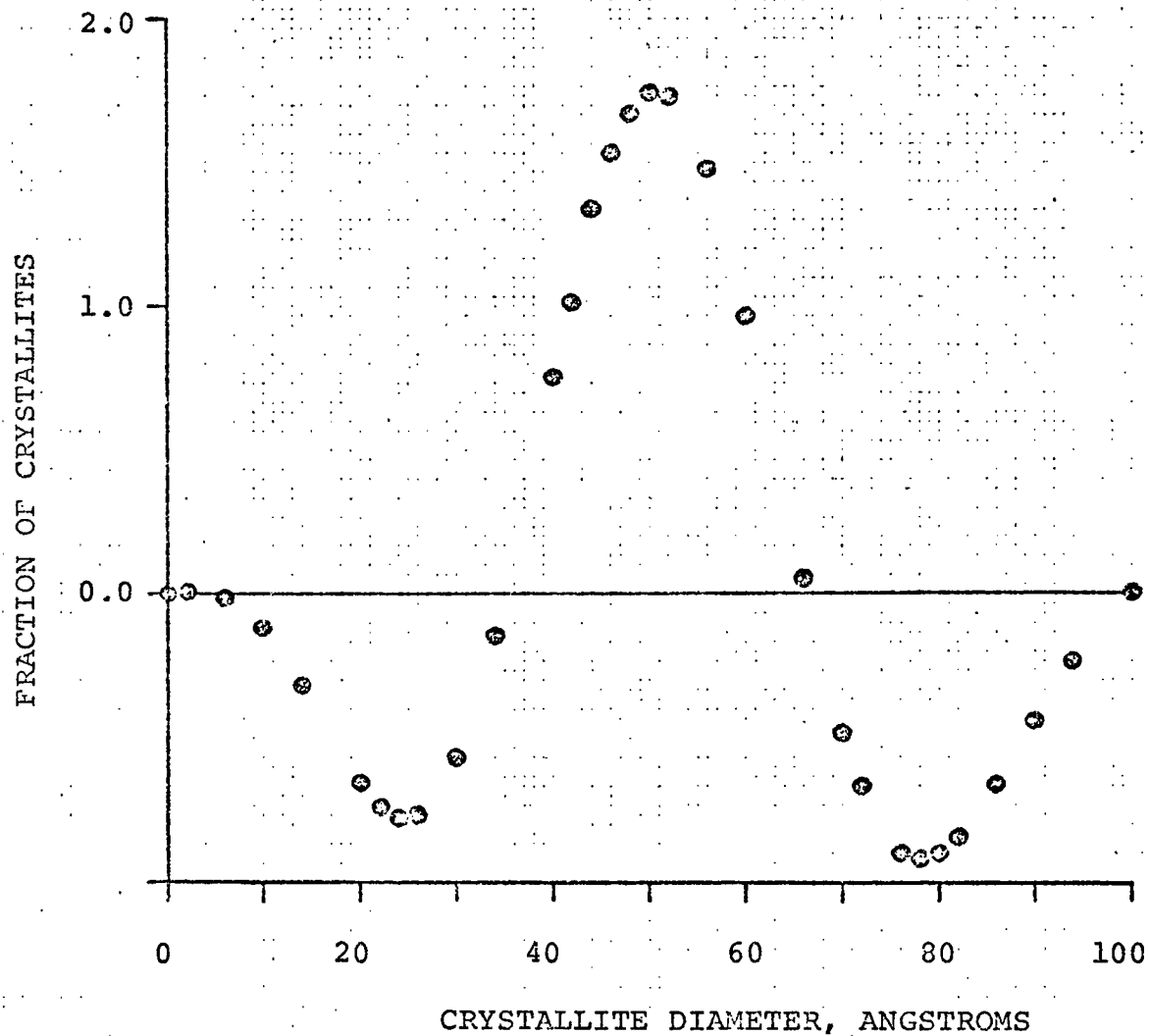


FIGURE 4.14 FOURIER SERIES APPROXIMATION TO CRYSTALLITE SIZE DISTRIBUTION FOR SAMPLE 5.

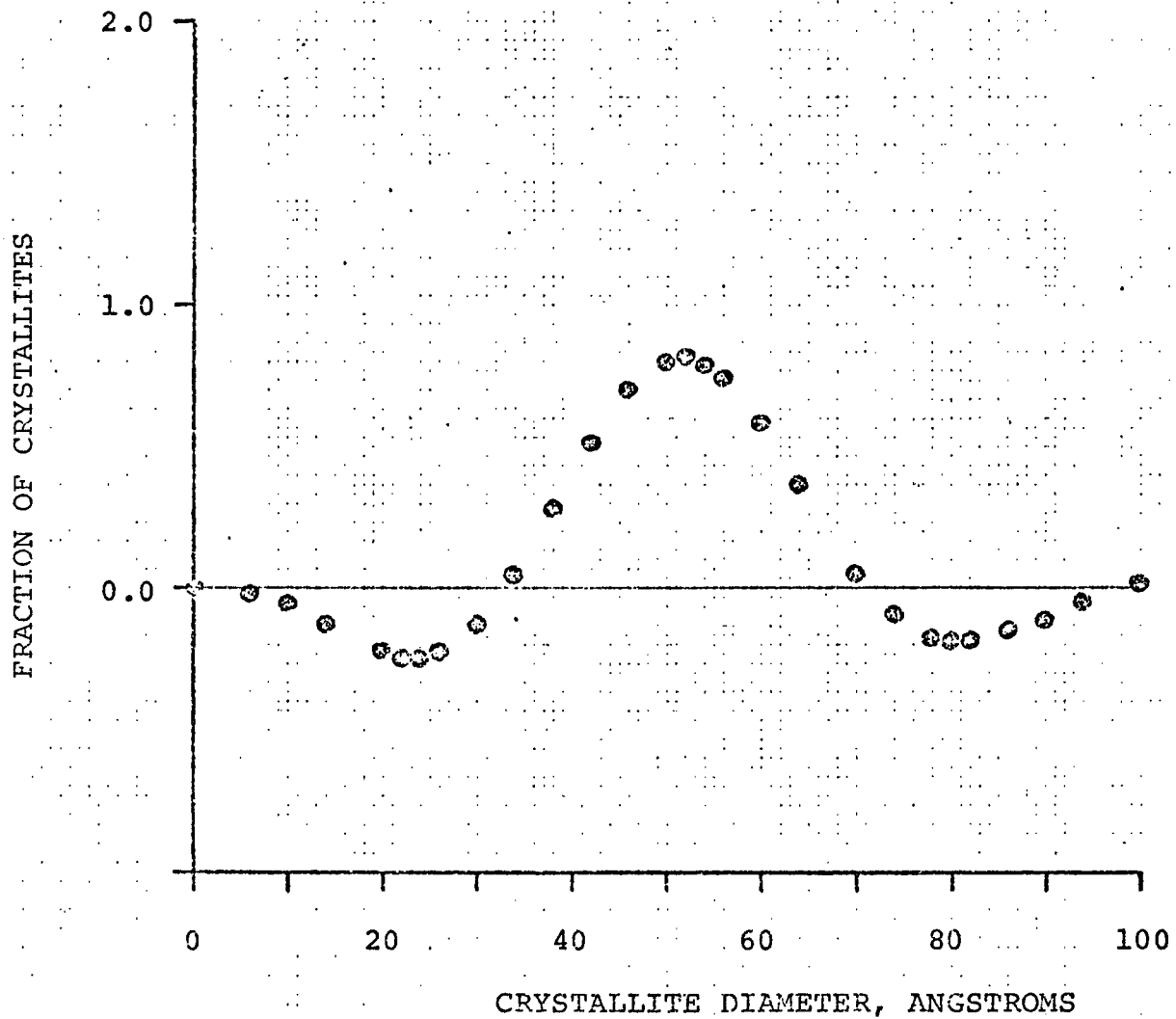


FIGURE 4.15 FOURIER SERIES APPROXIMATION TO CRYSTALLITE SIZE DISTRIBUTION FOR SAMPLE 6.

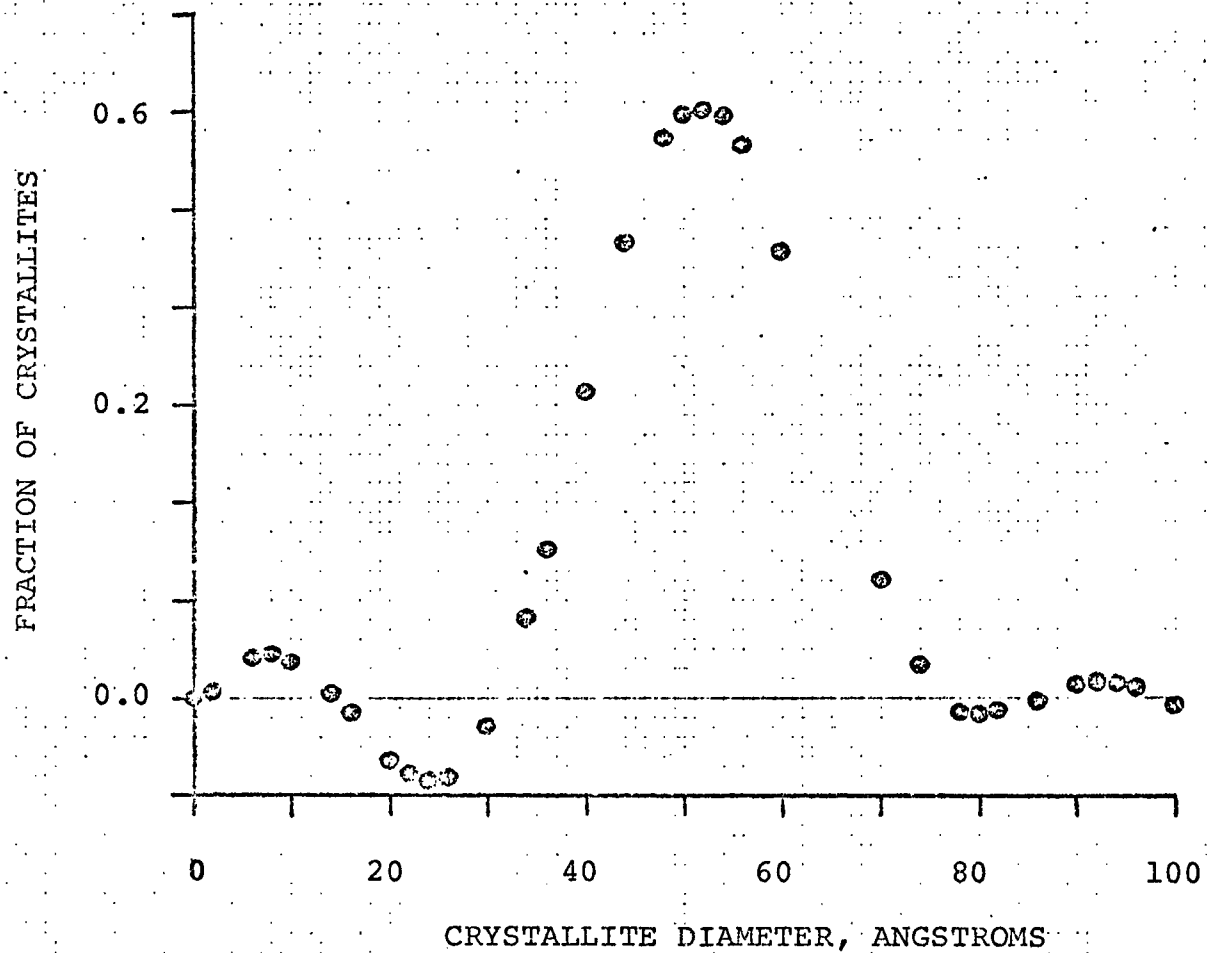


FIGURE 4.16 FOURIER SERIES APPROXIMATION TO CRYSTALLITE SIZE DISTRIBUTION FOR SAMPLE 7.

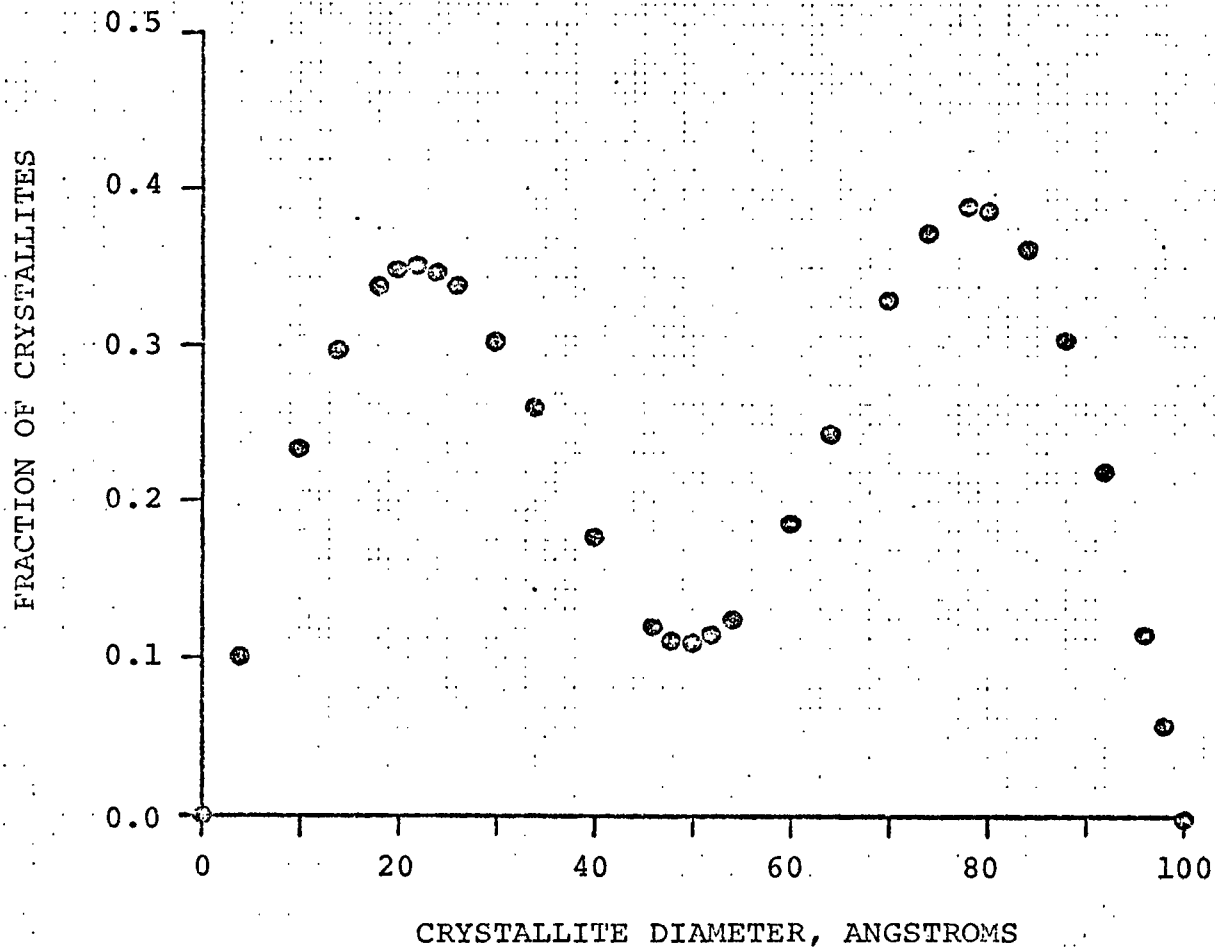


FIGURE 4.17 FOURIER SERIES APPROXIMATION TO CRYSTALLITE SIZE DISTRIBUTION FOR SAMPLE 8.

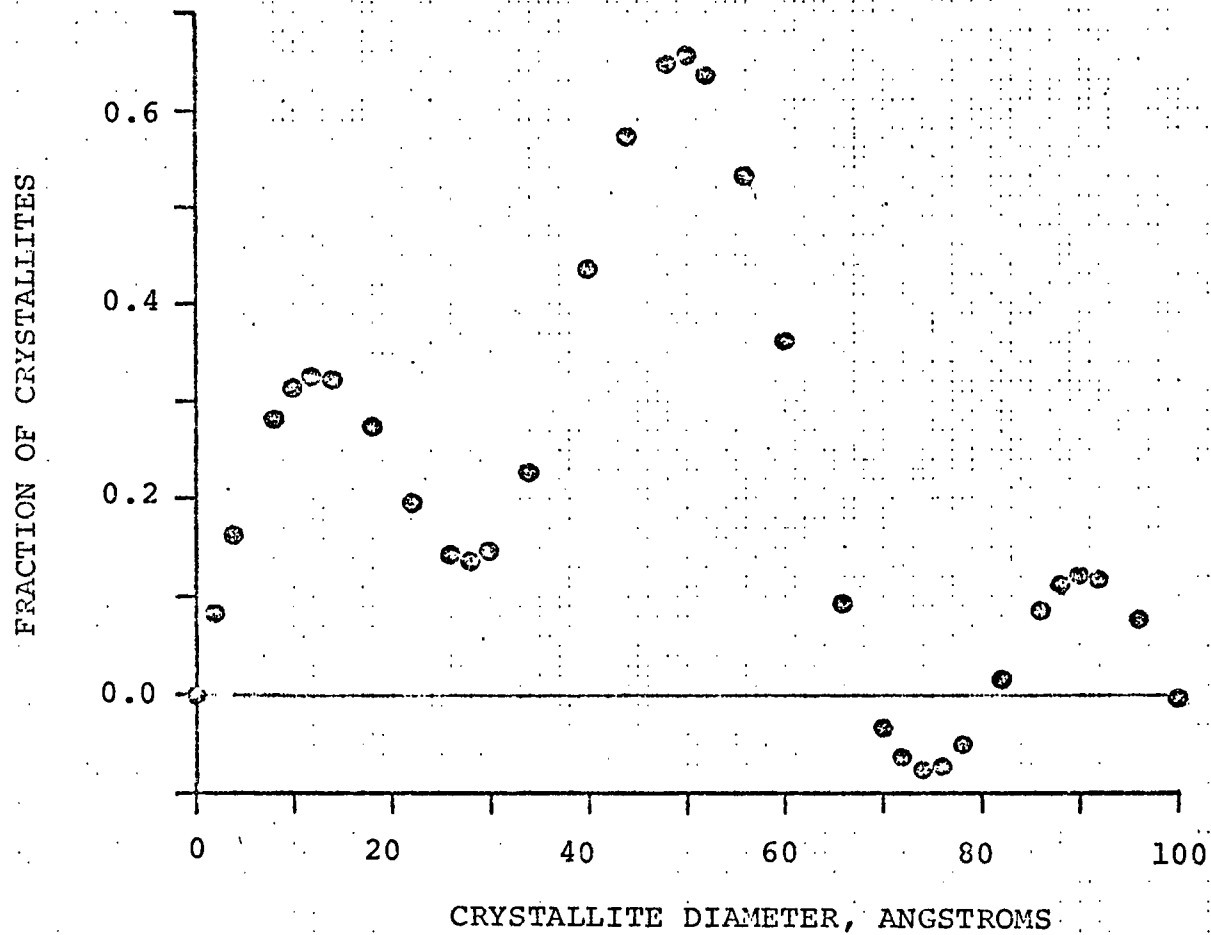


FIGURE 4.18 FOURIER SERIES APPROXIMATION TO CRYSTALLITE SIZE DISTRIBUTION FOR SAMPLE 9.

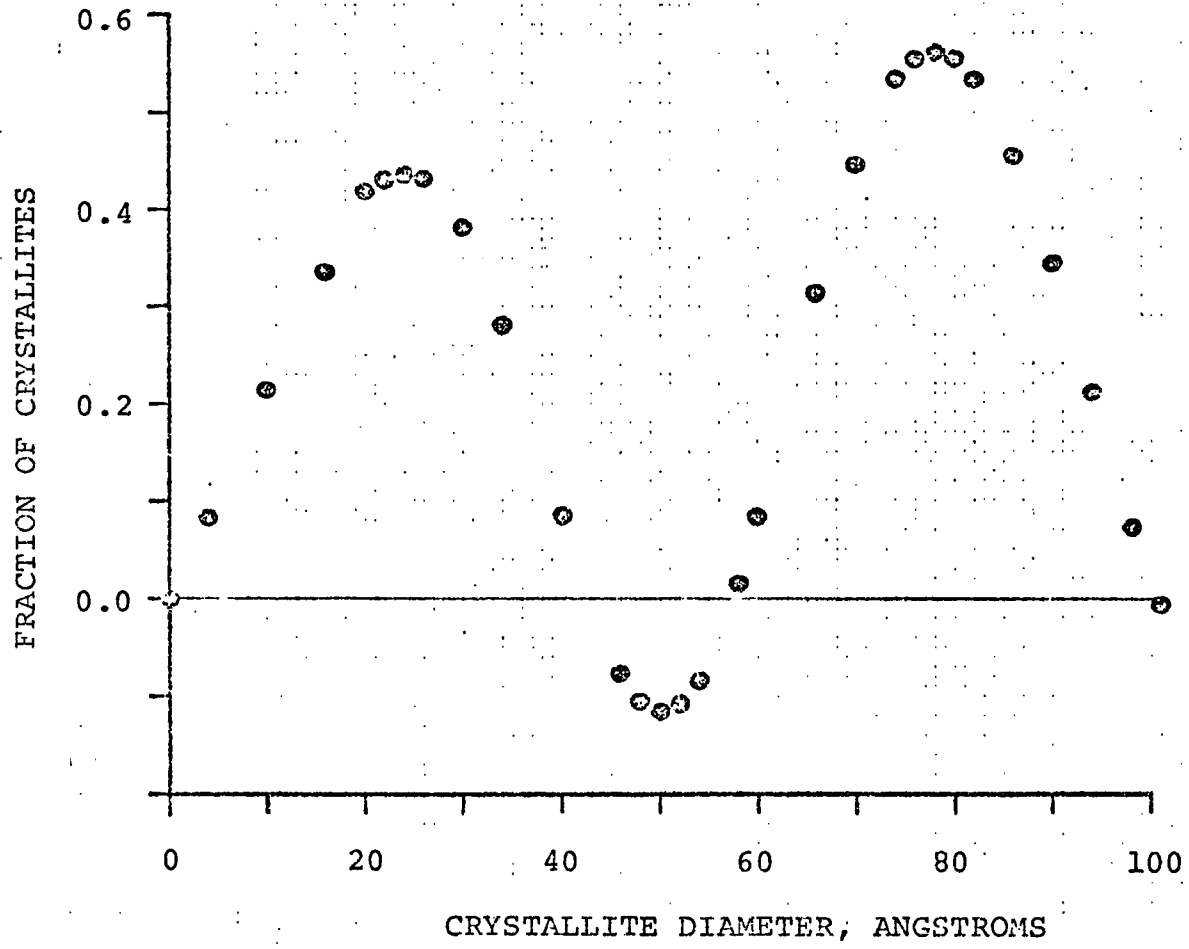


FIGURE 4.19 FOURIER SERIES APPROXIMATION TO CRYSTALLITE SIZE DISTRIBUTION FOR SAMPLE 10.

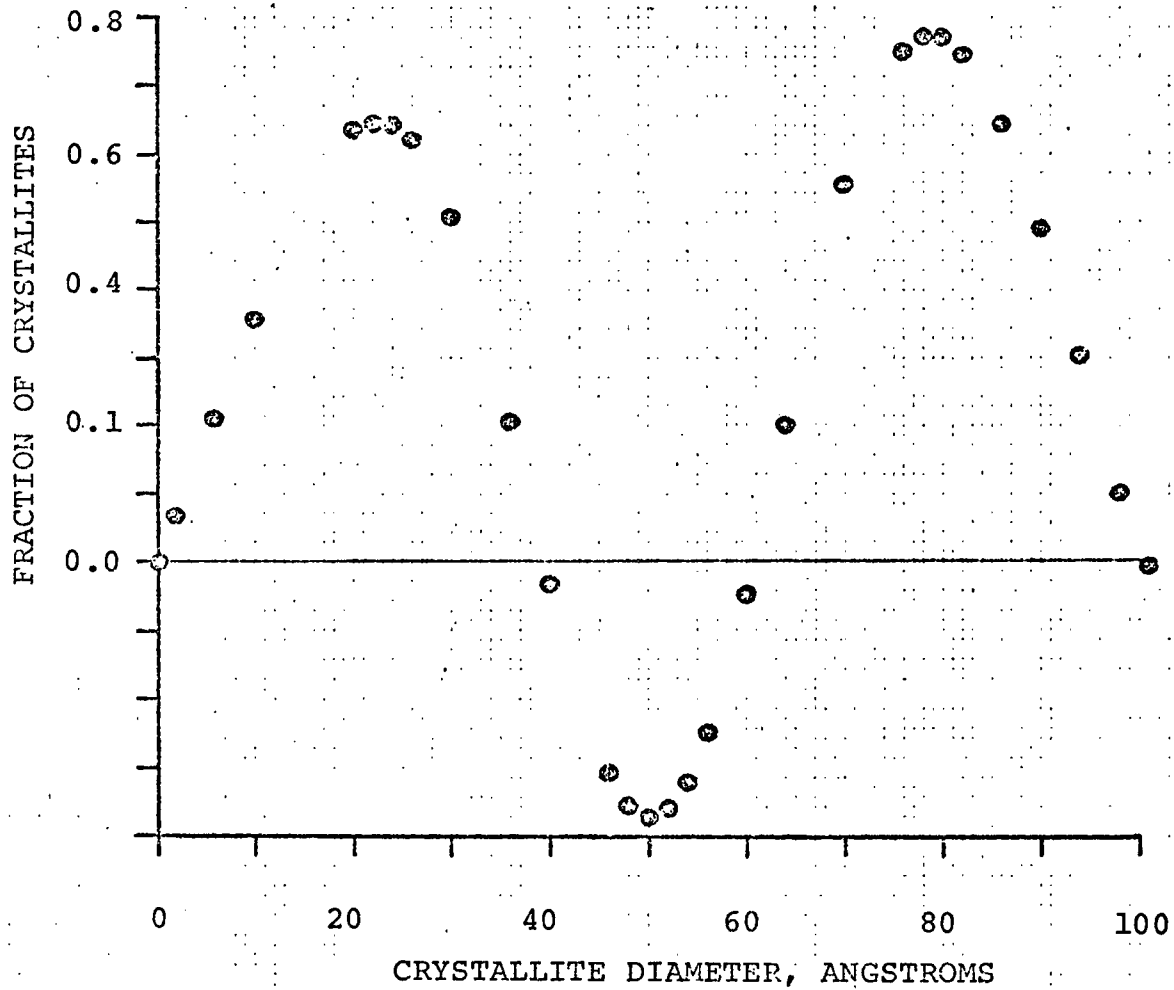


FIGURE 4.20 FOURIER SERIES APPROXIMATION TO CRYSTALLITE SIZE DISTRIBUTION FOR SAMPLE 11.

## CHAPTER V

### CONCLUSIONS AND RECOMMENDATIONS

The results of this magnetic investigation of dispersed nickel catalyst based on the data presented in Chapter IV are as follows:

(1) The saturation data obtained from magnetic measurements at 295 degrees Kelvin and extending to the 20 to 30 kilo-oersted range was considerably lower ( in one case 20 percent lower ) than the estimate obtained by using magnetic measurements up to 90 kilo-oersteds on dispersed nickel systems with most of their crystallite diameters in the 10 to 100 Angstrom range.

The use of low temperatures would hopefully be avoided not only because of the adverse effects on the superparamagnetic behavior of small crystallites but also due to the inconvenience of working with cryogenic sample equipment ( reduction of magnet work volume, time required to change and cool sample, etc.). However, to avoid the use of low temperature samples will require the use of magnetic field strengths extending into the 50 to 100 kilo-oersted range in order to obtain magnetic saturation data of small crystallite systems.

(2) Measurement of the low and high magnetic field strength estimates of the average crystallite size yields information

on the dispersion of the system which will be valuable for better characterizing dispersed catalytic systems. However, a measure of dispersion usually requires that a type of distribution function be assumed. In this investigation, two measures of dispersion were calculated assuming a normal distribution and a log-normal distribution function. From Figures 4.12 to 4.20, it is seen that many crystallite size distributions may not be of these types. Therefore, although low and high magnetic field strength average crystallites sizes provide useful information, it is preferable to know the crystallite size distribution.

(3) Two different methods were proposed for approximating the crystallite size distributions of dispersed catalyst. One of these methods, the direct matrix method, appears to give unsatisfactory results. The second method, the Fourier integral method, is possibly a technique for determining crystallite size distributions.

(4) The Fourier integral method was used to approximate the crystallite size distribution of several catalyst samples. Five coefficients of the distribution were determined using a five by five segment of the coefficient array of the Langevin function given by equation ( 2.44 ) and five coefficients of the experimental data given by equation ( 2.50 ). The results of the computations are given in Figures 4.12 to 4.20. Although these results give only

qualitative information about the crystallite size distribution, further work with this method may provide better approximation of the crystallite size distribution.

It is recommended, that in future studies with this equipment, that electronic integration of the measuring coil signal be attempted. This would expedite the collection of the experimental data and hopefully improve the reliability of the data. It is also suggested that further work be directed to improving the results of the Fourier integral method, specifically by first investigating better determination of the Fourier coefficients of the Langevin function given by equation ( 2.44 ) by digital and analytical means and then by the utilization of a larger number of coefficients.

Further work could consider not only the effects on the crystallite size distribution of the reduction temperature and the reduction time, but also the effects of the support and the effects of adsorbates as a means of investigating adsorption bonding and the active crystallite sizes for different adsorbed species. The results of such investigations should prove interesting and useful for better characterization of dispersed catalytic systems.

## BIBLIOGRAPHY

1. Boudart, M., Aldag, A., Benson, J. E., Dougherty, N. A., and Harkins, C. G., *Journal of Catalysis*, 6, 92 ( 1966 ).
2. Luss, D., *Journal of Catalysis*, 23, 119 ( 1971 ).
3. Langevin, P., *J. Phys.*, 4, 678 ( 1905 ).
4. Kittel, C., Introduction to Solid State Physics, fourth edition, John Wiley and Sons, Incorporated, New York, 1971.
5. Selwood, P. W., Adsorption and Collection Paramagnetism, Academic Press, New York, 1962.
6. Heukelom, W., Broeder, J. J., and van Reijen, L. L. J. *Chim. Phys.*, 51, 474 ( 1954 ).
7. Bean, C. P., and Jacobs, I. S., *J. Applied Physics*, 27, 1448 ( 1954 ).
8. Becker, J. J., *Transactions of the American Institute of Mining, Meterlurgical, and Petroleum Engineers*, 209, 59 ( 1957 ).
9. Luborsky, F. E., and Lawrence, P. E., *J. Applied Physics*, 32, 231S ( 1961 ).
10. Jacobs, I. S., and Bean, C. P., Magnetism, ed. G. Rado and H. Suhl, Volume III, Academic Press, New York, 1963.
11. Selwood, P. W., Magnetochemistry, second edition, Interscience Publishers Incorporated, New York, 1956.
12. Neel, L., *Anal. Geophysics*, 5, 99 ( 1949 ).
13. Brown, W. F., Jr., *J. Applied Physics*, 30, 130S ( 1959 ).
14. Knappwost, A., and Illenberger, A., *Naturwissenschaffer*, 45, 238 ( 1958 ).
15. Vogt, E., Henning, W., and Hahn, A., in "Berichte Arbeitsgemeinschaft Ferromagnetismus 1958", ed. Dr. Reiederer Verlag, Stuttgart, 43 ( 1959 ).
16. Bean, C. P., Livingston, J. D., and Rodbell, D. S., *Le Journal de Physique et le Radium*, 20, 298 ( 1959 ).

17. Dorling, T. A., and Moss, R. L., *Journal of Catalysis*, 7, 378 ( 1967 ).
18. Spenadel, L., and Boudart, M., *J. Phys. Chem.*, 64, 204 ( 1960 ).
19. Adams, C. R., Benesi, H. A., Curtis, R. M., and Meisenheimer, R. G., *Journal of Catalysis*, 1, 336 ( 1962 ).
20. Reinen, D., and Selwood, P. W., *Journal of Catalysis*, 2, 109 ( 1963 ).
21. Richardson, J. T., and Beaxis, J. O., *Review of Scientific Instruments*, 34, 887 ( 1957 ).
22. Barrnett, S. J., *J. Applied Physics*, 23, 975 ( 1952 ).
23. Broersma, S., *Review of Scientific Instruments*, 20, 660 ( 1949 ).
24. Cahn, J. W., *Transactions of the American Institute of Mining, Meterlurgical, and Petroleum Engineers*, 209, 1309 ( 1959 ).
25. Dietz, R. E., Thesis, Northwestern University, Evanston, Illinois, 1960.
26. Richardson, J. T., Personal Communication.
27. Weil, L., *Compt. Rend. Acad. Sci.*, 229, 584 ( 1949 ).
28. Weil, L., in "Colloque National de Magnitism, Strasbourg 1957", p. 147, CNRS, Paris ( 1958 ).
29. Luborsky, F. E., *J. Applied Physics*, 33, 1909 ( 1962 ).
30. Elmore, W. C., *Physics Reviews*, 54, 1092 ( 1938 ).
31. Dreyer, H., *Zeitschrift fur Anorganische und Allgemeime Chemie*, 362, 233 ( 1968 ).
32. Elliott, D., Doctoral Dissertation, University of Houston, Houston, Texas, May 1972.
33. Rosser, E. J., Master's Thesis, University of Houston, Houston, Texas, May 1972.
34. Richardson, J. T., *J. Scientific Instruments*, 1, 456 ( 1963 ).

APPENDIX A

LANGEVIN AND BRILLOUIN FUNCTIONS

LANGEVIN FUNCTION

When a material containing  $n$  crystallites per unit volume, each with magnetic moment  $\mu$ , is subjected to an externally applied magnetic field, the magnetic moments tend to align with the applied field. However, thermal agitation tends to keep the moments disaligned. The interaction energy is

$$U = \mu H \cos(\theta) \quad \text{A.1}$$

where  $\theta$  is the angle between the applied field and the magnetic moments. The magnetization per unit volume is then

$$M = n \overline{\cos(\theta)} \quad \text{A.2}$$

Langevin assumed that there was a Boltmann distribution of orientations so that the probability of finding a moment aligned in an element of solid angle is proportional to  $\exp(-U / kT)$  hence

$$\overline{\cos(\theta)} = \frac{\int_0^\pi \sin(\theta) \cos(\theta) \exp(\mu H \cos(\theta) / kT) d\theta}{\int_0^\pi \sin(\theta) \exp(\mu H \cos(\theta) / kT) d\theta} \quad \text{A.3}$$

$$\overline{\cos(\theta)} = \text{COTH}(\mu H / kT) - [1 / (\mu H / kT)] \quad \text{A.4}$$

$$\overline{\cos(\theta)} = L(\mu H / kT) \quad \text{A.5}$$

Therefore

$$M = n\mu L( \mu H / kT ) \quad \text{A.6}$$

### BRILLOUIN FUNCTION

Kittel ( 4 ) has shown how that for simple spin systems that the only energy levels are

$$U = \pm\mu_B H \quad \text{A.7}$$

where  $\mu_B$  is the Bohr magneton. Hence the relative proportions of the two energy levels are

$$n_1 / n = \frac{\text{EXP}( \mu H / kT )}{\text{EXP}( \mu H / kT ) + \text{EXP}( -\mu H / kT )} \quad \text{A.8}$$

$$n_2 / n = \frac{\text{EXP}( -\mu H / kT )}{\text{EXP}( \mu H / kT ) + \text{EXP}( -\mu H / kT )} \quad \text{A.9}$$

where

$$n_1 + n_2 = n \quad \text{A.10}$$

The magnetization is then

$$M = ( n_1 - n_2 )\mu = n\mu \text{TANH}( \mu H / kT ) \quad \text{A.11}$$

A.12

where

$$\text{TANH}( \mu H / kT ) = \frac{\text{EXP}( \mu H / kT ) - \text{EXP}( -\mu H / kT )}{\text{EXP}( \mu H / kT ) + \text{EXP}( -\mu H / kT )}$$

Similarly, for a system of angular momentum quantum number  $J$ , there are  $2J + 1$  energy levels and the magnetization becomes

$$M = ngJ\mu_B \text{ Br} ( gJ\mu H / kT ) \quad \text{A.13}$$

where

$$\text{Br} ( C ) = \left[ \frac{2J + 1}{2J} \right] \text{COTH} \left( \frac{[2J + 1] C}{2J} \right) - \left[ \frac{1}{2J} \right] \text{COTH} \left( \frac{C}{2J} \right) \quad \text{A.14}$$

is the Brillouin function.

APPENDIX B

EXPERIMENTAL DATA

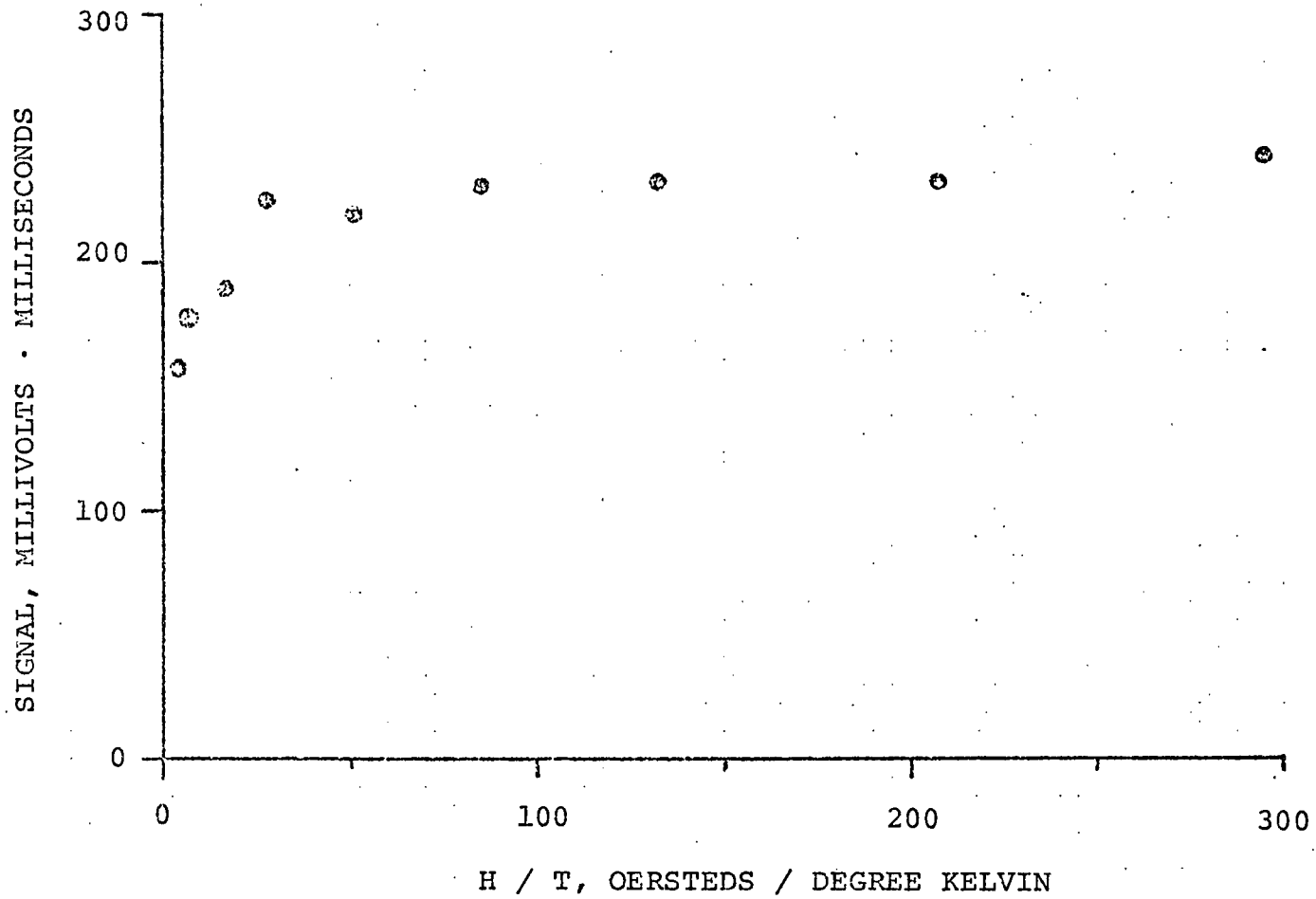


FIGURE B.1 EXPERIMENTAL DATA FROM HIGH FIELD MEASUREMENTS FOR SAMPLE 2 AT 295 DEGREES KELVIN.

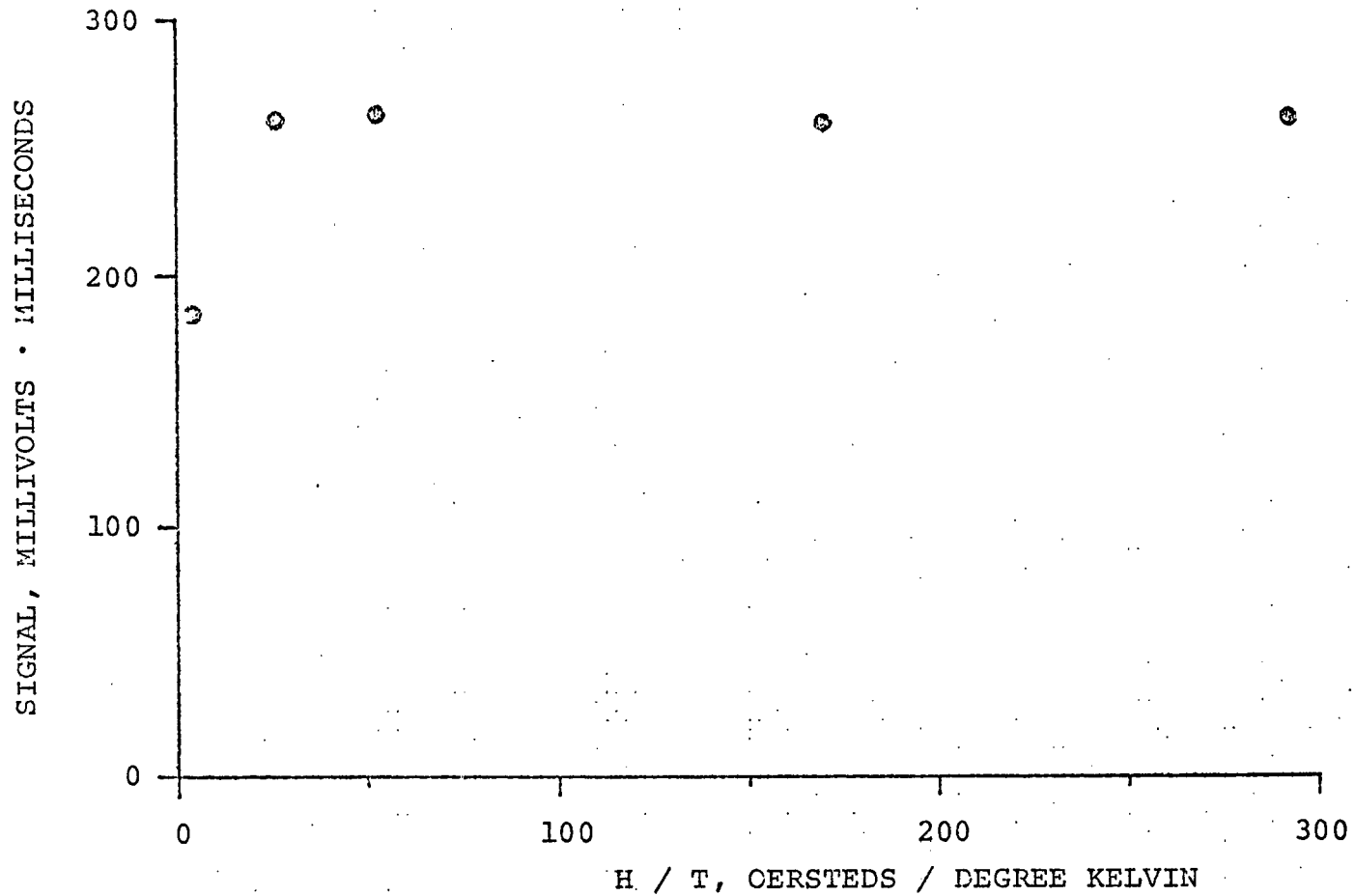


FIGURE B.2 EXPERIMENTAL DATA FROM HIGH FIELD MEASUREMENTS FOR SAMPLE 4 (BULK NICKEL) AT 295 DEGREES KELVIN.

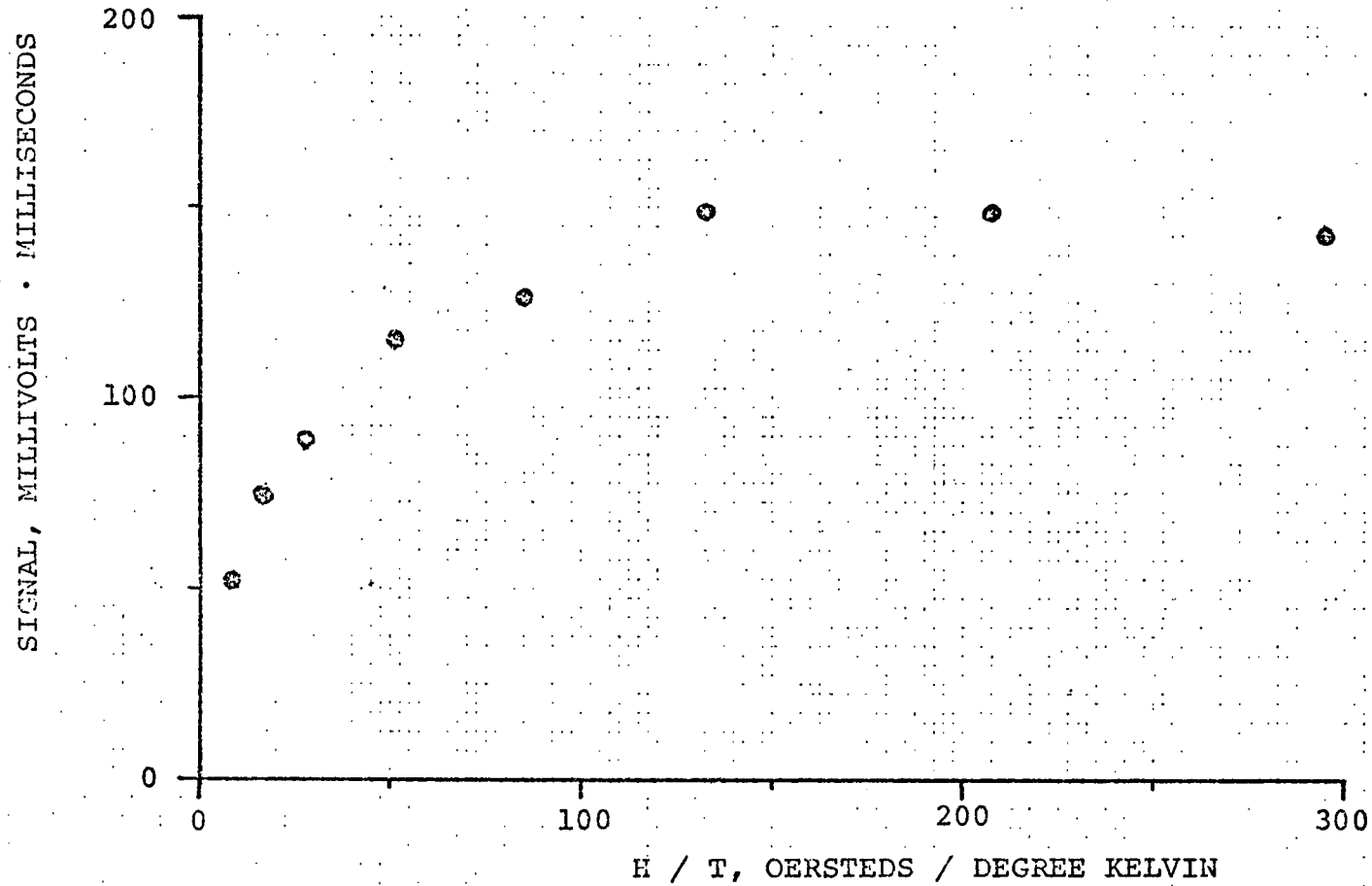


FIGURE B.3 EXPERIMENTAL DATA FROM HIGH FIELD MEASUREMENTS FOR SAMPLE 5 AT 295 DEGREES KELVIN.

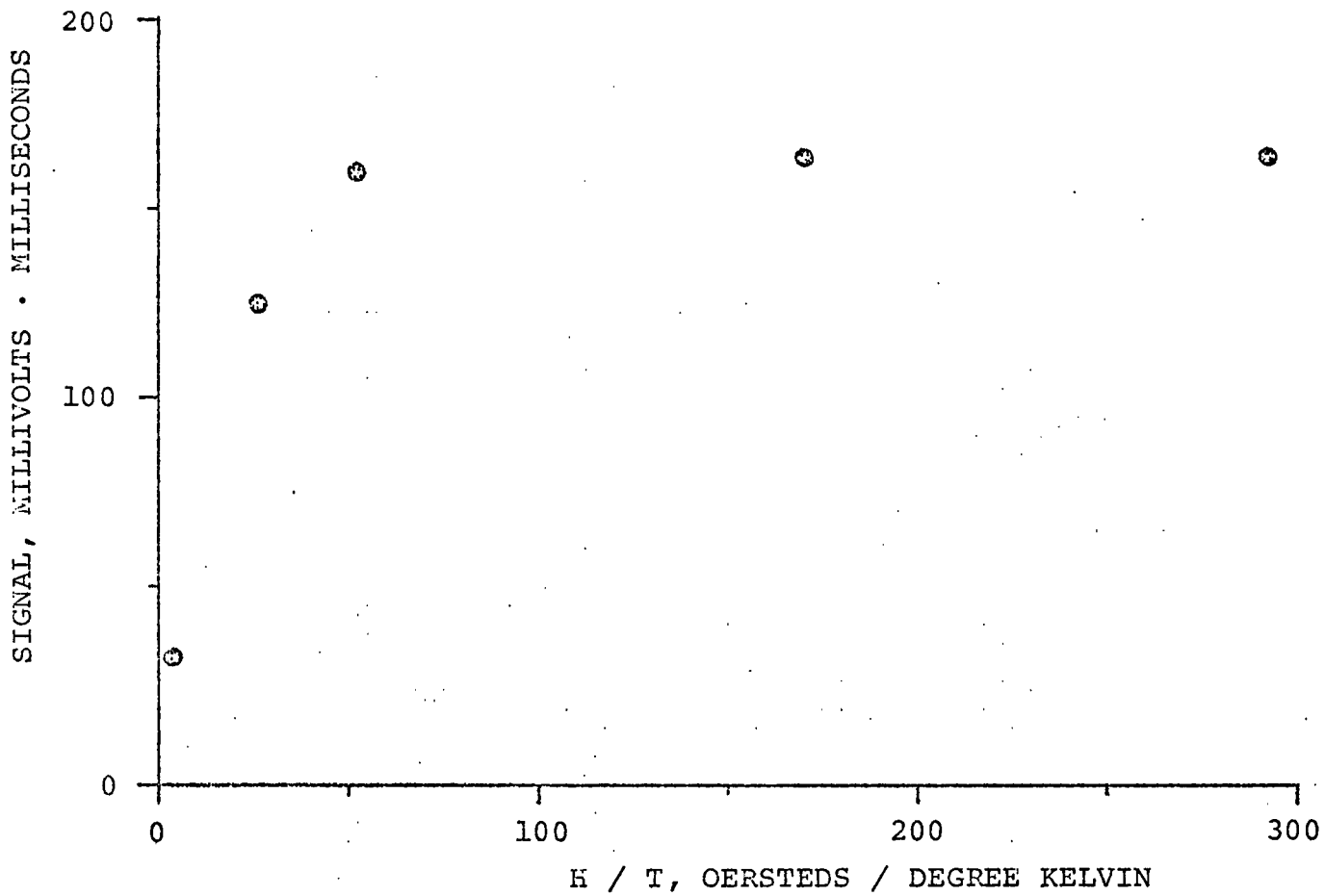


FIGURE B.4 EXPERIMENTAL DATA FROM HIGH FIELD MEASUREMENTS FOR SAMPLE 6 AT 295 DEGREES KELVIN.

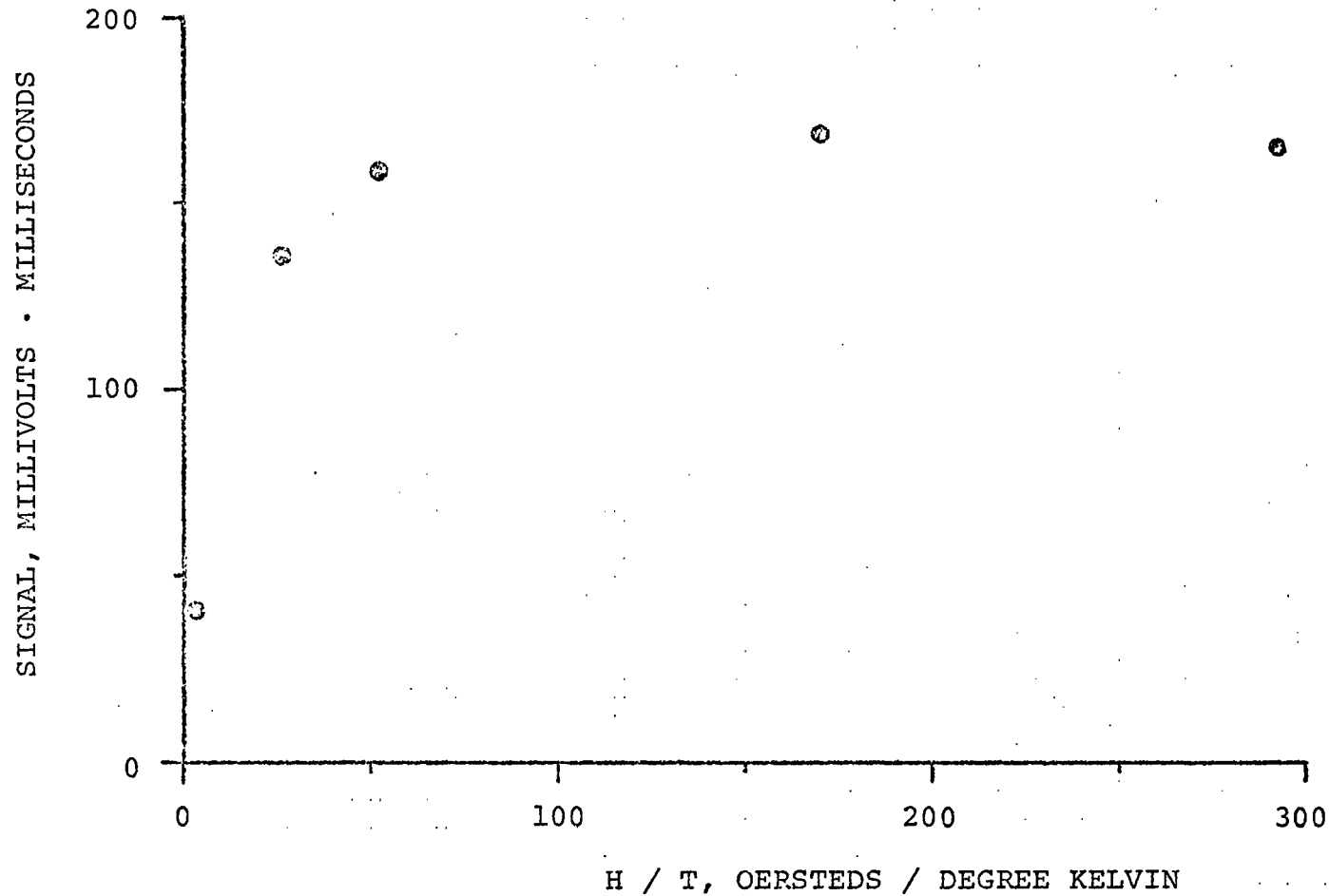


FIGURE B.5 EXPERIMENTAL DATA FROM HIGH FIELD MEASUREMENTS FOR SAMPLE 7 AT 295 DEGREES KELVIN.

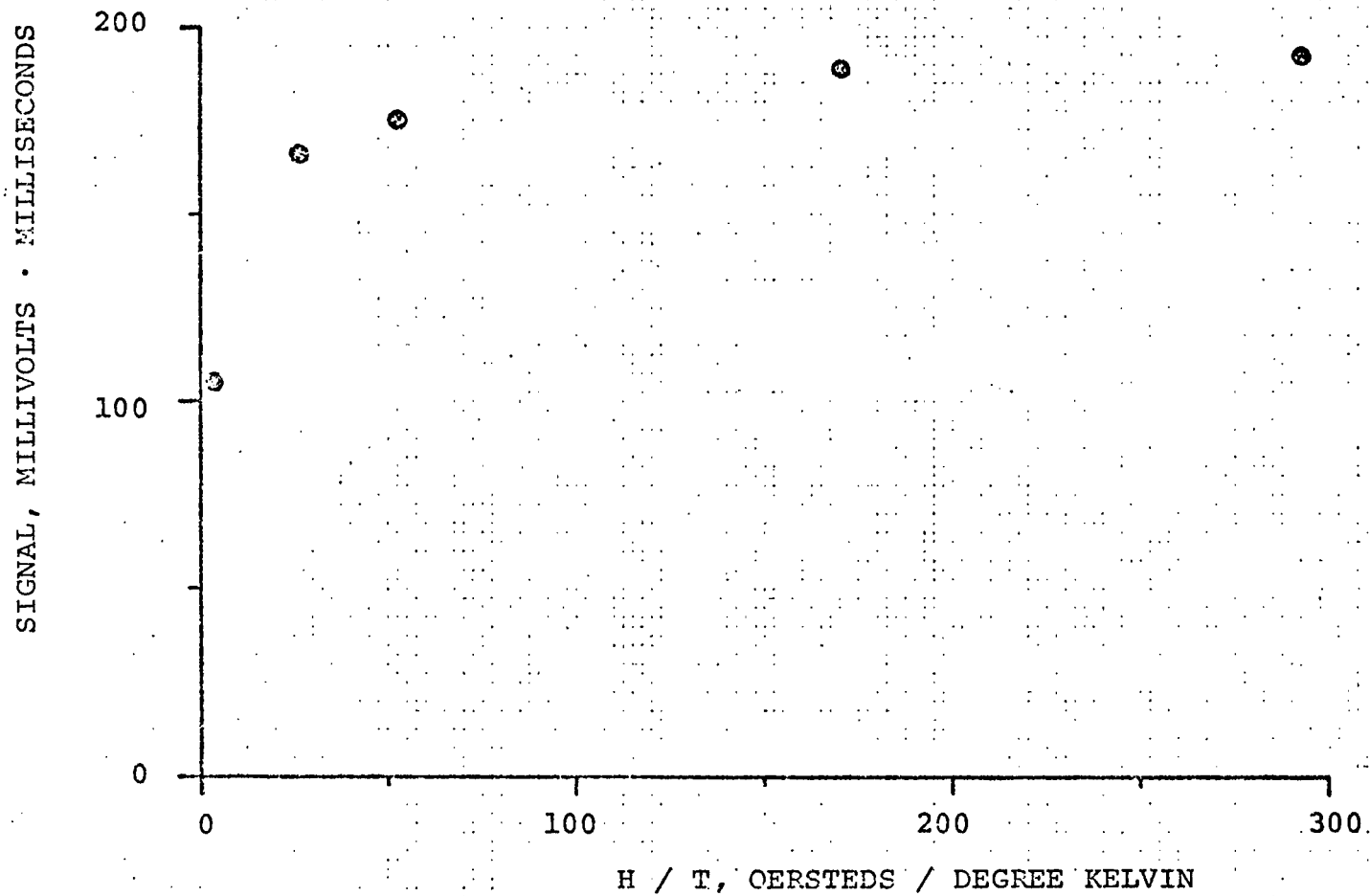


FIGURE B.6 EXPERIMENTAL DATA FROM HIGH FIELD MEASUREMENTS FOR SAMPLE 8 AT 295 DEGREES KELVIN.

SIGNAL, MILLIVOLTS · MILLISECONDS

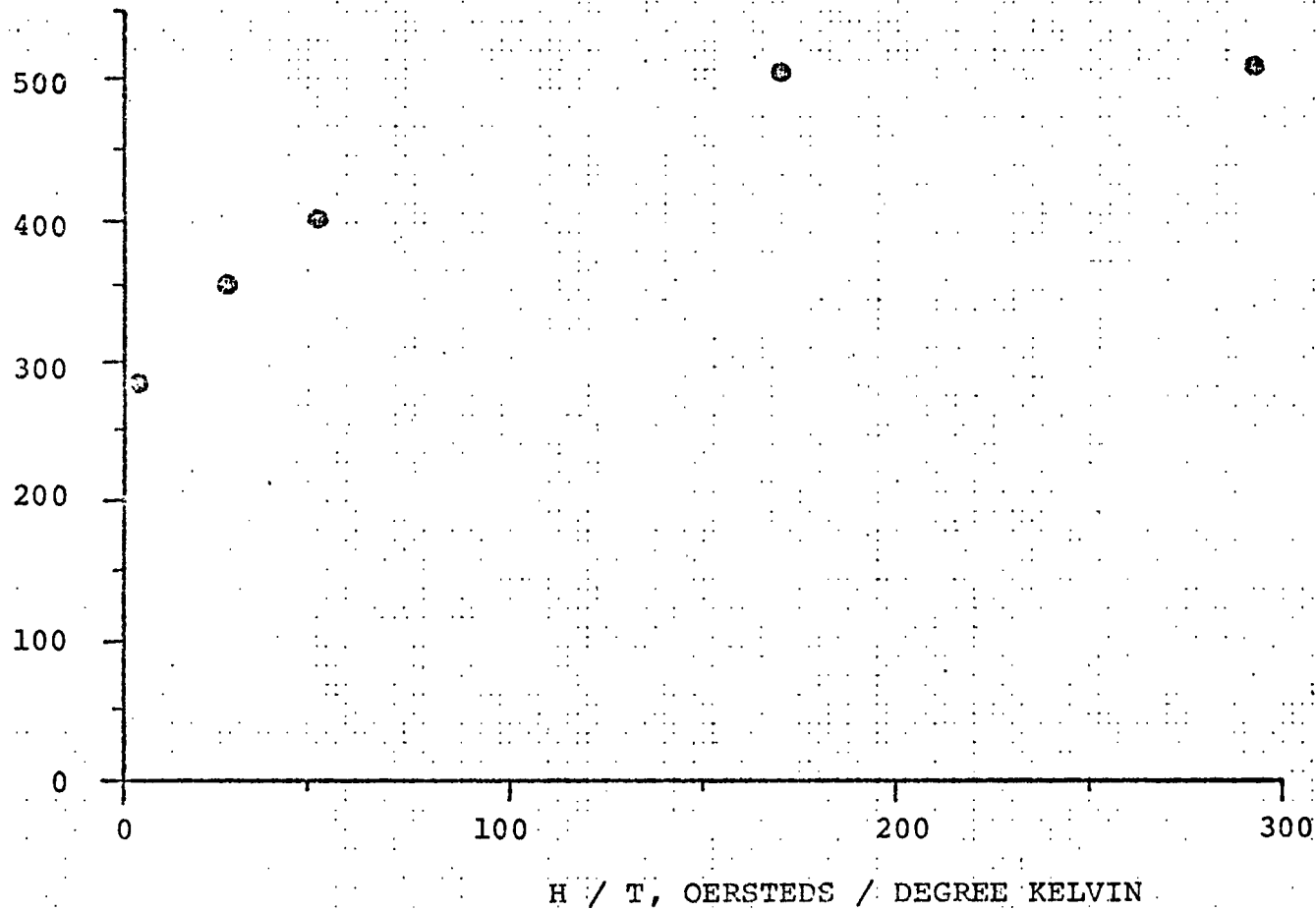


FIGURE B.7 EXPERIMENTAL DATA FROM HIGH FIELD MEASUREMENTS FOR SAMPLE 9 AT 295 DEGREES KELVIN.

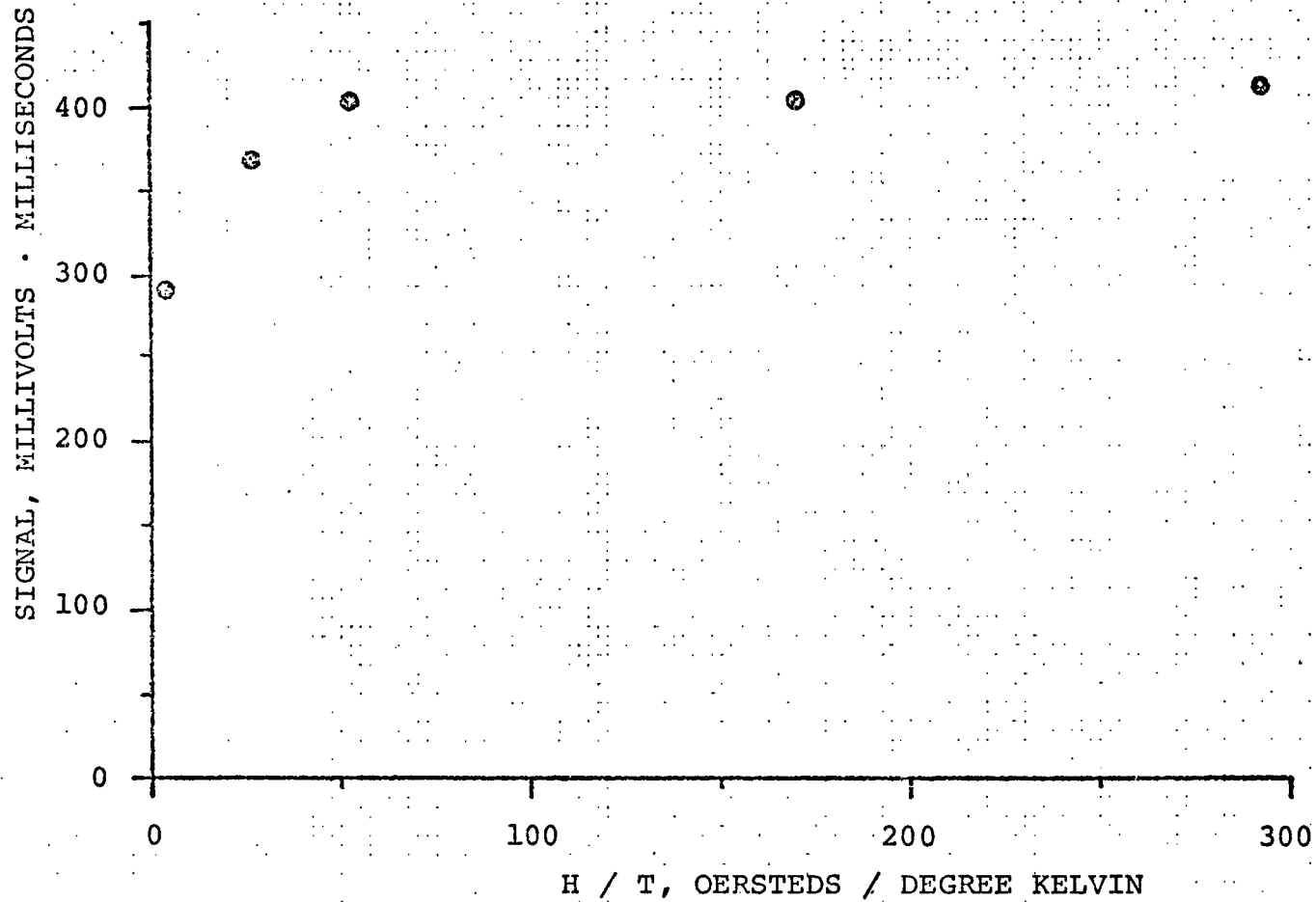


FIGURE B.8 EXPERIMENTAL DATA FROM HIGH FIELD MEASUREMENTS FOR SAMPLE 10 AT 295 DEGREES KELVIN.

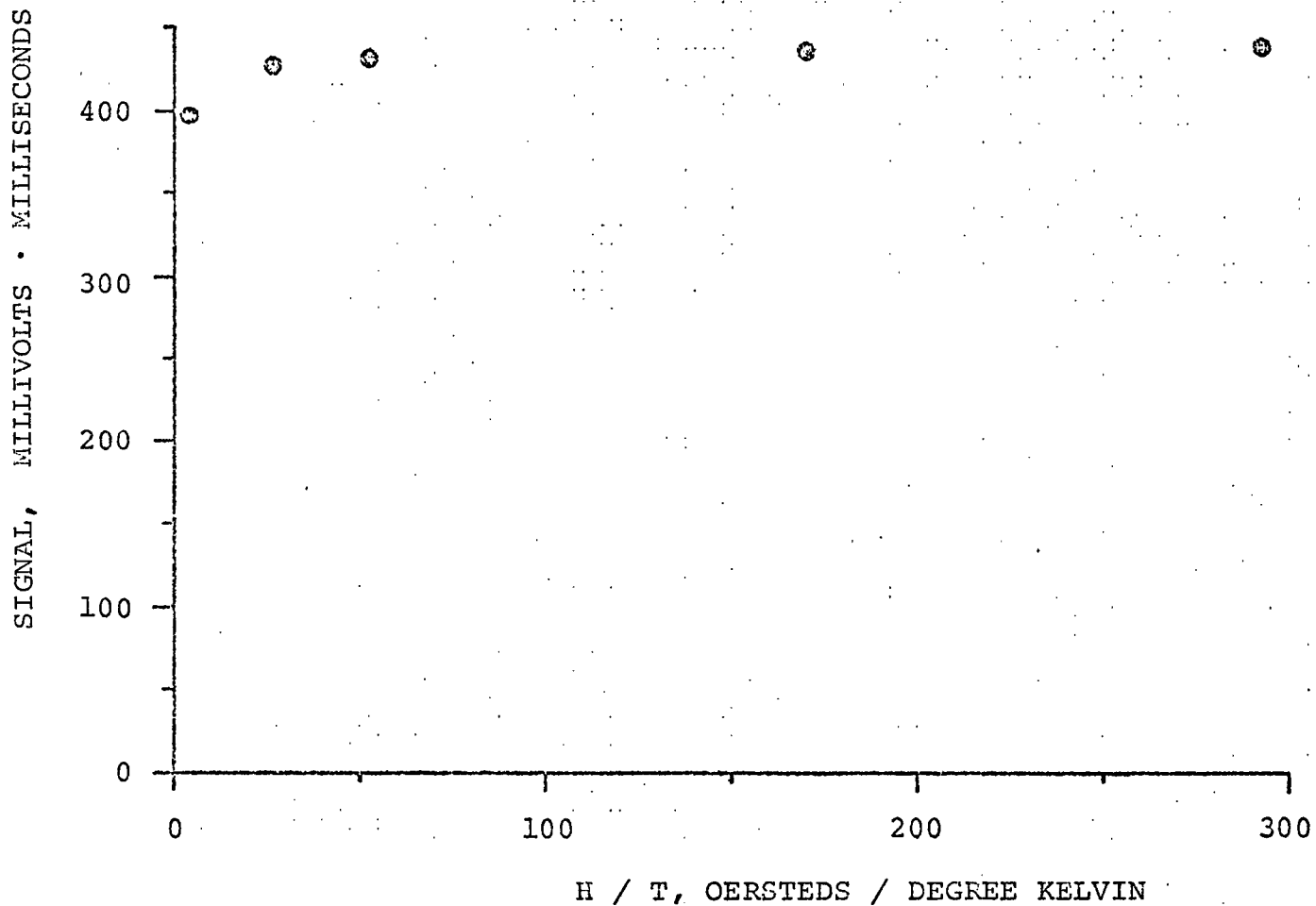


FIGURE B.9 EXPERIMENTAL DATA FROM HIGH FIELD MEASUREMENTS FOR SAMPLE 11 AT 295 DEGREES KELVIN.

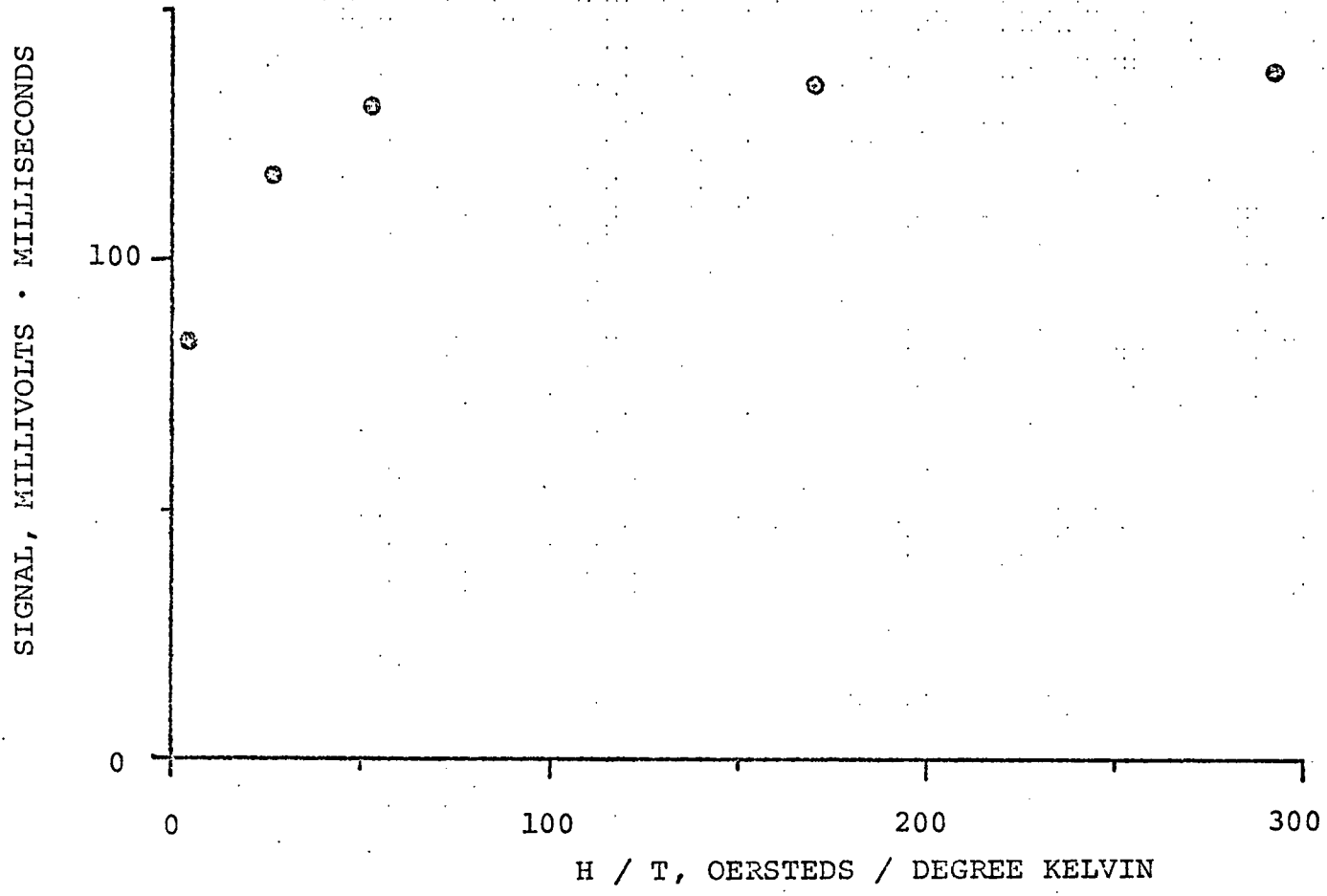


FIGURE B.10 EXPERIMENTAL DATA FROM HIGH FIELD MEASUREMENTS FOR SAMPLE 12 AT 295 DEGREES KELVIN.

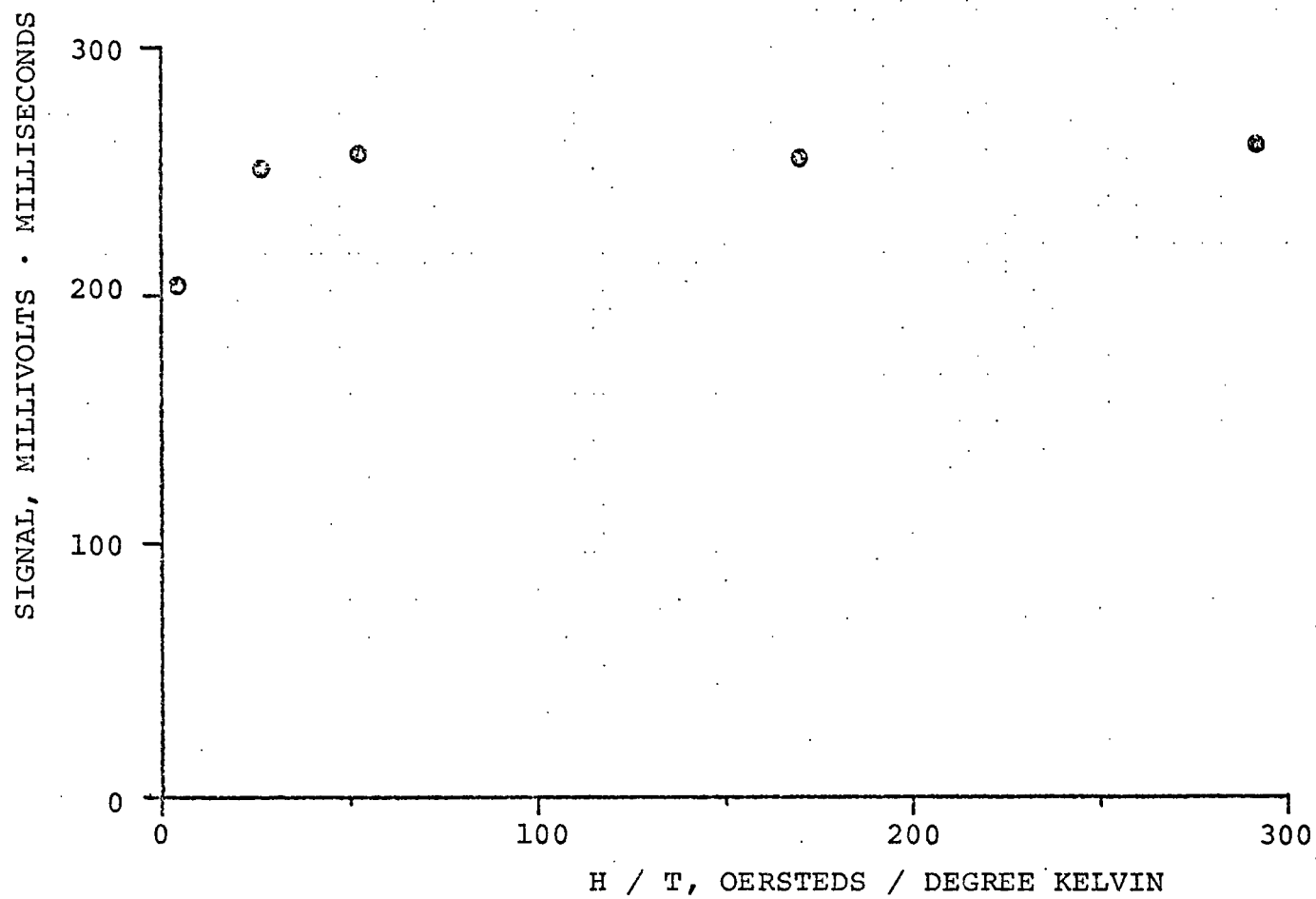


FIGURE B.11 EXPERIMENTAL DATA FROM HIGH FIELD MEASUREMENTS FOR SAMPLE 13 AT 295 DEGREES KELVIN.

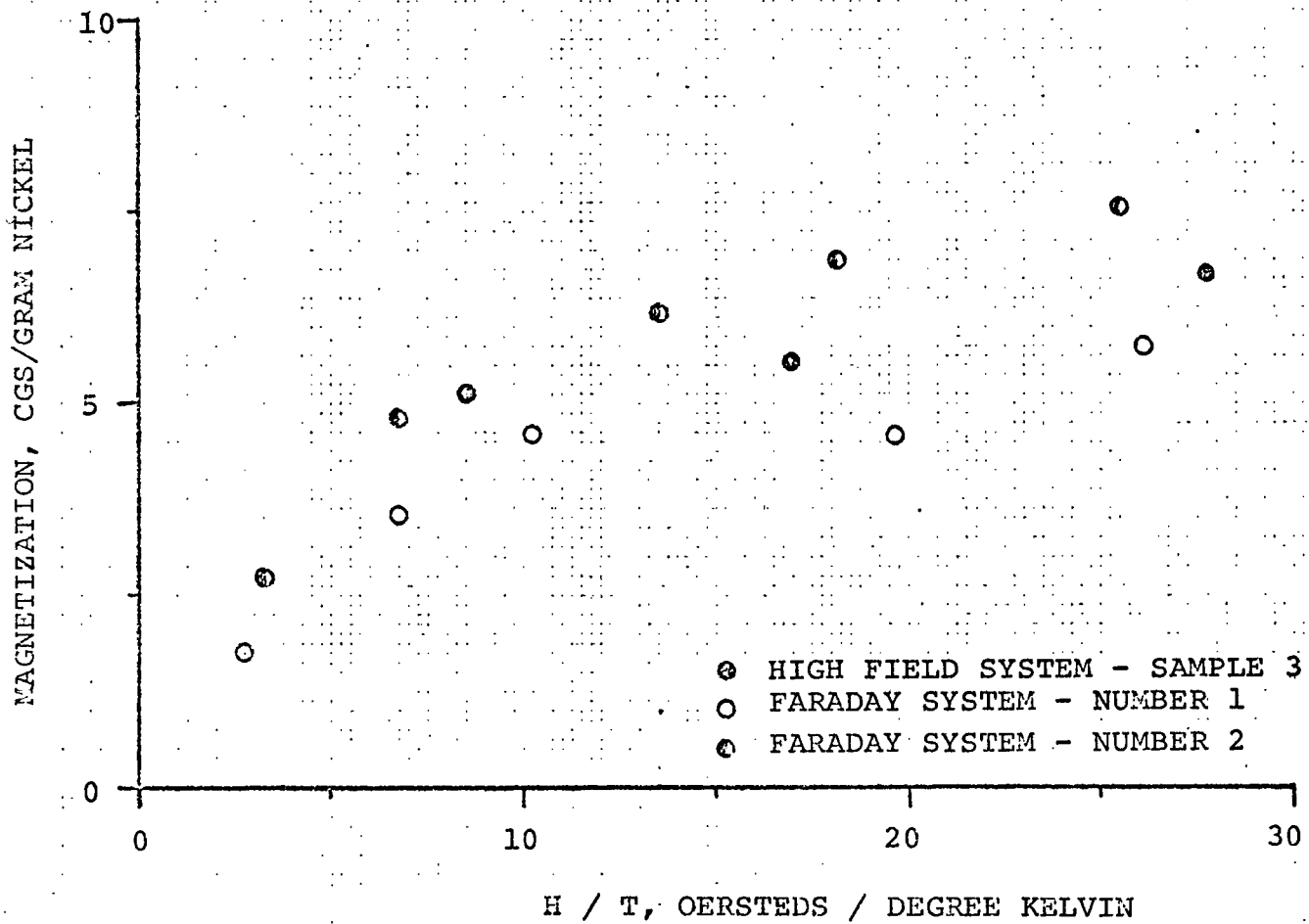


FIGURE B.12 COMPARISON OF HIGH FIELD SYSTEM DATA WITH FARADAY SYSTEM DATA. FARADAY DATA AFTER ROSSER ( 33 ).

APPENDIX C  
COMPUTER PROGRAM

```

C *****
C *
C * PROGRAM TO CALCULATE CRYSTALLITE SIZE DISTRIBUTIONS OF SUPPORTED *
C * CATALYST FROM MAGNETIC DATA USING THE FOURIER INTEGRAL METHOD *
C * LONNIE REED VINCENT - UNIVERSITY OF HOUSTON - FEBRUARY, 1973 *
C * VERSION AS OF JULY 25, 1973 *
C *
C *****
0001 INTEGER C, R, ALARM, PROCED
0002 DIMENSION A( 10, 10), ALABEL( 20), B( 10), C( 10),
1 D( 10, 10), FRAC( 200), HOT( 200), R( 10), REXP( 200),
2 TEMP( 200), VOL( 200)
0003 DATA A/ 100*0.0/, B/ 10*0.0/, C/ 10*0/, D/ 100*0.0/,
1 FRAC/ 200*0.0/, HOT/ 200*0.0/, R/ 10*0/, REXP/ 200*0.0/,
2 TEMP/ 200*0.0/, VOL/ 200*0.0/, ALARM/0/, EPS/ 1.0E-30/,
3 PROCED/ 0/, PI/ 3.141593/
0004 NAMELIST / ALIST / REXP, HOT, M, N, INCR, MA, NA, A
C NOMENCLATURE
C A : ARRAY OF SINE COEFFICIENTS OF DOUBLE FOURIER SERIES OF
C LANGEVIN FUNCTION, DIMENSION NA BY MA
C ALABEL : VECTOR FOR LABELING PURPOSES
C ALARM : WARNING FLAG, SEE AMATSO, (INTEGER)
C B : VECTOR OF SINE COEFFICIENTS IN FOURIER SERIES OF
C EXPERIMENTAL DATA, DIMENSION M
C C : WORK VECTOR, (INTEGER)
C D : WORK ARRAY
C FRAC : FRACTION OF PARTICLES WITH VOLUME VOL, DIMENSION M
C HOT : FIELD STRENGTH DIVIDED BY TEMPERATURE( KILOERSTEDS(CGS)/
C DEGREE SELVIN ), DIMENSION N
C PROCED : CONTROL FLAG, SEE AMATSO
C R : WORK VECTOR, (INTEGER)
C REXP : EXPERIMENTAL VALUES OF THE RELATIVE SATURATION, DIMENSION N
C TEMP : WORK VECTOR
C VOL : VOLUME OF CRYSTALLITE( ANGSTROMS CUBED), DIMENSION M
C
0005 READ(5,600) ALABEL
0006 READ(5,ALIST)
0007 HMAX = HGT( N )
0008 DO 10 I = 1, N, 1
0009 HOT( I ) = (HOT( I ) / HMAX ) * PI
0010 CALL CONSTR( REXP, HOT, TEMP, VOL, FRAC, N, INCR )
0011 DO 12 I = 1, M, 1
0012 AM = I - 1
0013 12 VOL( I ) = AM
0014 VMAX = VOL( M )
0015 DO 15 I = 1, M, 1
0016 15 VOL( I ) = ( VOL( I ) / VMAX ) * PI
0017 16 CALL FCOEFF( D, REXP, HOT, N, NA, D )
0018 CALL DATOUT( A, NA, MA, -1 )
0019 CALL DATOUT( D, NA, MA, -1 )
0020 CALL AMATSO( A, D, C, R, MA, PROCED, DET, EPS, ALARM )
0021 WRITE(6,650) ALARM, DET
0022 650 FORMAT(' ',13,02X,E11.4)
0023 DO 25 I = 1, NA, 1

```

```
0024      R( I ) = D( I, 1 )
0025      25 CONTINUE
0026      CALL DATOUT( A , NA, MA, -1)
0027      CALL DATOUT( D , NA, MA, -1)
0028      CALL FSER( FRAC , B , VOL , MA , M )
0029      WRITE(6,610)
0030      WRITE(6,620) ALABEL
0031      WRITE(6,635)
0032      DO 220 I = 1, M , 2
0033      TEMP( I ) =(VOL( I ) * VMAX ) / PI
0034      VOL( I ) = ( PI * TEMP( I )**( 3.0 ) ) / 6.0
0035      WRITE(6,640) I , TEMP(I) , VOL(I) ,FRAC(I)
0036      VOL( I ) = VOL( I ) * 1.0E-04
0037      220 CONTINUE
0038      225 CONTINUE
0039      630 FORMAT( 20A4)
0040      610 FORMAT('1',05(//) )
0041      620 FORMAT(' ', 20A4, 2(//) )
0042      635 FORMAT(' ',07X,'I',06X,'DIAMETER',05X,'VOLUME',06X,'FRACTION')
0043      640 FORMAT(' ',06X,I3,03(02X,E11.4))
0044      END
```

```

0001 SUBROUTINE AMATSO( A , B , C , R , N , PROCED , DET , EPS , ALARM)AMS 1
C A MATRIX SOLUTION PROGRAM - L. REED VINCENT , JANUARY 15, 1973 AMS 2
C DEPARTMENT OF CHEMICAL ENGINEERING AMS 3
C UNIVERSITY OF HOUSTON AMS 4
C A PROGRAM TO INVERT THE MATRIX A OR TO SOLVE THE MATRIX EQUATION AMS 5
C  $A * X = B$  BY DIRECT POW OPERATIONS USING COMPLETE MATRIX PIVOTING AMS 6
C TO REDUCE A TO IDENTITY MATRIX AND PRODUCE INVERSE OR X IN B AMS 7
C NOMENCLATURE : AMS 8
C A : MATRIX TO BE INVERTED OR COEFFICIENT MATRIX OF EQUATION  $A * X$  AMS 9
C = B , DIMENSION N BY N AMS 10
C B : FOR INVERSE , AMATSO WILL CONSTRUCT IDENTITY MATRIX IN B; B AMS 11
C WILL CONTAIN INVERSE ON RETURN , DIMENSION N BY N AMS 12
C TO SOLVE  $A * X = B$  , B MUST BE SPECIFIED ON ENTRY; B WILL CONTAINAMS 13
C SOLUTION X ON RETURN , DIMENSION 1 BY N AMS 14
C ALARM : ( INTEGER ) WARNING FLAG WHOSE VALUE INDICATES FOLLOWING AMS 15
C CONDITIONS AMS 16
C 1 : PIVOT IS 0.0 , A IS SINGULAR AMS 17
C 2 : ( ABS(PIVOT).LE. ABS(EPS) ) AMS 18
C 3 : INVERSE OR SOLUTION PROCEDURE NOT SPECIFIED , SEE 'PROCED' AMS 19
C 4 : THE MATRIX A HAS NOT BEEN REDUCED TO IDENTITY MATRIX AMS 20
C C : ( INTEGER ) COLUMN WORK VECTOR , DIMENSION 1 BY N AMS 21
C DET : DETERMINANT OF A AMS 22
C EPS : MAGNITUDE OF PIVOT IS LESS THAN OR EQUAL FOR WHICH A WILL BEAMS 23
C CONSIDERED SINGULAR AMS 24
C N : ( INTEGER ) ORDER OF A AMS 25
C PROCED : ( INTEGER ) FLAG TO INDICATE SOLUTION DESIRED ACCORDING TOAMS 26
C FOLLOWING VALUES AMS 27
C 0 : SOLUTION X OF  $A * X = B$  AMS 28
C 1 : INVERSE OF A AMS 29
C R : ( INTEGER ) ROW WORK VECTOR , DIMENSION 1 BY N AMS 30
C AMS 31
0002 REAL A , B , DET , EPS , HOLD , PIVOT AMS 32
0003 INTEGER ALARM , C , I , IPOSIT , J , JPOSIT , K , N , NOUSE , AMS 33
1 PROCED , R AMS 34
0004 DIMENSION A( N , N ) , B( N , N ) , C( N ) , R( N ) AMS 35
C AMS 36
C AMS 37
C START:PROCEDURE CHECK AMS 38
C AMS 39
0005 1 IF( PROCED.EQ. 1 ) GO TO 4 AMS 40
0006 2 IF( PROCED.EQ. 0 ) GO TO 10 AMS 41
0007 3 GO TO 130 AMS 42
C AMS 43
C END:PROCEDURE CHECK AMS 44
C AMS 45
C START:CONSTRUCTION OF IDENTITY MATRIX AMS 46
C AMS 47
0008 4 DO 9 I= 1,N AMS 48
0009 5 DO 8 J= 1,N AMS 49
0010 6 B( I , J ) = 0.0 AMS 50
0011 7 IF( I.EQ.J ) B( I , J ) = 1.0 AMS 51
0012 8 CONTINUE AMS 52
0013 9 CONTINUE AMS 53
C AMS 54

```

	C	END:CONSTRUCTION OF IDENTITY MATRIX	AMS	55
	C		AMS	56
	C	START:SET VALUES OF R, C, PIVOT, DET, AND ALARM	AMS	57
	C		AMS	58
0014		10 ALARM = C	AMS	59
0015		PIVOT = C.0	AMS	60
0016		DET = 1.0	AMS	61
0017		DO 16 I= 1,N	AMS	62
0018		C( I ) = 0	AMS	63
0019		R( I ) = 0	AMS	64
0020		16 CONTINUE	AMS	65
	C		AMS	66
	C	END:SETTING VALUES OF R, C, PIVOT, DET, AND ALARM	AMS	67
	C		AMS	68
	C		AMS	69
	C	START:REDUCTION	AMS	70
	C		AMS	71
0021		DO 70 I= 1,N	AMS	72
0022		PIVOT = C.0	AMS	73
	C		AMS	74
	C	START:SEARCH FOR PIVOT	AMS	75
	C		AMS	76
	C	ROW IPOSIT	AMS	77
	C		AMS	78
0023		DO 44 IPOSIT= 1,N	AMS	79
	C		AMS	80
	C	START:CHECK IF ROW HAS BEEN USED BEFORE	AMS	81
	C		AMS	82
0024		I = I - 1	AMS	83
0025		20 DO 26 K= 1,I	AMS	84
0026		IF( R( K ).EQ.IPOSIT ) GO TO 23	AMS	85
0027		NOUSE = C	AMS	86
0028		GO TO 26	AMS	87
0029		23 NOUSE = 1	AMS	88
0030		K = I	AMS	89
0031		26 CONTINUE	AMS	90
0032		I = I + 1	AMS	91
0033		IF( NOUSE.EQ. 1) GO TO 44	AMS	92
	C		AMS	93
	C	END:CHECK IF ROW HAS BEEN USED BEFORE	AMS	94
	C		AMS	95
	C	ELEMENT JPOSIT OF ROW IPOSIT	AMS	96
	C		AMS	97
0034		DO 42 JPOSIT= 1,N	AMS	98
0035		30 IF( ABS( A( IPOSIT , JPOSIT ) ).NE. 1.0 ) GO TO 37	AMS	99
0036		PIVOT = A( IPOSIT , JPOSIT )	AMS	100
0037		R( I ) = IPOSIT	AMS	101
0038		C( I ) = JPOSIT	AMS	102
0039		IPOSIT = N	AMS	103
0040		35 JPOSIT = N	AMS	104
0041		GO TO 42	AMS	105
0042		37 CONTINUE	AMS	106
0043		IF( ABS( PIVOT ).GE. ABS( A( IPOSIT , JPOSIT ) ) ) GO TO 42	AMS	107
0044		PIVOT = A( IPOSIT , JPOSIT )	AMS	108

0045	40 R( I ) = IPOSIT	AMS	109
0046	C( I ) = JPOSIT	AMS	110
0047	42 CONTINUE	AMS	111
0048	44 CONTINUE	AMS	112
	C	AMS	113
	C	AMS	114
	C	AMS	115
	C	AMS	116
	C	AMS	117
	C	AMS	118
0049	45 IF( PIVOT.EQ. 0.0 ) GO TO 110	AMS	119
0050	46 IF( ABS( PIVOT ).LE. ABS( EPS ) ) GO TO 120	AMS	120
	C	AMS	121
	C	AMS	122
	C	AMS	123
0051	DET = DET * PIVOT	AMS	124
	C	AMS	125
	C	AMS	126
	C	AMS	127
	C	AMS	128
	C	AMS	129
0052	IF( PIVOT.EQ. 1.0) GO TO 51	AMS	130
	C	AMS	131
	C	AMS	132
	C	AMS	133
	C	AMS	134
	C	AMS	135
0053	IPOSIT = R( I )	AMS	137
	C	AMS	138
	C	AMS	139
0054	DO 50 JPOSIT= 1,N	AMS	140
0055	A( IPOSIT , JPOSIT ) = A( IPOSIT , JPOSIT ) / PIVOT	AMS	141
0056	B( IPOSIT , JPOSIT ) = B( IPOSIT , JPOSIT ) / PIVOT	AMS	141
0057	50 CONTINUE	AMS	142
	C	AMS	143
	C	AMS	144
	C	AMS	145
	C	AMS	146
	C	AMS	147
	C	AMS	148
	C	AMS	149
	C	AMS	150
	C	AMS	151
0058	51 IPOSIT = R( I )	AMS	152
0059	JPOSIT = C( I )	AMS	153
0060	DO 65 K= 1,N	AMS	154
	C	AMS	155
	C	AMS	156
	C	AMS	157
0061	IF( K.EQ.IPOSIT ) GO TO 65	AMS	158
0062	HOLD = A( K , JPOSIT )	AMS	159
0063	DO 60 J= 1,N	AMS	160
0064	A( K , J ) = A( K , J ) - A( IPOSIT , J ) * HOLD	AMS	161
0065	B( K , J ) = B( K , J ) - B( IPOSIT , J ) * HOLD	AMS	162
0066	60 CONTINUE	AMS	163

0067	65 CONTINUE	AMS 164
	C	AMS 165
	C	AMS 166
	C	AMS 167
	C	AMS 168
0068	70 CONTINUE	AMS 169
	C	AMS 170
	C	AMS 171
	C	AMS 172
	C	AMS 173
	C	AMS 174
	C	AMS 175
0069	JPOSIT = N - 1	AMS 176
0070	DO 100 J= 1,JPOSIT	AMS 177
0071	IF( A( J , J ).EQ. 1.0 ) GO TO 100	AMS 178
0072	75 DO 95 I= J,N	AMS 179
0073	IF( A( I , J ).NE. 1.0 .AND. A( I , J ).NE. 0.0 ) GO TO 160	AMS 180
0074	IF( A( I , J ).NE. 1.0 ) GO TO 95	AMS 181
	C	AMS 182
	C	AMS 183
	C	AMS 184
0075	DO 85 K= 1,N	AMS 185
0076	HOLD = A( I , K )	AMS 186
0077	A( I , K ) = A( J , K )	AMS 187
0078	A( J , K ) = HOLD	AMS 188
0079	HOLD = B( I , K )	AMS 189
0080	B( I , K ) = B( J , K )	AMS 190
0081	B( J , K ) = HOLD	AMS 191
0082	85 CONTINUE	AMS 192
0083	I = N + 1	AMS 193
	C	AMS 194
	C	AMS 195
	C	AMS 196
0084	95 CONTINUE	AMS 197
0085	100 CONTINUE	AMS 198
	C	AMS 199
	C	AMS 200
	C	AMS 201
0086	105 RETURN	AMS 202
	C	AMS 203
	C	AMS 204
	C	AMS 205
0087	110 ALARM = 1	AMS 206
0088	DET = 0.0	AMS 207
0089	115 RETURN	AMS 208
	C	AMS 209
	C	AMS 210
	C	AMS 211
	C	AMS 212
0090	120 ALARM = 2	AMS 213
0091	DET = 0.0	AMS 214
0092	125 RETURN	AMS 215
	C	AMS 216
	C	AMS 217

	C		AMS 218
	C	START:WARNING FOR NO PROCEDURE SPECIFICATION	AMS 219
	C		AMS 220
0093		130 ALARM = 3	AMS 221
0094		150 RETURN	AMS 222
	C		AMS 223
	C	END:WARNING	AMS 224
	C		AMS 225
	C	START:WARNING FOR A NOT REDUCED TO IDENTITY MATRIX	AMS 226
	C		AMS 227
0095		160 ALARM = 4	AMS 228
0096		DET = 0.0	AMS 229
0097		170 RETURN	AMS 230
	C		AMS 231
	C	END:PROGRAM	AMS 232
	C		AMS 233
0098		END	AMS 234

```
0001      SUBROUTINE CONSTR( Y , X , SLOPE , YP , XP , N , INCR )
0002      DIMENSION Y( INCR ), X( INCR ), SLOPE( N ), YP( N ), XP( N )
0003      DO 10 I= 1, N, 1
0004      YP( I ) = Y( I )
0005      XP( I ) = X( I )
0006      10 CONTINUE
0007      LIMIT = N - 1
0008      DO 20 I = 1, LIMIT , 1
0009      SLOPE( I ) = ( YP( I+1) - YP( I ) ) / ( XP( I+1) - XP( I ) )
0010      20 CONTINUE
0011      LIMIT = INCR - 1
0012      DEL = XP( N ) / LIMIT
0013      X( 1 ) = 0.0
0014      DO 30 I = 2, INCR , 1
0015      X( I ) = X( I-1) + DEL
0016      30 CONTINUE
0017      LIMIT = INCR
0018      J = 0
0019      DO 40 I = 1, LIMIT , 1
0020      IF( X( I ).GE. XP( J+1) ) J = J + 1
0021      Y( I ) = SLOPE( J ) * ( X( I ) - XP( J ) ) + YP( J )
0022      40 CONTINUE
0023      N = INCR
0024      RETURN
0025      END
```

```
0001      SUBROUTINE FCOEFF( A , F , X , N , NA , D )
0002      DIMENSION A( NA ) , F( N ) , X( N ) , D( NA , NA )
0003      PI = 3.141593
0004      NMAX = N - 1
0005      DELX = X( N ) - X( N - 1 )
0006      DO 200 I = 1, NA , 1
0007         II = I
0008         A( I ) = 0.0
0009         A( I ) = ( F( 1 ) * SIN( II * X( 1 ) ) ) / 2.0
0010         DEL = ( F( N ) * SIN( II * X( N ) ) ) / 2.0
0011         A( I ) = A( I ) + DEL
0012         DO 100 J = 2, NMAX , 1
0013            DEL = ( F( J ) * SIN( II * X( J ) ) )
0014            A( I ) = A( I ) + DEL
0015      100 CONTINUE
0016         A( I ) = A( I ) * 2.0 * DELX / PI
0017      200 CONTINUE
0018      DO 20 I = 1, NA, 1
0019         D( I , 1 ) = A( I )
0020      20 CONTINUE
0021      RETURN
0022      END
```

```
0001      SUBROUTINE FSER( F , A , X , MA , M )
0002      DIMENSION F( M ) , X( M ) , A( MA )
0003      PI = 3.141593
      C      PROGRAM TO CALCULATE FOURIER SERIES REPRESENTATION OF FUNCTION F
      C      FROM COEFFICIENTS A AND B
      C      UNEQUAL INTERVALS OF X CAN BE USED
0004      DO 200 I = 1, M , 1
0005      F( I ) = 0.0
0006      DO 100 J = 1, MA , 1
0007      JJ = J
0008      DEL = A( J ) * SIN( JJ * X( I ) )
0009      F( I ) = F( I ) + DEL
0010      100 CONTINUE
0011      F( I ) = F( I ) / PI
0012      200 CONTINUE
0013      RETURN
0014      END
```

0001	SUBROUTINE DATOUT ( RST , N , NN , ICARDS )	DATOUT 1
0002	DIMENSION RST ( N , NN )	DATOUT 2
0003	DO 200 I = 1, N, 1	DATOUT 3
0004	200 WRITE ( 6, 600) ( RST( I , K ) , K = 1, NN, 1)	DATOUT 4
0005	WRITE (6, 610)	DATOUT 5
0006	IF ( ICARDS .LT. 0) GO TO 9999	DATOUT 6
0007	DO 310 K = 1, NN, 1	DATOUT 7
0008	310 PUNCH 650,(RST( I , K ) , I = 1, N , 1)	DATOUT 8
0009	600 FORMAT ( ' ', 10( 2X,E11.4) )	DATOUT 9
0010	610 FORMAT ( 'C' )	DATOUT 10
0011	650 FORMAT( 8X, 5(1X,E11.4,' '),/, 8X, 5( 1X,E11.4,' ') )	DATOUT 11
0012	9999 RETURN	DATOUT 12
0013	END	DATOUT 13

APPENDIX D

SAMPLE CALCULATIONS

## SAMPLE CALCULATIONS

From photograph 13-9

$$\text{Area} = 1.10 \text{ in}^2$$

$$\int E dt = (1.10 \text{ in}^2) \left( 8.34 \frac{\text{vdiv} \cdot \text{tdiv}}{\text{in}^2} \right) \\ \left( 20 \frac{\text{msec}}{\text{tdiv}} \right) \left( 2.0 \frac{\text{mvolts}}{\text{vdiv}} \right) = 367 \text{ mv} \cdot \text{msec} \\ \text{at } 7.80 \times 10^3 \text{ oersteds}$$

After all data for this sample are calculated, saturation signal is obtained as

$$\left( \int E dt \right)_{\infty} = 430 \text{ mv} \cdot \text{msec}$$

hence

$$M/M_{\infty} = \frac{367}{430} = .854$$

From data on nickel at saturation

$$m_{Ni} (54.4) = C_{\eta} \int E dt$$

$$C_{\eta} = \frac{(54.4)(.114 \text{ gm Ni})}{262} = 2.50 \times 10^{-2}$$

$$M_{\infty} = \frac{C_{\eta}}{m_{Ni}} \left( \int E dt \right)_{\infty}$$

$$M_{\infty} = \frac{2.50 \times 10^{-2}}{.199 \text{ gm reduced Ni}} (430) = 54.0 \frac{\text{cgs units}}{\text{gm reduced Nickel}}$$

Average Crystallite Sizes :

Low field:

$$(\bar{v}^2/\bar{v}) = \left[ \frac{(3)(1.38 \times 10^{-16})(295)}{485} \right] \left[ \frac{.671}{1.08 \times 10^{-3}} \right] \text{ cm}^3$$

$$(\bar{v}^2/\bar{v}) = 127 \times 10^3 \text{ \AA}^3$$

$$d = 62.5 \text{ \AA}$$

High field:

$$\bar{v} = \left[ \frac{(1.38 \times 10^{-16})(295)}{485} \right] \left[ \frac{1.00}{1.00 - .955} \right] \left[ \frac{1.00}{86.5 \times 10^3} \right] \text{ cm}^3$$

$$\bar{v} = 303 \times 10^2 \text{ \AA}^3$$

$$d = 38.7 \text{ \AA}$$

## NOMENCLATURE

A	Area, squared centimeters
B	Magnetic Flux Density, gauss
Br	Brillouin Function
C	A constant
c	Capacitance, farads
d	Diameter, centimeters or Angstroms
E	Electrical Potential Difference, volts
f	Distribution Function
H	Magnetic Field Strength, oersteds
K	M / H, magnetic susceptibility per unit volume
k	Boltzmann Constant, $1.38 \times 10^{-16}$ ergs / degree Kelvin
L	Langevin Function
l	Distance, centimeters
M	Intensity of Magnetization, magnetic moment per unit volume or gauss
m	Mass, gram
$M_{sp}$	Spontaneous Magnetization, magnetic moment per unit volume or gauss
N	Number of Turns
n	Number of Crystallites
Q	$1 / 2\pi R_c$
R	Resistance, ohms
r	Radius, centimeters or Angstroms

s	Dispersion
T	Temperature, degrees Kelvin or degrees Centigrade
t	Time, seconds
U	Energy, ergs
V	Volume, cubic centimeters or cubic Angstroms
W	Fourier Coefficient
$\beta$	$H / T$ , oersteds / degree Kelvin
$\theta$	Angle, radians
$\mu$	Magnetic Moment
$\nu$	Frequency, hertz
$\pi$	3.141593
$\rho$	Density, grams per cubic centimeter
$\sigma$	$M / \rho$ , Specific Magnetization, magnetic moment per unit mass
$\tau$	Relaxation Time, seconds
$\Phi$	Magnetic Flux, maxwell
$\chi$	$K / \rho$ , magnetic susceptibility per unit mass

## SUBSCRIPTS

b	Bulk
c	Curie Point
max	Maximum Value
Ni	Nickel
o	Observed
r	Remanance
s	Sample
$\infty$	At Infinite Magnetic Field Strength or at Saturation Condition

## SUPERSCRIPTS

— Average Value